

Nonlinear Robust Control and Optimisation of Microgrids



Grigorios Michos

Department of Automatic Control and Systems Engineering
The University of Sheffield

A thesis submitted in partial fulfillment of the requirements
for the award of the degree of

Doctor of Philosophy

Sheffield 2023

*To my parents,
Kiriaki and Stavros*

Acknowledgements

First and foremost, I would like to thank my family for their endless support, both mentally and financially. I would like to acknowledge the effort of my parents, Kiriaki and Stavros, to provide me with the means to become the person I am today. Undoubtedly, without their sacrifices, I would not be in the privileged position to chase and achieve my dreams. I would also like to express my thanks to my girlfriend, Agathi, for her patience and support throughout the past few years. Despite the difficulties of this journey, she selflessly stood by my side and always found a way to cheer me up.

Next, I would like to express my gratitude to my supervisors Dr. George Konstantopoulos and Dr. Paul Trodden. Dr. George Konstantopoulos provided persistent support, excellent mentoring and constructive feedback. His influence allowed me to mature as a researcher and had a profound positive impact on my research work. My deepest thanks also extend to Dr Paul Trodden, who undertook the difficult project of becoming my main supervisor the later years of my PhD studies. I will forever be thankful for his support and the helpful commentary he provided during the conceptualisation and writing of research papers, as well as during the writing of this thesis.

I am also immensely grateful to Pablo R. Baldivieso Monasterios for his guidance, without which this journey would be undoubtedly much harder. Finally, I would like to thank my colleagues Panos Skentzos, Andrei Braiton, Alex Paspatis and Seyfullah Dedeoglou. Their support and friendship meant a lot.

Abstract

The modern power grid is entering a new “smart grid” era, which promises more efficient power transmission/distribution, decentralised power generation and seamless integration of renewable energy resources to the electricity distribution grid. In the heart of this new era lies the Microgrid, which represents a scaled, local version of the grid and allows the integration of various renewable energy resources, energy storage systems and loads via power converters. Along with a plethora of distinct advantages, Microgrids also introduce many new challenges in designing an appropriate controller that ensures tight regulation of the grid voltage/frequency and economic operation of the network. The continuous advancement of technology enabled the rise of complex and sophisticated load architectures, the majority of which are of DC nature. A prime example is the constant power load, which introduces a nonlinear, destabilising behaviour and poses a threat to the operation of the network. Another issue is associated with the long physical distances between the individual units and the requirement to exchange information in a fast communication rate. Despite the existence of a vast literature on Microgrid control, the majority of the studies are case-specific, offer only numerical investigations of system stability and focuses on the implementation of each proposed control scheme with extensive simulation scenarios or experiments. Due to the continuously increasing complexity of loads and network topologies, it is essential to study the problem from a control-theoretic perspective, in order to provide a deep insight into the dynamical behaviour of the system and develop control techniques that provide strong theoretic guarantees regarding a safe and reliable operation. Furthermore, even though it has not been extensively studied so far, the ability to satisfy constraints is crucial to the Microgrid operation in order to protect the electronic components from overcurrent surges or overvoltage cases that can cause expensive damages and disrupt the network operation. This thesis aims to fill this gap by thoroughly investigating the nonlinear behaviour of the Microgrids under the influence of nonlinear loads. More specifically, the first main contribution is the development of a distributed control scheme for meshed DC Microgrids that employs neighbour-to-neighbour communication and guarantees both local and cou-

pled constraint satisfaction. Contrary to the majority of the approaches found in the literature, the proposed method utilises only locally available information at each node in order to enhance the system scalability and enlarge the range of potential applications. This first part includes a rigorous theoretic analysis to formulate explicit conditions such that the system achieves the desired behaviour and admits asymptotically stable equilibrium points. The following parts of this thesis focus specifically on the effect of the nonlinear loads. The problem is studied from a geometric point of view in order to shed light into the dynamic interaction between the loads and the network and design a control scheme that enhances the system robustness to perturbations of the load demand. First, a local low-level current controller is proposed that guarantees overcurrent protection without the use of saturation devices. Then, theoretic tools are used to guarantee that the voltage trajectory of each local node remains close to a desired reference trajectory and prove that the deviations between the two are bounded in a positive invariant set. This is ultimately used to design a unified control scheme, *i.e.* for both the output voltage and inner current states of each interfacing power converter, that achieves a constraint-based operation with reduced conservativeness compared to the original method. The overall system stability is analytically proven by the use of control Lyapunov functions. The final contribution of this thesis is the extension of the provided theoretic analysis from a DC to the case of an isolated AC Microgrid. A robust controller is proposed in order to show that similar results can be obtained even in the case of a more complicated system model. An analytic characterisation of a closed positive invariant subset of the system state space is obtained and it is shown how this property can be used to design a constraint-based approach for AC Microgrids. Each proposed method is tested in a simulation scenario to validate the results and illustrate the associated theoretic properties.

Contents

1	Introduction	1
1.1	Motivation	1
1.2	Aims and Objectives	5
1.3	Publications List	5
1.3.1	Published	5
1.3.2	In preparation	6
1.4	Thesis Outline	6
2	Literature review	9
2.1	The Microgrid Architecture	9
2.2	Microgrid Types	10
2.3	Power Converters	13
2.3.1	Buck Converters	15
2.3.2	Boost Converters	16
2.3.3	Buck-Boost Converters	16
2.3.4	Three-phase Inverter	17
2.4	Loads	19
2.4.1	Constant Impedance Loads	19
2.4.2	Constant Current Loads	20
2.4.3	Constant Power Loads	20
2.5	Compensation of Microgrid Systems	22
2.5.1	Primary Control	23
2.5.2	Supervisory Control	28
2.6	Microgrid Stability in the Presence of CPLs	35
2.7	Constraint-Based Operation	37
2.7.1	Constraint-Based Operations in Microgrid Literature	37
2.7.2	Constraint-Based Operations in Control Theory Literature	37
2.8	Gaps in the Literature	39

3	Distributed Constrained-Based Control of DC Microgrids	41
3.1	System Modelling	42
3.2	Primary Control Design	43
3.3	Supervisory control structure	46
3.4	Upper Level - Target Computation	47
3.5	Lower-Level distributed control	48
3.5.1	Recursive Feasibility	50
3.5.2	Stability of the Closed-Loop Dynamics	57
3.6	Simulation Results	61
3.7	Conclusions	62
4	Tube-based Control of DC Microgrids	65
4.1	Problem Statement	66
4.2	Inner Current Control	69
4.3	Voltage Control	70
4.3.1	Formulation and boundedness of the error dynamics	71
4.3.2	Formulation of the nominal voltage controller	77
4.4	Stability analysis of the cascaded dynamics	80
4.5	Simulations	82
4.6	Conclusions	84
5	Dynamic tube control scheme for islanded DC Microgrids	87
5.1	Problem Formulation	88
5.2	Voltage dynamics and boundedness analysis	89
5.3	Regulation of the Nominal Dynamics	95
5.4	Stability and Recursive Feasibility	97
5.5	Simulations	99
5.6	Conclusions	101
6	Tube-based Control for Islanded AC Microgrids	105
6.1	Problem Statement	106
6.2	Control Scheme Formulation	107
6.3	Positive invariance of the dynamics	109
6.4	Simulations	117
6.5	Conclusions	118
7	Conclusions and future work	120
7.1	Summary	120
7.2	Discussion of assumptions and limitations	121
7.3	Future directions	123

A Preliminaries: Theory and Notation	125
A.1 Common notations	125
A.1.1 Function properties	126
A.2 Linear Algebra	127
A.3 Nonlinear System Analysis	127
A.4 Graph Theory	129

List of Figures

2.1	An AC Microgrid consisting of several renewable resource units and consumers.	11
2.2	A DC Microgrid consisting of several renewable resource units and consumers. Each unit is interfaced with the network via a power converter.	12
2.3	A Hybrid Microgrid consisting of an AC and a DC subgrid interfaced by an interlinking converter.	13
2.4	Circuit diagram of a buck converter connected in parallel to a local load.	15
2.5	Circuit diagram of a boost converter connected in parallel to a local load.	16
2.6	Circuit diagram of a buck-boost converter connected in parallel to a local load.	17
2.7	Circuit diagram of an DC/AC inverter connected an AC bus.	17
2.8	V-I characteristics of a constant impedance load	20
2.9	V-I characteristics of a constant current load	20
2.10	V-I characteristics of a constant power load	21
2.11	Hierarchical control of a Microgrid. Dashed arrows indicate flow of information and solid arrows depict the control inputs.	23
2.12	Voltage and current Inner loops of a power converter	24
2.13	The droop controller linearly adjusts the output voltage according to the measured feedback value.	25
2.14	The three strategies for the design of secondary Microgrid control. Three different cases of isolated Microgrids are illustrated with a circular topology. Dashed lines depict an exchange of information, while the solid lines are the transmission lines of the network.	30
3.1	Generic meshed Microgrid consisting of DER units and local loads.	43

3.2	Simplified node circuit of a power converter connected to a local load an the common DC bus. The input takes the form of a controlled current source.	43
3.3	Coupled constraint and reachability sets for a two-node system.The product of the resulting two reachability sets is always within the constraint set.	60
3.4	A MG network with nine converters and seven local loads	61
3.5	Converter voltage trajectories of Node 1 (—), Node 2 (—), Node 3 (—), Node 4 (—), Node 5 (—), Node 6 (—), Node 7 (—), Node 8 (—), Node 9 (—), and setpoints (· · ·) of all converter subsystems with the use of the proposed control scheme.	63
3.6	Power supply to CPL_1 (—), CPL_2 (—), CPL_3 (—), CPL_4 (—), CPL_5 (—), CPL_6 (—), CPL_7 (—), CPL_8 (—), CPL_9 (—) and respective power demands (· · ·)	63
3.7	Line power trajectories and the respective boundaries for $Line_{12}$ (—), $Line_{23}$ (—), $Line_{34}$ (—), $Line_{41}$ (—), $Line_{35}$ (—), $Line_{56}$ (—), $Line_{47}$ (—), $Line_{68}$ (—), $Line_{89}$ (—).	64
3.8	Trajectory evolution of node 1 and node 2 voltages within the coupled constraint set.	64
4.1	Network topology of a meshed islanded DC MicroGrid.	67
4.2	Node circuit modelled as a DC/DC Buck converter connected in parallel to a local constant power load.	67
4.3	Vector field and positive invariant set N for a two node system.	76
4.4	Network topology of a meshed islanded MicroGrid.	83
4.5	Voltage and nominal voltage trajectories for Node 1(—, · · · · ·), Node 2(—, · · · · ·), Node 3(—, · · · · ·), Node 4(—, · · · · ·), Node 5(—, · · · · ·), Node 6(—, · · · · ·) and Node 7(—, · · · · ·) respectively. The constrained region is represented with black solid lines (—) and the voltage references by black dashed lines (---). The voltage trajectories are within the respective \mathcal{S}_i (□) at all times.	84
4.6	Converter Current trajectories for Node 1(—), Node 3(—) and Node 7(—) respectively.The constrained region \mathbb{C} is represented by black solid lines (—) and the current references \hat{i}_i by black dashed lines (---).	85
4.7	Load fluctuations around the nominal value \bar{P} for Node 1. A similar load profile is shared among the rest of the Nodes.	85
5.1	Meshed MG with seven nodes locally connected to a CPL.	99

5.2	State space of Node 1. The constraint set $\mathbb{Y} = \mathbb{X} \times \mathbb{C}$ is depicted as  and the tube cross-sections with  . The nominal voltage defining the centre of the tube is depicted with (---) and the uncertain trajectory with (—).	101
5.3	Cross-sections of the tube at time $t = 0s$ depicted with  and at time $t = 15s$ depicted as  . It can be seen that the closer the nominal voltage is to the lower bound of the constraint set the larger is the tube size.	102
5.4	Comparison between the rigid-tube (—) approach presented in Chapter 4 and the dynamic tube (—) of this chapter. The rigid tube activates the constraint set and results in larger convergence time. .	102
5.5	Node uncertain and nominal voltages of Node 1 (—,⋯⋯), Node 2 (—,⋯⋯), Node 3 (—,⋯⋯), Node 4 (—,⋯⋯), Node 5 (—,⋯⋯), Node 6 (—,⋯⋯), and Node 7 (—,⋯⋯). The black solid lines represent the upper and lower bound respectively of the nodal constraint set.	103
5.6	Current trajectories and references provided by the voltage layer. .	103
6.1	Example of the geometric effect of the CPL on the velocity of the energy-like function. (Left) The surface where $h_i(e_{d,i}, e_{q,i}, \delta P_i, \delta Q_i)$ is mapped to non-negative values. (Right) The projection of the surface on the state space (<i>red</i>) and the boundary of $\mathcal{N}_i(z_{d,i})$ (<i>black</i>). It can be seen from this figure that the control design and analysis in this case is indeed not as straightforward as in the DC scenario. The coupling between the d and q components leads to an invariant set that is not just a Cartesian product of the invariant sets depicted in the previous chapters.	112
6.2	Voltage trajectories for nodes \mathcal{V}_1 (—), \mathcal{V}_2 (—), \mathcal{V}_3 (—), \mathcal{V}_4 (—) and respective nominal trajectories (---). It is seen that the RMS voltage of each node is kept close to the rated value despite the constant perturbations of the load demand.	118
6.3	Input current trajectories for nodes \mathcal{V}_1 and \mathcal{V}_3	118

List of Tables

3.1	Network component and control parameter values.	62
4.1	Network component and control parameter values.	84

Chapter 1

Introduction

This chapter will present the main motivation behind this thesis. The first section presents the general topic and defines the necessary concepts that will be encountered throughout the thesis. While a detailed presentation of the relative literature will be provided in the next chapter, a concise summary of the findings will also be given here in order to clearly define the aims and objectives of this study. An outline of the thesis structure and a list of contributions will also be provided in this chapter.

1.1 Motivation

During the past decade, the world has experienced unprecedented climate changes. The frequency and intensity of extreme weather phenomena has increased, causing catastrophic damages to infrastructure and having a high socioeconomic impact on the local communities [1, 2]. The global energy-production industry has been identified as one of the main contributors of the climate change, where the majority of the current energy production is done by burning fossil fuels. This has resulted in the release of greenhouse gases, which trap heat in the atmosphere and cause a greenhouse effect. In order to address this problem, many governments are beginning to pass legislation that favours the development and adoption of “greener” energy production resources. In particular, under the revised European Climate Law, the member states of the European Union are required to reduce the greenhouse gas emissions by 55% by 2030 and achieve net zero of emissions by 2050.

The effort to reduce greenhouse gas emissions has highlighted the need of a paradigm shift in the structure of the traditional energy distribution network, also known as power grid. In the conventional power production architecture, the power flow is unidirectional, where the power is produced by large power plants and electrically transmitted to distribution centres by long transmission lines. From there,

the power is supplied directly to the consumers via the distribution network. Many techniques have been developed to make the overall process more efficient and reliable. Despite of this, in its current setup, there are still many drawbacks that are fundamentally difficult to overcome. At its core, the power production process is done by burning coal, natural gas and oil, which results in a substantially large carbon footprint. In addition, the power losses at the transmission lines and the distribution network are far from negligible. Taking Greece as an example, the annual power losses from the electric power transmission accounts for about 8% of the total power production output, which is translated in approximately 5 TWh within an annual period. A large penetration of distributed generation (DG) units could potentially result in a substantial reduction of these losses. Assuming a 30% distribution of the load to close proximity renewable energy resources, then up to 1.2 TWh can be saved, while the carbon footprint of the energy production process is minimised. Nevertheless, due to their high reliance to environmental conditions, the integration of a large number of DG units directly in the power grid displays significant challenges. Most notably, their intermittent behaviour could amplify the already challenging task of providing an uninterrupted power supply to the consumers. Therefore, the traditional concept of the power grid needs to be restructured in a way such that it is able to accommodate this change.

The concept of “smart grid” has emerged as a potential solution, where the conventionally centralised structured of the power grid is transformed in a decentralised network [3], [4]. Each cluster of the network, known as a “Microgrid”, represents a collection of consumer loads, energy storage devices, and DG units such as wind turbines, photovoltaic panels etc. This structure enables the direct supply of energy to the consumers by geographically-adjacent DG units, decreasing the need of long transmission lines to only instances where the load demand exceeds the local DGs capabilities. This can potentially reduce the power losses, improve the power quality and facilitate the distribution of energy in remote and distant areas. Furthermore, in cases where the local power demand is met, the Microgrid can either inject the excess power to the network or locally store it to cover future load requirements. Therefore, the power flow of the overall network becomes bidirectional, creating an extra degree of flexibility in its operation. However, the most significant advantage of the Microgrid is the ability to separate itself from the main grid and operate in an isolated mode, known as “islanded”. This setting is autonomously enabled either in the cases where the provided power quality from the grid is inadequate to meet the consumer desired standards or during abnormal conditions such as faults or voltage collapse. As a result, the ability to dynamically isolate the Microgrids from the network enhances the system reliability and robustness, while also eliminates

the susceptibility to single points of failure, which is a well-known disadvantage of a centralised structure.

One of the core components within a Microgrid architecture is the power converter. These devices are used to interface each DG unit with the rest of the network and regulate the output voltage by sending a pulse-width-modulation signal to the converter's switching device. This improves the flexibility of the system and enables sophisticated network operations such as: (a) accurate load sharing, (b) improving the quality of the provided power or (c) economic operation through power and energy management. Nevertheless, due to the continuing evolution in the complexity of the consumer load requirements, as well as the inherent fundamental properties of the energy distribution network, the design of a control scheme to achieve the desired operation is not straightforward. A major challenge is presented when the loads in the network adopt a nonlinear structure. This type of load is commonly referred to as a "ZIP" load, stemming from the combination of a constant impedance load "Z", a constant current load "I" and a constant power load "P". The latter part is shown to be the most challenging, due to its nonlinear characteristics. Designing a control scheme for a network with constant power loads is a challenging task, as these exhibit negative impedance characteristics and tend to destabilize the system. The majority of the works in the literature address this problem by either employing local approximation of the dynamics, assuming that the load itself provides sufficient positive damping to counteract the effect, or are limited in numerically validating the stability of a system under a proposed control law. Therefore, despite the high interest this problem has attracted, the behaviour of a network in the presence of "ZIP" loads, as well as providing sufficient stability guarantees that can be generalised for any case study, are still open problems in the literature.

Even though Microgrids are clusters of the overall network, in many cases are still considered a geographically large-scale system. Therefore, the physical distance between each unit is not negligible and has to be considered in the control development process. Any information exchange infrastructure in place has to operate in a sufficiently low bandwidth, such that it accounts for possible delays due to the need for the information to travel over large geographical distances. As a result, the number of feasible applications of a centralised structure, where each unit has to communicate with a central unit and receive a centrally computed control input, is severely limited. In addition, as it will be analytically shown in the following chapters, there exist a strong coupling among the local node dynamics of the network. This implies that the operation of each local unit is heavily affected by the neighbouring units and errors in the transmitted information have a high effect on

the overall system regulation. Ultimately, even though the exchange of information presents difficult practical challenges, the presence of a communication link is still desired to achieve tight regulation and reduce errors.

As evidenced by the above, along with a plethora of distinct advantages, Microgrids also introduce many new challenges. The various DG units are interfaced to the network by power converters, which, contrary to the traditional synchronous machines, are low-inertia units. As a result, the effect of external disturbances to the network is more predominant, which can potentially lead to voltage/frequency fluctuations and destabilize the overall system. Especially in the case of islanded Microgrids, high voltage fluctuations can damage the interfacing power converters and reduce the Microgrid ability to provide an uninterrupted power supply to the loads. Therefore, the design of a control scheme for the regulation of Microgrid systems is far from trivial and requires a careful theoretical analysis in order to reduce the potential risk of faults and guarantee that the system achieves the desired behaviour. In the following we outline the main challenges and open questions in the literature of Microgrid control.

- Design of a model-based control framework to regulate both the converter current and voltages to desired values and ensure overcurrent and overvoltage protection of the interfacing power converters.
- A major challenge is the design of a distributed control scheme; the DG units need to exchange minimum amount of information in order to satisfy the small time-scale of the dynamics, while ensuring that the thermal capacities of the connection lines are not exceeded.
- Incorporate additional objectives in the control design process to improve the overall Microgrid performance; These may include achieving economic operation by minimising generation costs and minimising unnecessary power losses, avoiding unnecessary circulating currents and sharing the power demand proportionally to each unit according to the individual power rating.
- Analytically guarantee the system stability, even in the presence of destabilising time-varying components.

The following sections will present the aims and objectives of this thesis, followed by an overview of the thesis structure and a list of its contributions.

1.2 Aims and Objectives

The aim of this thesis is to address these outstanding challenges by developing new theory and control algorithms for isolated Microgrids with nonlinear dynamics. A key feature of the proposed algorithms is strong control theoretic properties and guarantees, including asymptotic stability of the system equilibria, enforced constraint satisfaction and system robustness to uncertain external inputs. This way, the results of this thesis can be generalized beyond a single case-study or a particular network topology. More specifically, the main aims and objectives are formulated as:

1. Analytically investigate the induced nonlinear behaviour of the constant power loads and use this information to develop a control theoretic framework that guarantees the desired behaviour
2. Design a unified, *i.e.* for both inner current and output voltage converter states, model-based control framework for the regulation of isolated Microgrids that:
 - Achieves tight regulation of both the output voltage and inner current of the converters to desired values
 - Allows distributed operation with only neighbour-to-neighbour communication and locally available information
 - Guarantees boundedness of the converter states in a desired set in the presence of both linear and nonlinear loads, even during the transient phase
 - Guarantees boundedness of the transmission line currents in a desired set with minimum communication among the DG units
3. Provide analytic stability guarantees that are not affected by linearisation errors and can be generalised beyond a specific operating point
4. Numerically validate the theoretic results

1.3 Publications List

1.3.1 Published

1. Michos, G., Konstantopoulos, G.C., Trodden, P.A. and Kadiramanathan, V., Control of Isolated AC Microgrids with Constant Power Loads: A Set

- Invariance Approach. In 2022 30th Mediterranean Conference on Control and Automation (MED) (Accepted)
2. Michos, G., Baldivieso-Monasterios, P.R., Konstantopoulos, G.C. and Trodden, P.A., 2023. Robust Two-Layer Control of DC Microgrids with Fluctuating Constant Power Load Demand. *IEEE Transactions on Control of Network Systems*.
 3. Michos, G., Baldivieso-Monasterios, P.R. and Konstantopoulos, G.C., 2022. Distributed economic nonlinear MPC for DC Micro-Grids with inherent bounded dynamics and coupled constraints. *Systems & Control Letters*, 167, p.105327.
 4. Michos, G., Baldivieso-Monasterios, P.R. and Konstantopoulos, G.C., 2022, June. Robust Distributed Control for DC Microgrids with System Constraints. In 2022 30th Mediterranean Conference on Control and Automation (MED) (pp. 1036-1041). IEEE.
 5. Michos, G., Baldivieso-Monasterios, P.R. and Konstantopoulos, G.C., 2021, October. Nonlinear primary and supervisory control of dc microgrids for distributed optimal operation with neighbour-to-neighbour communication. In 2021 25th International Conference on System Theory, Control and Computing (ICSTCC) (pp. 302-307). IEEE.

1.3.2 In preparation

Michos, G., Baldivieso-Monasterios, P.R., Konstantopoulos, G.C. and Trodden, P.A., Dynamic Tube-Based Control for DC Microgrids, (In preparation)

1.4 Thesis Outline

The remainder of this thesis is organised as followed. Chapter 2 presents an overview of the mathematical modelling of the various types of converters that are considered in this study. In addition, a mathematical model for each case of DC load is included, accompanied by a discussion on their effect on the network and the challenges these introduce in the control design process. The remaining of this chapter presents a thorough literature review of the control strategies that have been proposed for the regulation of DC Microgrids. This is split in two major parts; the first part introduces the hierarchical control architecture of the Microgrid regulation and provides a range of studies for each hierarchical level and the respective subcategories. Then, in order to reflect the aims and objectives of this thesis, the second

part pays particular attention to the regulation of Microgrids under the effect of nonlinear loads. This is followed by a literature review on the studies that achieve some form of constrained-based operation, e.g. overcurrent or overvoltage protection of the equipment. Studies are also included from the control theory literature to highlight the challenges and gaps this thesis attempts to address in both fields.

Each of the following chapters is associated with a different study from the list of publications. More specifically, Chapter 3 is associated with the fifth and third published study, Chapter 4 with the fourth and second, Chapter 6 with the first, while Chapter 5 is a work under preparation for submission.

Chapter 3 proposes a distributed control scheme for isolated DC Microgrids that achieves both local and coupled constraint satisfaction in the form of upper bounds on the line currents between nodes. This study considers meshed network topology with local constant power loads, neighbour-to-neighbour communication and local optimisation objectives. This way, the results are scalable to networks with arbitrarily large number of nodes. The problem is viewed from the conventional approach of considering the external inputs, *i.e.* the interaction term and the load demand, as disturbances to the local dynamics. An extensive theoretic analysis is provided to derive sufficient conditions such that all the control objectives are guaranteed and show that the equilibrium points within the desired constraint set are asymptotically stable. An effort is made to reduce the complexity one may face in the implementation of the proposed method by removing the need to compute terminal sets and by providing conditions for the tuning variables that require only the knowledge of locally available information. Simulation results are also provided to demonstrate the performance of the proposed method.

Chapter 4 builds upon the results of Chapter 3 to propose a unified control scheme. Contrary to the previous chapter, this work also considers the converter current dynamics and incorporates desired input current operation limits in the control design process. Furthermore, a detailed analysis is included, studying the effect of the nonlinear load from a geometric perspective, and utilises this information to design a control law that guarantees boundedness of the voltage trajectory in a desired set. This property is used to remove the load term from the bound on the rate of change of the disturbance, introduced in Chapter 3, thus simplifying the implementation and reducing the conservativeness that may arise from the previous approach. The proposed method generates a reference voltage trajectory and is analytically guaranteed that the distance of the true voltage trajectory from the reference is bounded at all times. A centralised control scheme is designed for the regulation of the nominal dynamics to desired reference points. However, it is explained that by adopting a method similar to Chapter 3, one may also achieve a

distributed operation. Furthermore, it is shown that the solution of the inner converter current dynamics is always bounded. Finally, an analytic proof is provided to show that the cascaded system admits asymptotically stable equilibrium points by the use of Control Lyapunov Functions and tools from the theory of interconnected systems. Simulation results are provided to support the theoretic findings.

Chapter 5 aims to extend the results of the previous chapters and provide a thorough analysis on the interaction between the nonlinear load and the proposed control law. It is shown that it is possible to reduce the conservativeness of the sufficient conditions that were formulated in the previous chapter and construct a time-varying bound on the voltage that depends on its position in the state space. Similarly, for simplicity a centralised control law is developed for the nominal dynamics which can be translated to a distributed control by following the process outlined in Chapter 3. It is ultimately shown that similar guarantees can be achieved, while increasing the size of the set of available control actions. The results are accompanied by theoretic guarantees regarding the recursive feasibility of the control law and asymptotic stability of the closed-loop system. The introduced time-varying concept of the bound between the reference and the true voltage trajectories, as well as the Microgrid operation under the proposed control law, is illustrated in a simulated scenario.

Chapter 6 studies the case of an isolated, meshed, AC Microgrid with local constant power loads. The model of the system is expressed in the dq -frame that will be presented in Chapter 2. The primary aim of this chapter is to investigate the behaviour of the closed loop system under the effect of the nonlinear load and propose a control law that achieves similar results with the DC scenario. It is shown that the proposed control law can indeed bound the trajectory of the voltage d and q components in a two dimensional subspace of the state space. An analytic characterisation of this subspace is provided by studying the geometric behaviour of each component and it is shown that this characterisation can be approximated by a convex set in order to allow the formulation of an optimisation-based approach. The properties of the proposed control scheme are demonstrated in a simulated scenario, where it is shown that the voltage root-mean-square value of each node in the network is bounded around a generated reference trajectory.

Finally, Chapter 7 provides a brief summary of the thesis and draws conclusions on the results. In addition, a few ideas are included that can be used in future directions of this work.

Chapter 2

Literature review

This chapter presents a detailed review of the literature regarding Microgrid control. At first, an overview of the Microgrid structure will be provided in order to identify the key components and shed light into the operational principles. Then, the main control challenges and objectives will be formulated. A significant portion of this chapter will be dedicated in outlining both the conventional and the current state-of-the-art control approaches. Particular emphasis will be given in the provided theoretical guarantees, in an effort to identify the gaps in the literature and give an insight in the practical limitations of the suggested methods.

2.1 The Microgrid Architecture

There are numerous definitions of a Microgrid in the literature, see for example [5] or [6]. The consensus is that at its essence, a Microgrid is defined as a local energy distribution system that serves a distinct geographical area. Examples of this are an isolated community, a small suburban city or specific facilities such as a sports stadium, a hospital complex or aviation and maritime vehicles. As the name suggests, a Microgrid is a scaled version of a grid that interconnects various distributed generation units with loads, consumers and, as it is often the case, energy storage devices such as batteries or supercapacitors. The key characteristic of the Microgrid is the ability to be self-sustained, meaning that it is not reliant on the main grid to satisfy the local energy requirements. As it was also discussed in the previous chapter, this “local” characteristic is the reason why this is such an attractive solution, since it substantially improves the efficiency of the electricity transportation of the overall network.

The capability to operate independently from the main grid improves the overall network’s susceptibility to faults during abnormal operation such as storms or other events that can cause an outage of the power grid. This is particularly important

in complex and large networks such as in the US or China. In 2003, the US experienced the second worst worldwide power outage in history, an event known as the “Northeast Blackout”. A series of faults occurred when a tree branch fell on a power line in the state of Ohio, causing the majority of the Northeast states to lose power supply for several hours. Events such as this, highlight the need for the network to isolate itself from faults and provide an uninterrupted power supply and distribution.

The third and, arguably, most important characteristic is that more sophisticated and intelligent operations can be achieved due to the Microgrid’s scaled size. While many different approaches have been suggested for achieving this, in its most basic form a central controller for the entire Microgrid is used to regulate the power flow between the DG units and the loads. More specifically, some of the Microgrid control objectives are [7]:

- Constrained-based regulation of the network voltage and current; In case of an AC Microgrid, regulation of the frequency is also a common requirement.
- Proportional load sharing among the DG units.
- Smooth transition from islanded to grid-connected mode and vice versa.
- Reducing the running costs and achieving economic operation by solving an optimisation problem.
- Regulation of the power flow between the Microgrid and the main grid during grid-connected mode.

Developing a unified control framework to achieve all, or even some, of the above objectives is not a trivial task. Therefore, numerous studies have been devoted to address some of the current issues, with the number rising as more diverse and complex Microgrid architectures are becoming feasible.

2.2 Microgrid Types

This section will discuss the three different types of Microgrids that are commonly encountered in the literature; the AC, DC and Hybrid Microgrid.

AC Microgrid

The first type that will be discussed is the AC Microgrid. A typical AC Microgrid is depicted in Fig. 2.1. This type usually consists of one or more AC buses, thus requiring a conversion to an AC power output in order to connect a unit to the

2.2. MICROGRID TYPES

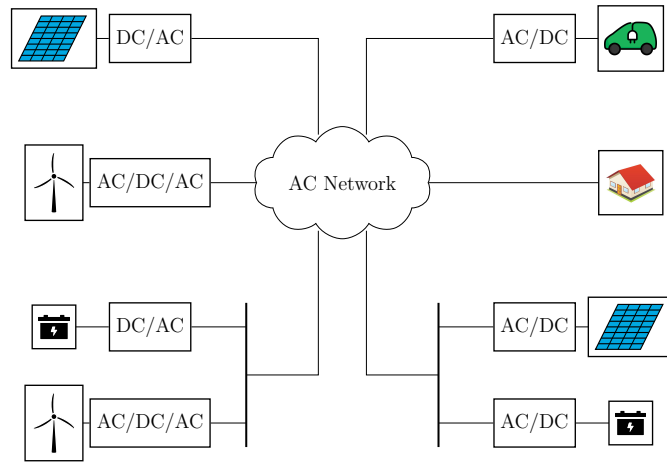


Figure 2.1: An AC Microgrid consisting of several renewable resource units and consumers.

to the main or local bus. In addition, there exists a static switch that allows the network operator to connect or disconnect the Microgrid from the main utility grid. This connection point is commonly referred to as the point of common coupling (PCC). There are two main modes of operation that each require a different type of control: grid-connected and islanded.

In grid-connected mode, only a current controller needs to be employed, since the voltage and the frequency are usually determined by the main grid. The main control objective in this mode is to maximise the power supply of the local loads from local DG units and minimise the Microgrid dependence from the main grid, [8]. To achieve this, the network operator usually determines pre-specified real and reactive power values that each DG unit needs to supply. In the case that the local power supply is not sufficient to meet the local power demand, then the main utility grid is required to satisfy the remaining power requirements [9]. In islanded or autonomous mode, the local energy demand must be less or equal to the power supply of the DG units in the Microgrid. Furthermore, the DG units need to proportionally share the load according to the power rating, while the voltage and the frequency of each unit need to be controlled independently [10].

DC Microgrid

A representation of a DC Microgrid is given in Fig. 2.2, where every unit is connected to a local or main DC bus. DC Microgrids have gathered a substantial interest over the past few years due to their high reliability and efficiency compared to their AC counterparts. The increasing penetration of renewable sources of DC nature have made the DC Microgrid an attractive choice due to the need for fewer

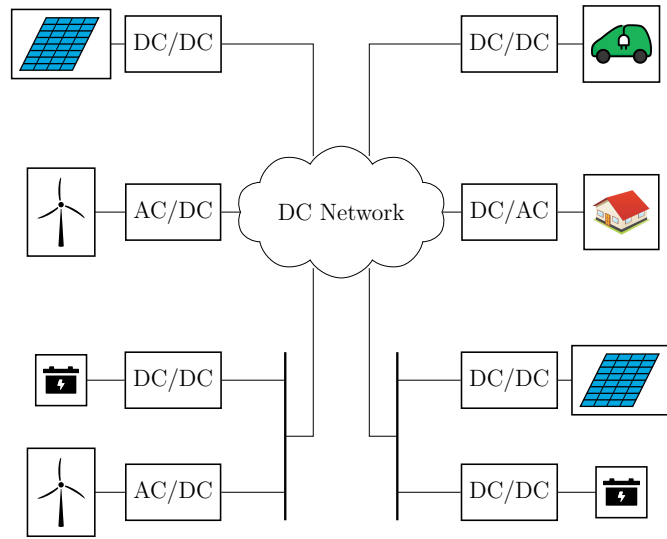


Figure 2.2: A DC Microgrid consisting of several renewable resource units and consumers. Each unit is interfaced with the network via a power converter.

points of AC/DC and DC/AC conversions [11]. This reduces the potential points of failure and avoids instability issues during abnormal conditions. Furthermore, the conversion power losses are mitigated, increasing the overall efficiency of the network. Another advantage of the DC Microgrid is that the the control design process is substantially simplified, since the issues of power quality, as well as reactive power and frequency regulation, are no longer present [12, 13]. Applications of DC Microgrid include electric ships [14, 15], High-Voltage-Direct-Current (HVDC) networks [16], railworks [17, 18, 19] and data centres [20, 21], to name a few.

Hybrid Microgrid

The previous sections highlighted the distinct advantages of a DC Microgrid. Nevertheless, the majority of the distribution network is of AC nature and a transition to a entirely-DC network is immensely costly and may take decades. Therefore, the concept of the hybrid Microgrid was conceptualised, which combines both architectures as subgrids tied under a single hybrid network. The interface of the two subgrids is made via a bidirectional interlinking converter, that regulates the power flow between the two sides and aims to stabilize the network and achieve power balance [22]. Hybrid Microgrids are a relatively new concept that has attracted the interest of many researchers, e.g. [23, 24, 25]. One of the challenges of regulating a hybrid Microgrid is the requirement to interface and manage the fast-response nature of the DC Microgrids with the slower AC. This is not a trivial problem and has been shown to be destabilizing in [26, 27]. A Hybrid Microgrid is depicted in Fig. 2.3.

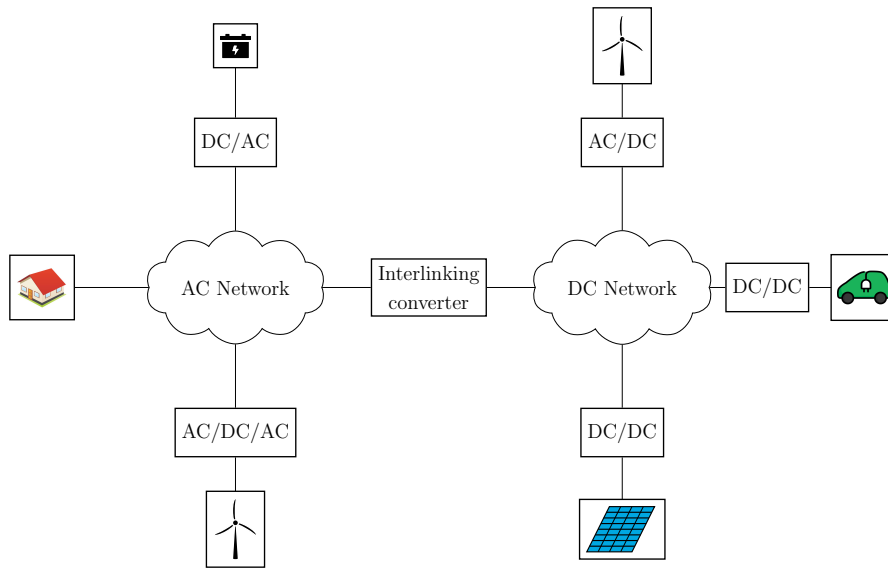


Figure 2.3: A Hybrid Microgrid consisting of an AC and a DC subgrid interfaced by an interlinking converter.

In order to clearly present the current state-of-the-art regarding Microgrid regulation and define the areas for further improvement, the remaining part of this chapter will provide an outline of the mathematical modelling of each Microgrid component. To this aim, two main categories can be distinguished; the power generation units and the power consumption elements. The former are interfaced with the network through power converters, which are responsible for the regulation of the output voltage and power. The next section will introduce the predominant variations of the power converter structure in both the DC and the AC case. It is noted that particular emphasis will be given in the modelling and the dynamic characteristics of each type, since each case requires a different approach during the control design process. Then, Section 2.4 will present the different type of loads and discuss the respective stability implications on the overall network in each case.

2.3 Power Converters

It has already been discussed that the main function of the power converters is to interface the power generation units with the Microgrid network. The necessity for such devices stems from the fact that, contrary to the conventional synchronous generators, the renewable energy resource units are electromechanical systems that generate a variable voltage/electricity/frequency. Therefore, a power converter is required in order to facilitate the interface with an utility grid that has a constant voltage/electricity/frequency. In the control literature, both the power generation

units and the utility grid are considered a subsystem of the overall network. Thus, a common categorization of the power converters is based on the type of systems that they interface. That is, the following types exist:

- DC/DC converters that interface two DC subsystems.
- AC/AC converters that interface two AC subsystems
- DC/AC and AC/DC converters that facilitate the interface of an AC with a DC subsystem or a DC with an AC subsystem respectively.

Furthermore, there exist two more characterisations for the AC/DC or DC/AC converter. Specifically, if the power flows from the AC side to the DC side, then the converter is called a rectifier, whereas in the case that the power flows from the DC side to the AC side then it is called an inverter. It is noted that the latter is the most common scenario one encounters in Microgrids. The reasoning for this is that most of the renewable resource units are of a DC nature, while electricity distribution via an AC network still remains a widely adopted practice.

The main building block of a power converter is the switching device. In order to control the converter output voltage and power, a PWM signal is supplied to the switch, which takes either an switched-on or switched-off position. That is, when the switch position is described by a switching function, this takes values in the discrete set $\{0, 1\}$. Then, one may derive a *switched model* of the power converter by a direct application of the Kirchhoff voltage and current laws. However, as it was also highlighted in [28], this model has a high degree of complexity and is not particularly useful for the control design process and the analysis of the converter dynamical behaviour. Therefore, it is common in the literature to adopt an *average model* instead, where the average value of the switch position is considered in the model dynamics, *i.e.* the switching function now takes values in the closed continuous set $[0, 1]$. Therefore, throughout this thesis the average model will be used to describe the converter dynamics.

There is a plethora of textbooks in the literature that present the modelling procedure of the power converter dynamics. In particular, both Yazdani et al. [28] and Hornik et al. [29] demonstrate the derivation of the switched model for various types of power converters. In addition, the average model is provided in Middlebrook et al. [30], while a passivity-based approach can be found in the book of Ortega et al. [31].

The majority of this thesis is devoted in the theoretical analysis of DC Microgrids, while the last chapter also includes some results in the AC scenario, where the DC/AC power converter is adopted. For this reason, the following sections will present the three predominant types of DC/DC conversion, namely the Buck,

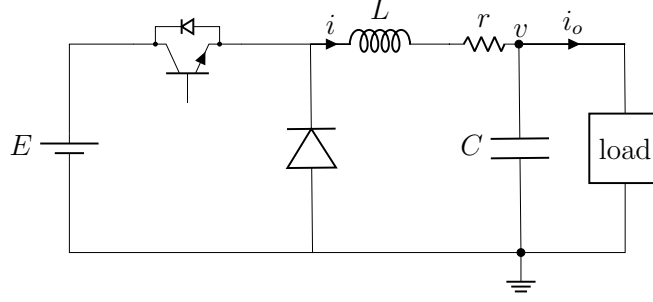


Figure 2.4: Circuit diagram of a buck converter connected in parallel to a local load.

Boost and Buck-Boost converters. Then, the DC/AC inverter will be briefly presented with emphasis given in the modelling of this type of systems. For additional results on the AC conversion, the interested reader is referred to the aforementioned textbooks, as well as to Bose et al. [32] and Erickson et al. [33].

2.3.1 Buck Converters

The buck converter, also referred to as the step-down converter, is used when the desired output voltage needs to be lower than the input voltage, *i.e.* the voltage of the DG unit. A circuit diagram of a buck converter is given in Fig. 2.4, which consists of the DC input voltage source, a switching element, a diode, an inductor L connected in series with a parasitic resistance r , and an output capacitor C . It is noted that the inductor and the capacitor act as a filter that improve the quality of the current drawn by the load and the output voltage of the converter. In order to derive the model of the power converter, the Kirchhoff laws are applied to the circuit, yielding the following linear differential equation

$$L \frac{di}{dt} = uE - v - ri, \quad (2.1)$$

$$C \frac{dv}{dt} = i - i_o, \quad (2.2)$$

where i denotes the inner converter current flowing through the inductor, E and v are the input and output voltages respectively, i_o is the output current drawn by the load and $u \in [0, 1]$ is the duty-ratio of the switching element. It is noted that the duty ratio can take any value in the continuous interval $[0, 1]$, hence the above is an *average model* of the buck converter dynamics. It can be seen that the buck converter is a linear model, where the duty ratio is multiplied by the input voltage. The latter is usually assumed a constant value, where the intermittent nature of the renewable resource units is mitigated by storage elements, *e.g.* batteries. Furthermore, the duty ratio variable is only present in current model, which

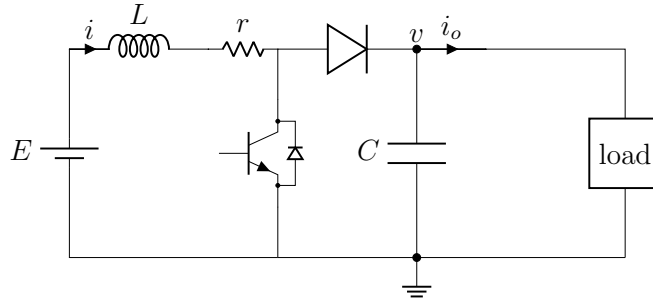


Figure 2.5: Circuit diagram of a boost converter connected in parallel to a local load.

in turn is considered an input to the voltage dynamics. Hence, the control design procedure can be simplified by a time-scale separation analysis, without adopting overly conservative assumptions.

2.3.2 Boost Converters

The boost converter, also known as a step-up converter, is employed when the utility grid operates in a higher voltage than the output of the DG unit. Therefore, in this case, the output voltage of the converter v is always higher than the input voltage E . The circuit diagram of a typical boost converter is depicted in Fig. 2.5. Similar to the case of buck converter, the boost converter consists of an inductor L connected in series with a parasitic resistance r , an output capacitor C , a diode, a switching element with duty ratio $u \in [0, 1]$ and an input voltage E . A direct application of the Kirchhoff laws yields the boost converter dynamics

$$L \frac{di}{dt} = -(1 - u)v + E - ri, \quad (2.3)$$

$$C \frac{dv}{dt} = (1 - u)i - i_o, \quad (2.4)$$

Contrary to the previous case of the buck converter, the boost converter model is nonlinear. In both the current and the voltage models, the control input u is multiplied by a state, which does not allow the direct decoupling of the dynamics by including a feedforward term in the control law parametrisation.

2.3.3 Buck-Boost Converters

The Buck-Boost converter allows for an output voltage that can be greater than or less than the input voltage from the DG unit. The respective circuit diagram is given in Fig. 2.6, where it can be seen that the converter is comprised of similar components with the previous two cases. However, it is noted that the output

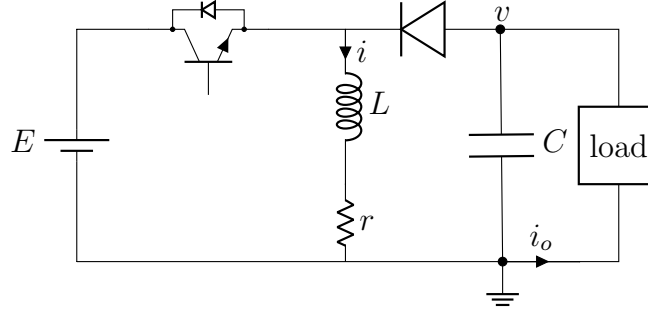


Figure 2.6: Circuit diagram of a buck-boost converter connected in parallel to a local load.

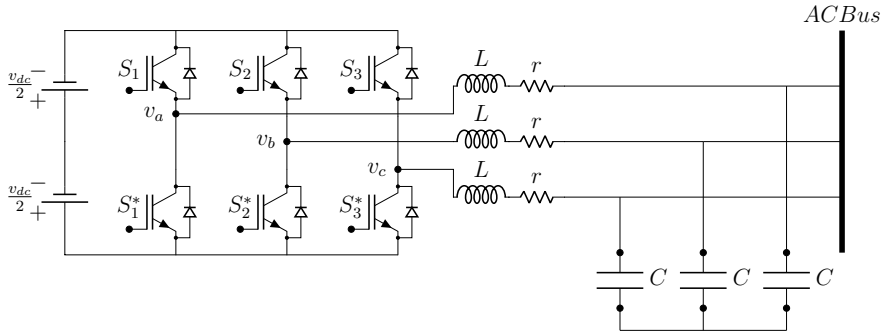


Figure 2.7: Circuit diagram of an DC/AC inverter connected an AC bus.

voltage is reversed in polarity to the input. An application of the Kirchhoff laws in this case result in the average model

$$L \frac{di}{dt} = -ri - (1 - u)v + uE, \quad (2.5)$$

$$C \frac{dv}{dt} = (1 - u)i - i_o. \quad (2.6)$$

Given a constant duty-ratio $u = \bar{u}$, it can be seen that the resulting voltage equilibrium point is given by the relation

$$\bar{v} = \left(\frac{\bar{u}}{1 - \bar{u}} \right) E - \frac{r}{\bar{u}} \bar{i}. \quad (2.7)$$

Therefore, for $\bar{u} > 0.5$ the converter operates in the boost mode and for $\bar{u} \leq 0.5$ in the buck mode.

2.3.4 Three-phase Inverter

In order to interface a DC source to an AC utility grid, a three-phase inverter is required. A schematic of the three-phase inverter is provided in Fig. 2.7. Due to its more complicated configuration, the mathematical modelling and subsequent control design process display a higher degree of complexity, compared with the

2.3. THREE-PHASE INVERTER

DC/DC converters. Initially, the output voltages of the three phase inverter in the natural abc framework can be represented as

$$\begin{bmatrix} v_a \\ v_b \\ v_c \end{bmatrix} = \begin{bmatrix} v_m \cos(\theta) \\ v_m \cos(\theta - 2\frac{\pi}{3}) \\ v_m \cos(\theta + 2\frac{\pi}{3}) \end{bmatrix} \quad (2.8)$$

However, the above representation of the inverter voltages yield a complicated dynamical model, making the controller design procedure an arduous task. Therefore, the Clarke-Park transformation is often adopted to simplify the subsequent inverter model. First, following [34], the Clarke transformation [29] maps the abc state vector to a stationary reference frame $\alpha\beta$ by the transformation,

$$\begin{bmatrix} v_\alpha \\ v_\beta \end{bmatrix} = T_{\alpha\beta} \begin{bmatrix} v_a \\ v_b \\ v_c \end{bmatrix}, \quad (2.9)$$

where the transformation matrix $T_{\alpha\beta}$ is given by

$$T_{\alpha\beta} = \frac{2}{3} \begin{bmatrix} 1 & -\frac{1}{2} & -\frac{1}{2} \\ 0 & \frac{\sqrt{3}}{2} & -\frac{\sqrt{3}}{2} \end{bmatrix}. \quad (2.10)$$

Then, in order for the voltages to be considered stationary, and thus to no longer be perceived as functions of time, the $\alpha\beta$ -frame is transformed to a synchronously rotating reference frame, known in the technical literature as the dq -frame [35]. This is achieved by the dq -transformation from [32] as

$$\begin{bmatrix} v_d \\ v_q \end{bmatrix} = T_{dq} \begin{bmatrix} v_\alpha \\ v_\beta \end{bmatrix}, \quad (2.11)$$

where the transformation matrix T_{dq} is given by

$$T_{dq} = \begin{bmatrix} \cos(\theta_g) & \sin(\theta_g) \\ -\sin(\theta_g) & \cos(\theta_g) \end{bmatrix}, \quad (2.12)$$

with θ_g the angle between the two reference frames. Then, assuming a common constant rotating frequency ω_c , the mathematical model of an inverter connected an AC bus is given by

$$L \frac{di_d}{dt} = -ri_d + \omega_c Li_q + \bar{v}_d - v_d \quad (2.13)$$

$$L \frac{di_q}{dt} = -ri_q - \omega_c Li_d + \bar{v}_q - v_q \quad (2.14)$$

$$C \frac{dv_d}{dt} = i_d - i_{o,d} + \omega_c C v_q \quad (2.15)$$

$$C \frac{v_q}{dt} = i_q - i_{o,q} + \omega_c C v_d \quad (2.16)$$

where C and L are respectively the capacitance and inductance of the output filter, r is a parasitic resistance, i_o is the output current, \bar{v} is the input of the system, while (v_d, i_d) and (v_q, i_q) are the d and q components of the output voltage and inductor current. Depending on the configuration, the above model can be connected to a grid via a switch or locally connected to a load. The usefulness of this transformation is that the equations describing the system dynamics are similar to the DC case. Therefore, one does not need to deal with sinusoidal signals during the control design process. The following sections, will discuss the modelling and inclusion of loads in the network.

2.4 Loads

The loads of the network represent the units that consume power. A common representation of the loads is the “ZIP” model, which combines a constant impedance “Z”, a constant current “I”, and a constant power “P” component [36]. This model is commonly given by the linear relation describing the output current drawn by the load as

$$i_{\text{ZIP}} = i_Z + i_I + i_P \quad (2.17)$$

In the following, each of these components will be presented as a separate case in order to discuss the type of behaviour they introduce to the system. In the following discussion, each load will be considered to be connected in parallel to the output capacitor of the power converter.

2.4.1 Constant Impedance Loads

This type of load requires a constant impedance component, *i.e.* in the relation expressing the current drawn by the load

$$i_o = \frac{v_l}{R_l} \quad (2.18)$$

it holds that $\frac{1}{R_l} = \text{constant}$. The V - I characteristics of this type of load are also depicted in Fig. 2.8, where it can be seen that the load current increases and decreases proportionally to the load voltage. In addition, it is noted that the CIL introduces a linear term to the overall converter model, without adding any significant degree of complexity to the system.

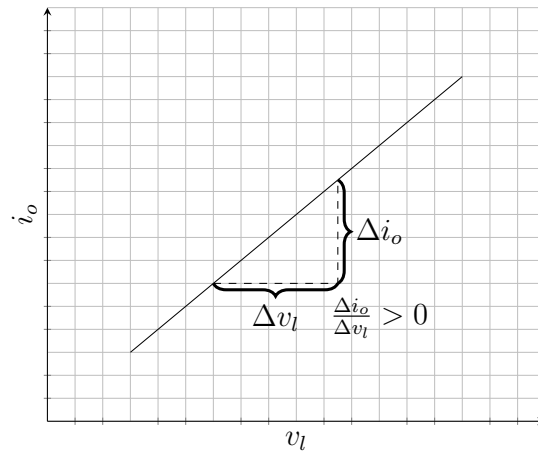


Figure 2.8: V-I characteristics of a constant impedance load

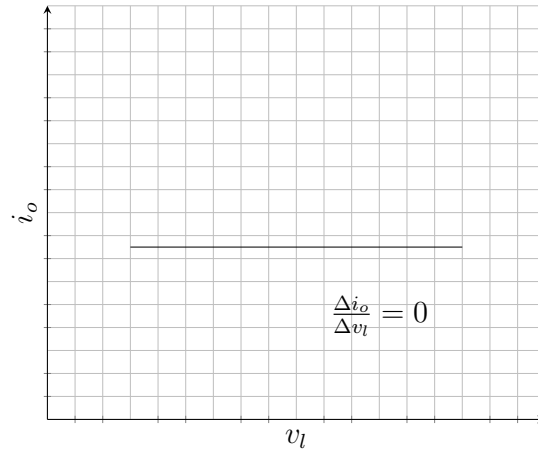


Figure 2.9: V-I characteristics of a constant current load

2.4.2 Constant Current Loads

Similarly to the CIL, the constant current load (CCL) introduces a linear term to the converter model. In this case, the load requires a constant current input, *i.e.*

$$i_o = \text{constant}. \quad (2.19)$$

The respective V - I characteristics are depicted in Fig. 2.9. Therein, it can be seen that the current drawn by the load attains a constant value for every value of the load voltage.

2.4.3 Constant Power Loads

The constant power loads (CPLs) are widely considered to represent the most challenging case [37], [38]. Contrary to the aforementioned loads, CPLs exhibit incremental negative impedance characteristics at steady state and tend to destabilize

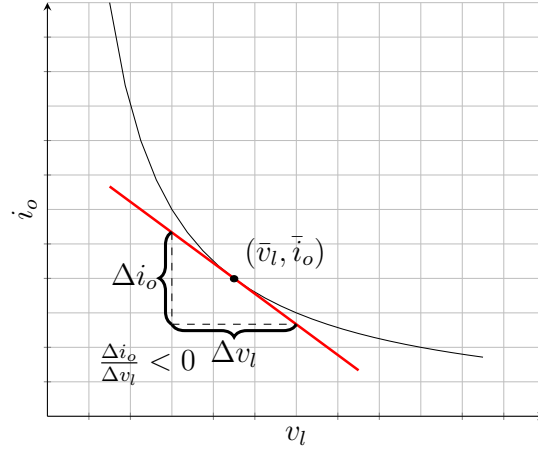


Figure 2.10: V-I characteristics of a constant power load

the overall system. More specifically, denoting the power demand as P , the output converter current i_o flowing in the load can be expressed as,

$$i_o = \frac{P}{v_l} \quad (2.20)$$

where v_l is the load voltage. Then, the partial derivative of (2.20) w.r.t. v_l yields

$$\frac{\partial i_o}{\partial v_l} = -\frac{P}{v_l^2}. \quad (2.21)$$

The V - I curve can be linearly approximated by adopting a Taylor expansion at an operating point (\bar{v}, \bar{i}) . This yields the linear relation,

$$i_o = -\frac{P}{\bar{v}^2}v_l + 2\frac{P}{\bar{v}} \quad (2.22)$$

which has a negative slope, implying that the CPL imposes a negative resistance that reduces the effective damping of the system. The V - I curve is also depicted in Fig. 2.10, where it can be seen that the current drawn by the load increases non-linearly when the load voltage decreases. It is noted that, as also shown in [39], in the case of an AC Microgrid following the dq system, modelling of (2.13), the constant power load is expressed through the relation

$$\begin{bmatrix} P \\ Q \end{bmatrix} = \frac{3}{2} \begin{bmatrix} v_d & v_q \\ v_q & -v_d \end{bmatrix} \begin{bmatrix} i_d \\ i_q \end{bmatrix}. \quad (2.23)$$

which by solving w.r.t. output current (i_d, i_q) yields

$$\begin{bmatrix} i_d \\ i_q \end{bmatrix} = \frac{2}{3} \begin{bmatrix} \frac{v_d}{v_d^2+v_q^2} & \frac{v_q}{v_d^2+v_q^2} \\ \frac{v_q}{v_d^2+v_q^2} & -\frac{v_d}{v_d^2+v_q^2} \end{bmatrix} \begin{bmatrix} P \\ Q \end{bmatrix}, \quad (2.24)$$

It can be seen that in the case of an AC Microgrid, the presence of CPL results in a more complicated dynamic modelling and, as shown in Chapter 6, requires a careful mathematical analysis.

2.5 Compensation of Microgrid Systems

A significant number of studies has been devoted in investigating the problems of regulating a Microgrid system, where, among others, the main control objectives usually are the tight regulation of the converter voltage and current, proportional load sharing, power flow management, optimal calculation of the operating points and protection of the electronic equipment from abnormal operating conditions. The number of different control objectives that need to be simultaneously satisfied, in combination with the requirement for an overall “intelligent” network behaviour, create the necessity of multilevel control design [40, 41, 38]. To this aim, the conventional controller architecture often follows a hierarchical approach, where each control level is responsible for achieving a specific task of the overall desired operation [42, 43].

The hierarchical control structure consists of three levels, see Fig. 2.11. The lowest control level achieves the “primary control”, where the adopted controller is responsible for the instantaneous regulation of the Microgrid state variables and, in some cases, defines the power sharing among the DG units of the network. As it will be demonstrated later, the primary controller can also be utilised to provide the additional damping that is required to stabilise the system in the case of CPLs in the network. Then, the secondary level controller is assigned the task of calculating the reference values that are provided to the primary controller. Calculation of these values can be done according to some desired criteria, such as restoring the Microgrid states deviations from the rated values, achieving economic operation or minimisation of circulating line currents [44, 45]. In order to realise this hierarchical operation, the two levels are often forced to operate in different timescales, where the primary control operates in milliseconds and the secondary control in minutes or hours [46]. Recently, some approaches have been proposed that combine the control objectives of the two levels into a single controller, e.g. see [47], thus dropping this requirement for time scale separation. Nevertheless, so far only a limited number of control objectives is shown to be achievable. Finally, the tasks of energy management and power flow regulation among the different Microgrids of the entire grid are assigned to a tertiary control level. However, the tertiary control is detached from the Microgrid operation and can be considered a part of the overall main grid. Therefore, the focus of this literature review will be solely shifted to the primary and secondary levels instead.

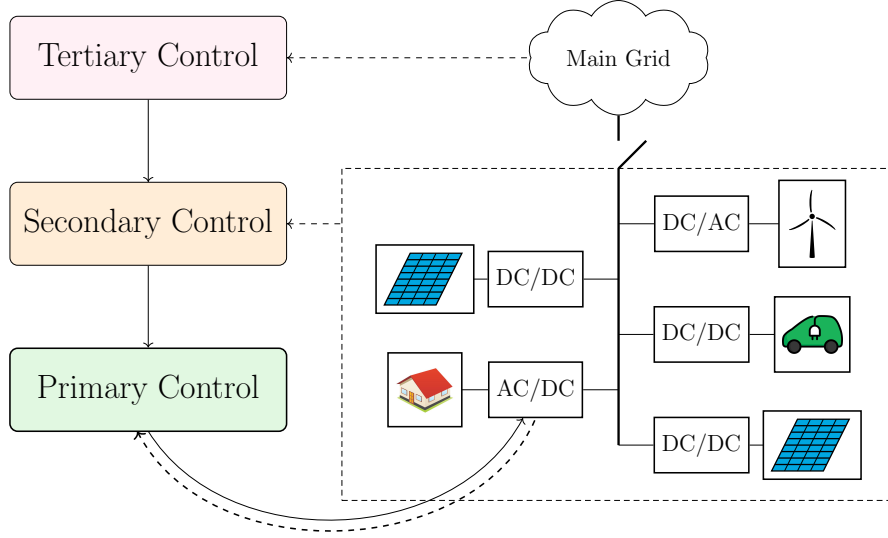


Figure 2.11: Hierarchical control of a Microgrid. Dashed arrows indicate flow of information and solid arrows depict the control inputs.

2.5.1 Primary Control

The primary control is at the bottom of the hierarchical control architecture. The traditional structure of the primary control level is two cascaded inner loops for the regulation of the converter voltage and current states, see Fig. 2.12, where each loop adopts a Proportional-Integral (PI) controller [48]. Then, a popular strategy that introduces damping to the system by mimicking the behaviour of a synchronous generator is the adoption of droop control [49]. Droop control is a technique that introduces a virtual resistance connected in parallel to the output of each converter. Considering a power converter connected to a common DC bus, then reference generation of the i^{th} voltage inner loop is formulated either by an output power or current feedback [50], such that

$$\begin{aligned}
 v_{ref,i} &= \bar{v}_i - m_i i_{o,i}, \\
 &\text{or} \\
 v_{ref,i} &= \bar{v}_i - m_i P_{o,i},
 \end{aligned} \tag{2.25}$$

where \bar{v}_i denotes the rated operating voltage of the converter, $v_{ref,i}$ is the reference voltage, $i_{o,i}$ and $P_{o,i}$ are the measured output current and power respectively, and $m_i \in [0, 1]$ is the droop coefficient. The purpose of the droop coefficient is to linearly adjust the reference voltage of the local converter according to the measured power demand or output current. The choice of the droop coefficient, and thus the slope of the V - I curve is made according to the desired power sharing among the parallel connected converters. In the conventional droop, the droop coefficient for

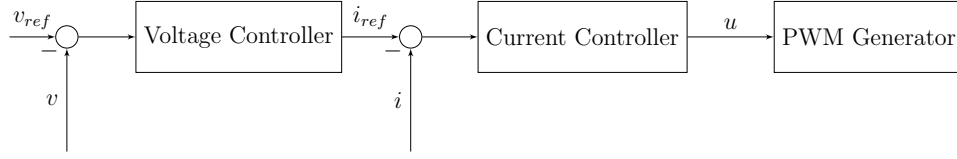


Figure 2.12: Voltage and current Inner loops of a power converter

two parallel connected converters is chosen in inverse proportion to their power ratings as [51, 52]

$$\frac{m_1}{m_2} = \frac{P_2^*}{P_1^*}. \quad (2.26)$$

The respective $V-I$ and $V-P$ characteristics of the droop controller are depicted in Fig. 2.13, where the droop controller linearly adjusts the output voltage according to the measured feedback value. While the droop control is widely adopted due to its completely decentralised structure and simplicity, it is known to have some major application drawbacks. As it can be seen from (2.25), larger values of the droop coefficient cause larger deviations between the reference $v_{ref,i}$ and the rated voltage \bar{v}_i . On the contrary, in order to achieve proportional power sharing, then larger values of the droop coefficient are desired, thus creating a trade-off between accurate voltage regulation and power sharing [53, 51]. The disadvantages of the conventional droop control have been sufficiently investigated in the literature. The main issue is that in order to achieve proportional power sharing according to each converter capabilities, the droop coefficients for two parallel connected converters need to satisfy the following sufficient condition [51]

$$\frac{m_1}{m_2} = \frac{r_1}{r_2}, \quad (2.27)$$

where r_1, r_2 are the output line resistances. Therefore, one requires knowledge of the line resistances, which is difficult to obtain and is subject to numerical errors. In order to cope with the disadvantages of the conventional droop control, numerous variations have been proposed in the literature, where the focus is given in both an improved overall performance and obtaining stronger theoretical guarantees.

A robust droop control for DC Microgrids is proposed in [52] that aims to address the effect of the load on the proportional power sharing of the conventional droop. Therein, the authors propose a novel droop control law, where an additional feedback term is introduced that requires knowledge of the load voltage. An improvement over the load sharing error with higher values of the additional gain is demonstrated. However, higher values of the additional gain reduce the stability margin of the system. Furthermore, the stability analysis is only numerically investigated and the results are restricted to cases of parallel connected networks

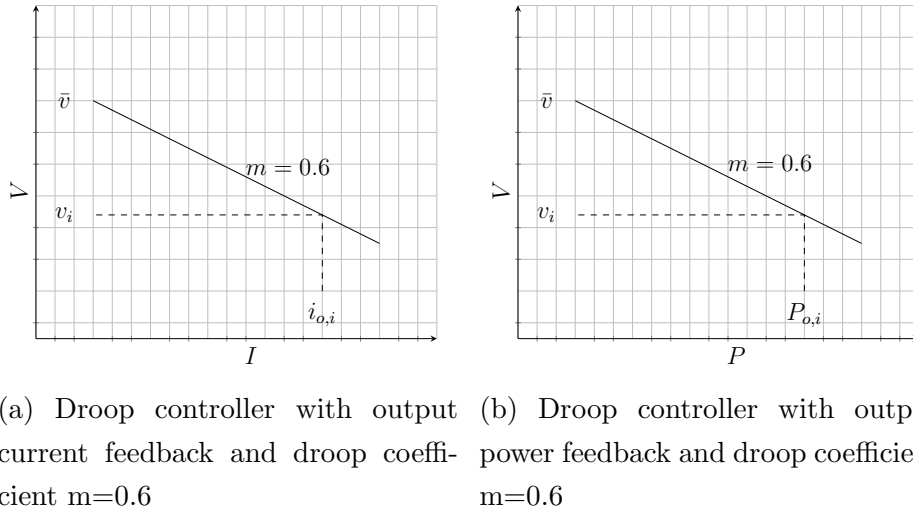


Figure 2.13: The droop controller linearly adjusts the output voltage according to the measured feedback value.

with a common, linear load. A robust droop method for parallel connected inverters was also proposed in [54] that is composed of two layers; an outer layer that includes a robust droop controller that improves the power sharing accuracy and an inner layer where a quasi-proportional resonant controller (QPR) is employed to reduce the offsets of the steady state voltages and minimise circulating currents. A variations of the robust droop controller is proposed in [55], where an uncertainty and disturbance estimator is adopted to compensate for the unknown exogenous signals to the system, such as variations of the output impedance or changes in the load demand. Similarly, an observer is also proposed in [56] in order to reduce the model uncertainties and achieve fast voltage regulation and improved power sharing. However, the performance of both methods depends on the accuracy of the observer. Overall, while displaying some advantages, the robust droop control uses the terminal voltage as a feedback signal which can severely limit the range of possible applications.

A popular variation of the droop control is the adaptive droop control, where the droop coefficients are adjusted in real time according to the current load conditions. An adaptive droop control for inverter-based Microgrids was proposed in [57] which was composed of two layers; one layer performs the estimation of the grid voltage and frequency when the Microgrid operates in grid-connected mode. Then, the droop controller injects active and reactive power to the grid according to these estimated values. While the application results of the proposed controller were thoroughly presented, this study lacks sufficient theoretic analysis of the closed loop system properties and the stability guarantees are obtained only in a small-signal sense. An adaptive droop control scheme was also proposed in [58], where

the controller includes an observer to estimate the average voltage across the Microgrid. Then, this estimated value is used in the local controller setting to adjust the terminal voltage setpoint. The respective current controller performs a similar task, where the local current value is compared with the ones of the neighbouring units to adjust the droop coefficient and improve the load sharing. However, again the theoretic contributions of the study are limited whereas an extensive demonstration of the controller application is provided. A similar approach was proposed in [59] for multi-terminal DC grids, where the droop coefficients are adjusted to achieve proportional load sharing according to each converter available capacity. The stability analysis is only investigated in a small-signal analysis. Other adaptive droop control approaches are proposed in [60] for parallel connected configurations of DC Microgrids, in [61] where an internal current loop is also implemented and [62] which suggests an adaptive droop control that achieves improvement of the Microgrid operation in terms of circulating currents minimisation and improved load sharing. While many different configurations of the adaptive droop control are suggested, a common denominator remains the weak stability guarantees of the proposed approaches.

A less adopted but promising approach is the quadratic droop controller proposed in [63, 64]. The authors derive a reduced form of the power flow equations and show that there exists a one-to-one correspondence between the solution of an optimised solution of the power flow and the voltage equilibrium point. This way, it is demonstrated that proportional load sharing can be achieved for any type of topology and number of converters. A long theoretic analysis of the controller properties is provided, however the case of CPLs in the Microgrid is only studied for a sufficiently small constant power component such that the system retains a stabilizing damping.

The nonlinear droop control has also gained an increased interest due to the substantial performance improvements that can be displayed. In [65], a completely decentralized nonlinear droop control scheme is proposed for parallel connected DC Microgrids. The conventional linear droop curves are substituted for nonlinear slopes, where each case is designed for different load conditions. A parabolic curve is proposed for high or low load demands, while a polynomial droop is suggested when the load demand is at an average value. The proposed control scheme is demonstrated in an experimental scenario where an improved current sharing and voltage regulation trade-off is displayed. A nonlinear droop control for DC Microgrids is proposed in [66]. The proposed scheme suggests a negative impedance slope for light load conditions and a nonlinear curve when the load demand is heavy. Other approaches include the nonlinear droop curve design proposed in [67], where

the parameters are chosen according to a minimisation of the Microgrid operating costs. In the above cases, the stabilities guarantees were only provided around a specific operating point, while a limited theoretic analysis was included, regarding the effect of the nonlinear droop curve on the closed loop system.

Apart from an analytic proof of stability that is not compromised by the nonlinear behaviour of the CPL, an implicit requirement is for every interfacing converter to operate within specific voltage limits in order to avoid damage to its components. Different load profiles may result in transients of voltage which could violate converter limits as the authors of [68] and [69] suggest. Furthermore, even though anti-wind-up techniques and saturated controller are simple solutions to this problem, it has been suggested that these can lead to performance degradation and closed loop instability [70]. Therefore, an effort is made to design a controller architecture that provides an inherent limitation property without the need of such devices. A current-limiting nonlinear controller was proposed in [71] for every type of DC/DC power converter. Therein, the current limitation is achieved by enforcing the existence of an unstable equilibrium point on the boundary of the desired set, thus limiting the evolution of trajectory of the closed loop system within that set. Variations of this controller were proposed in [72], where the proposed control scheme integrated the droop expression within the proposed control law to generate the voltage reference, as well as in [73, 25] for application in both AC and hybrid Microgrid architectures.

Considering the need of enforcing bounds on the evolution of the state trajectories, an interest is rising in optimisation-based methods for the regulation of the converter dynamics; this will also be discussed further in the following section, where this type of methods are more commonly used in the supervisory control level. A hybrid MPC method is proposed in [74], for the regulation of a boost converter connected to a CPL. The derived nonlinear model is discretized by an Euler forward method and an optimal control action is computed online to regulate the state trajectories to desired operating points. However, this approach studies only the case of a single converter connected to a local load, without expanding the results to the case of a Microgrid network. Expansion of an MPC approach to parallel connected converters is demonstrated in [75]. This study employs a sliding mode observer to estimate future perturbations of the load demand and a constrained receding optimisation problem to regulate the system states. Robustness to disturbances is demonstrated and an analytic proof of stability in the presence of CPLs in the network is provided. Nevertheless, a centralised structure is considered, which can complicate the implementation of the proposed controller. Furthermore, the stability guarantees are dependent on the accuracy of the estimated load values and the

computed control action is calculated offline, leaving no room for online adaptation of the control actions during abnormal conditions. A difficult obstacle in the design of the MPC is the requirement of an accurate model of the system [76]. A few approaches have been proposed that use an observer to predict model uncertainties and future variations of the load demand, e.g. in [77], where an Kalman filter is used in combination with an MPC in the case of DC Microgrids with CPLs. The main drawbacks of these approaches are that the provided theoretic guarantees are dependent on the accuracy of the predictions and most of the proposed strategies utilize a centralised structure, suffering from scalability issues and restricting the domain of possible application to small-scale Microgrids.

It is evident from the above that a substantial effort is given in improving the closed-loop performance of a droop controlled Microgrid. However, the completely decentralised structure limits the potential of substantial improvements, where a compromise is often made to accommodate the lack of a communication sub-network. To overcome this difficulty, a supervisory controller is commonly employed that operates in a different time scale and included some form of communication among the nodes of the network. The following section will provide a detailed overview of the proposed supervisory controllers in the literature.

2.5.2 Supervisory Control

The supervisory control is the highest level in the hierarchical structure. The purpose of this control level is to improve the overall performance of the Microgrid operation and deal with the shortcomings of the primary level. Traditionally, this control level operates in a slower time scale than the primary level, where the update rate of the reference points depends on the load profile and the desired operating target. This difference in the time-scales between the two levels allows an independent design, where the dynamic behaviour of the primary level is often ignored in the design of the supervisory controller. This way, the theoretic analysis of the closed loop system is substantially simplified, and the primary level has enough time to regulate the states to the computed references before these are updated. However, despite the simplicity of this methodology, it has been observed that designing a unified control framework paves the road for more sophisticated Microgrid operations, that have stronger safety guarantees compared to the conventional approaches, e.g. achieving optimality in the evolution of the state trajectories or enforcing some form of constrained operation [78].

In the case of a droop-controlled Microgrid, an additional term is introduced to the droop expression that is computed by the supervisory controller. Considering

the current feedback droop control of (2.25), then this is modified such that

$$v_{ref,i} = \bar{v}_i - m_i i_{o,i} + \delta v_i \quad (2.28)$$

where $\delta v_i \in \mathbb{R}$ is the input from the supervisory controller. Therefore, as it can be seen from (2.28), the reference generated by the droop controller is “shifted” by δv_i , where the value of δv_i is computed such that the Microgrid achieves some desired operation. The purpose of the supervisory level is highly dependent on the specific application, where the controller is tasked to achieve restoration of the steady state values to a desired operating point and, in some cases, economic operation and energy management by solving an optimisation problem formulated on minimising operating costs [79].

In many cases, the supervisory controller requires the existence of some form of communication framework in the network, *i.e.* information exchange among the DG units. Depending on the type of communication exchange, the supervisory controller implementations are categorised in three distinct cases [80]:

- *Centralised Control*: In this case, a centralised controller gathers information from every node in the network in order to compute a control action according to the designed control law. Then, it transmits the information back to the local controllers which regulate the local states to the computed reference point. A drawback of this method is that the centralised controller needs to have the processing capacity to solve complicated mathematical problems, where the complexity increases with the amount of nodes in the network. In addition, the communication infrastructure is required to operate in a high-transmission data rate to account for changes in the load profile. As it will be discussed in the following section, this type of controllers are heavily influenced by communication failures, reducing the overall network’s reliability and susceptibility to single points of failure [81, 82].
- *Distributed Control*: In this case, the control action is computed locally, where the information exchange is performed directly among the DG units, also called *agents*. Depending on the distributed controller configuration, each agent tries to meet a global or a local objective in a cooperative way. Due to the fact that the control action is computed locally, the complexity of the computations is often decreased compared to the centralised approach. As a result, the overall scalability of the network is improved [83]. Furthermore, this type of controller facilitates the development of control schemes with plug-and-play implementations, where a unit can be either removed or added to the network without compromising the performance of the entire system [47].

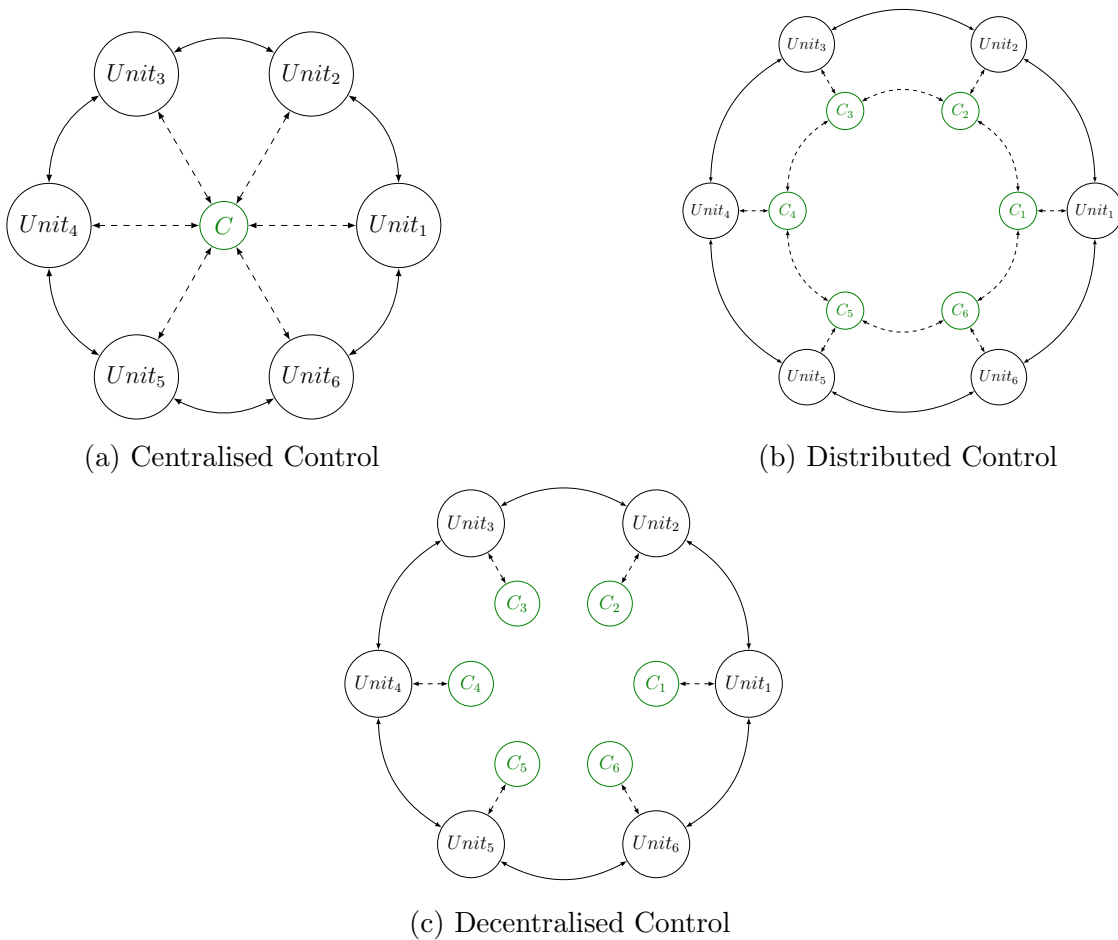


Figure 2.14: The three strategies for the design of secondary Microgrid control. Three different cases of isolated Microgrids are illustrated with a circular topology. Dashed lines depict an exchange of information, while the solid lines are the transmission lines of the network.

- *Decentralised Control*: In this case, each agent only considers local measurements in the calculation of the control action. This type of control is considered an extension of the conventional droop controller, where the control objective is often reaching a desired average value of the voltage and current of each DC/DC converter [84, 85]. Due to the lack of communication channels, the design and implementation of decentralised control schemes is challenging and can compromise the overall performance improvement.

The three control design strategies are depicted in Fig. 2.14. The following sections will present a collection of the past and current state-of-the-art literature works on each case of supervisory controller. Particular emphasis will be given in the distributed approaches, since these are shown to have the highest potential both in the sophisticated Microgrid operations that can be achieved and the practical

implementability regarding the technical requirements.

Centralised Schemes

As it was already highlighted in the previous section, the centralised structure is a convenient approach to design a supervisory Microgrid controller. Especially in the case of a meshed network, where the dynamic evolution of each individual node is heavily determined by the behaviour of the neighbouring nodes, a centralised control scheme can drastically simplify the control design process. The reason for this is that, contrary to the distributed approach, there is not the need for any requirement or particular assumption on the information exchange between the units.

A two-level supervisory control scheme for DC Microgrids is proposed in [86]. At primary level, an adaptive droop controller proportionally distributes the load sharing among the converters. Then, the first level of the supervisory control is responsible for voltage restoration and the second level uses genetic algorithms to compute optimal voltage references that improve the efficiency of the network. In addition it is shown that the first level of the supervisory control enlarges the effective damping of the closed loop system. However, this is only numerically investigated in the presence of resistive loads. The authors of [87] proposed a hierarchical control structure, where the supervisory dynamically adjusts the droop coefficients according to the average state-of-charge of the batteries across the Microgrid. It is shown that overall efficiency of the system is improved, while allowing the smooth integration of batteries with different state-of-charge capabilities. Nevertheless, the proposed control scheme requires accurate knowledge of the DC-bus voltage, which can limit the range of possible applications. The development of a resilient centralised controller was investigated in [88], where numerical simulations are used to demonstrate the controller robustness to transients caused during the connection of the Microgrid to the main grid.

The ability to concentrate information from every node in the network to a single controller unit has facilitated the development of efficient optimisation techniques that enforce some form of constrained operation. A comparison between the three supervisory control strategies is demonstrated in [89], where an MPC control scheme is adopted in each case to improve the power exchange and supply among the units of a group of home-Microgrids. This study shows that the centralised control scheme is able to achieve the highest performance improvement and reduce the number of extreme peaks experienced at both the consumption and the generation side of the point of common coupling with the main grid.

A centralised MPC approach is proposed in [90] to achieve constrained regulation of the system, where the control objective is achieving economic operation and

optimal power supply. However, the controller is formulated in a higher control level, where the approach is limited to solving the power flow equations, without considering the explicit Microgrid model. Similarly, an energy management system utilising an MPC is presented in [91]. It is demonstrated that economic costs are reduced despite the presence of errors or deviations from the available load forecast. The authors of [91] also proposed an MPC approach that provides system robustness to failures of the renewable energy resources, while in [92] a Gaussian process is used to accurately estimate the future solar generation and load demand of the network.

Even though MPC is an ideal approach to achieve constrained regulation of the system states, the literature regarding MPC applications in Microgrid control is limited to similar approaches with the above, where the primal concern is managing the energy distribution between the Microgrid and the main grid. Significant advantages can be achieved by enforcing a unified control framework, where the supervisory controller operates in similar time scales with the primary. This way, the Microgrid can inherit the attractive properties of an MPC control scheme, such as strong stability guarantees and enforcing system state and input constraints. This is demonstrated in [93], where a two-layer control layer is proposed for parallel connected converters. It is demonstrated that the proposed control approach constrains the voltage and current states of the interfacing converters, while also achieving optimal power management in the network. The number of similar approaches in the literature is severely limited mainly due to the practical need of solving an optimisation in such a short time. Nevertheless, the study of [94] shows that this is no longer a concern, presenting powerful and efficient optimisation solving algorithms applied to systems with sampling rate beyond 1 MegaHertz. Therefore, with the continuing parallel development of similar powerful tools, the application of fast time-scale MPC schemes in Microgrids becomes possible, opening a new field for further research.

Distributed Schemes

The previous section discussed the centralised control schemes for Microgrids. As it was highlighted, this type of control strategy can simplify the control design process, since the only communication link required is the one between each unit and the centralised controller. Furthermore, several advantages are demonstrated such as restoration of the system states to desired operating points, efficient power supply to the loads and enhanced management of the renewable energy resources. However, this method comes with several disadvantages, mainly in regards with the real-world implementation of each proposed control scheme. Firstly, this control strategy results in a controller that requires a constant communication channel

between each unit and the control unit. Therefore, any disruption in the communication framework jeopardises the operation of the entire Microgrid system, which can be particularly detrimental in remote areas that do not possess an adequate or reliable infrastructure. In addition, this creates the necessity of an expensive and complex communication framework, compared to the other control strategies. Another drawback is the reduced flexibility of the system, complicating the adoption of a Plug-and-Play type of operations, and reducing the ability of the system to adapt to new information and changes.

In order to overcome the aforementioned problems, a large portion of the literature has been dedicated to the development of distributed control strategies. This allows for the computation of a local control action at each DG unit, which utilises information gathered through the communication links. In particular, consensus-based methods have gained increasing interest [82, 95]. In distributed consensus control, each unit transmits and receives information only from its neighbours, *i.e.* the nodes of the graph that exist along a direct connection line. Each local controller utilises this exchange of information to fulfil a set of common control objectives in a cooperative fashion and improve the performance of the Microgrid network [96]. The adopted algorithm enforces the steady states of the DG units to reach an agreement, hence the terminology “consensus”, based on a cost minimisation criterion or a desired power sharing ratio for each unit. A secondary distributed consensus control is presented in [97] for DC Microgrids of meshed topology and linear loads. The proposed scheme addresses the voltage drift caused by the primary droop controller and computes optimal input injections considering the economic dispatch of the generating units. The original dynamics are augmented with an additional state of a “distributed consensus filter” that achieves proportional power sharing and exponential stability of the equilibrium points. A three-level hierarchical control scheme is proposed in [98] that aims to enforce proportional power sharing among a cluster of DC Microgrids. Therein, the controller does not require information regarding the topology of the network, thus enabling Plug-and-Play capability. The authors of [98] discuss the stability challenges for consensus-based hierarchical control of DC Microgrids. The primary focus of this study is the interaction between the communication and physical network, highlighting the need to integrate a discrete sampled-system with a dynamically continuous one. A power consensus algorithm for DC Microgrids is proposed by the authors of [99]. The design of a nonlinear capacitor is proposed that is shown to achieve proportional power sharing among the DG units according to a desired predefined ratio. While the existence of nonlinear loads is not excluded, the main result assumes that the negative impedance effect of the constant power load is mitigated by the other com-

ponents of the network, without compromising the system’s effective damping. In an effort to improve the convergence speed, a distributed control with finite-time protocol is proposed in [100]. The proposed control law is formulated by adopting a saturation unit in the input currents, and a Lyapunov-based analysis is provided to estimate an upper bound on the convergence time of the closed loop system.

Another control strategy that has been investigated is event-triggered control. In this secondary control scheme, a control action is computed each time a specific event occurs. Instead of a constant flow of information at a fixed sampling rate, the exchange of information is triggered at specific events, reducing the communication burden and often providing a satisfying performance [101]. The effects of this intermittent communication of the nodes is studied in [102]. It is shown that current sharing and average voltage regulation can be achieved, even in cases of communication delays. A theoretic analysis is provided for the proposed control, however the results are restricted by considering a static model of the network and linear loads. Similar control objectives were also considered by the authors of [103], where the theoretic analysis of the closed loop system is formulated on a dynamic network model. An interesting study is presented in [104], where an event-triggered distributed secondary controller is proposed for parallel connected DC/DC converters and both linear and nonlinear loads. Even though the effectiveness of the proposed scheme is thoroughly demonstrated in both simulations and experimental results, the analytic effect of the CPL on the local dynamics is not investigated and the authors do not provide explicit tuning guidelines that guarantee the desired behaviour. An event-triggered, average consensus secondary control is proposed in [105]. While an analytic dynamical model of each node of the network is formulated by an application of the Kirchhoff laws, the study considers solely constant impedance loads.

Decentralised Schemes

The third control strategy is decentralised control, where each unit computes a control action using only locally available information. A unified decentralised control strategy for DC Microgrids was proposed in [106] to achieve voltage restoration and improve the power sharing between the DG units. The authors propose a new feature in the droop control expression termed “injected AC frequency DC”, where a virtual frequency is employed to imitate the frequency droop control method in AC Microgrids. The virtual frequency implicitly operates as a communication link and it is argued that the proposed method improves the voltage drop due to changes in the load demand and enhances the accuracy of the current sharing. The study considers a static model of the network and provides stability guarantees through

a small-signal analysis. The authors of [107], also proposed a control scheme that introduces an additional term to the primary droop controller. In this study, a feedback term consisting of the total current drawn by the loads in the network is used to restore the DC bus voltage to the reference value. While this study considers the presence of CPLs in the network, the stability analysis is limited from a control-theoretic point of view, since similar to [106] a small signal analysis is included. Decentralised control strategies that modify the droop control expression are also proposed in [108, 109, 110, 111, 112], however a comprehensive theoretic analysis is not provided and the properties of the controllers are mainly validated through extensive experimental results. A fully decentralised approach was provided in [83] with the ability to enable Plug-and-Play operation. A Quasi-Stationary-Line approximation is used to augment the model of the local DG system with an additional model of the line dynamics. Then, the Lyapunov method for linear systems was used to design an appropriate feedback gain that achieves asymptotic stability of the local dynamics. A strong assumption is made in this study that the loads are acting as a unknown current disturbance, allowing the consideration of the load current as an additive, as opposed to parametric, disturbance to the voltage dynamics. Plug-and-Play capability is a popular control objective among many decentralised approaches, since there is no requirement of a communication link. These have been proposed for both droop-based [113] and droop-free [114, 115] methods. A port-Hamiltonian model is derived in [113] to derive sufficient conditions for asymptotic stability of the closed loop system under the proposed control law. A decentralised control for meshed islanded inverter-based Microgrids is proposed in [115]. Therein, the DG units that have a direct line to a plugged-in, or plugged-out, unit, retune the control parameters online to preserve the overall stability of the Microgrid system. The control strategy proposed in [114] requires the adoption of an additional control layer to compute global setpoints. Then, a linear decentralised controller is designed to robustly track the respective reference value.

2.6 Microgrid Stability in the Presence of CPLs

It is evidenced from the previous section that a large portion of the literature focuses on the operational properties of a specific case study, where it was often assumed that only linear loads are present in the network. The adopted assumptions allow for a numerical investigation to provide closed-loop stability guarantees, which, however, are compromised by the introduction of CPLs and deviations from the assumed system parameter values. Even though the nonlinear effect of the CPL can be linearised around an operating point to facilitate a stability analysis, this

reduces the stability margin of the system and does not allow the operation on voltage levels away from the operating point.

To overcome this problem, a few studies have been proposed in order to cope and analyse the destabilizing effect of the CPL. A simplified model of a droop-controlled DC Microgrid with CPLs was presented in [116] in order to reduce the complexity of the theoretic analysis and control design. The authors of [117] present an investigation of the effect of both the system parametric values and the type of loads present in the network. The effect of these factors on the system damping is studied via an eigenvalue analysis, showing that under-damped Microgrids may display high frequency unstable oscillations. Then, a virtual-impedance technique is proposed to counteract the effect of the CPL. Extensive simulations of a DC Microgrid with CPLs were used in [118] to identify the stable state subspace, by varying the load demand according to a specified range. This way, stability conditions of the operating points are identified in the presence of an varying-load demand. The system robustness to uncertain varying CPLs was also studied in [119]. The stability analysis is performed by considering the load demand to lie in an polytopic set, instead of a fixed value. Then, local stability of each point is shown when these are parametrised by any value in the uncertainty set. An energy-based approach is suggested in [120]. Therein, a mixed potential model of a DC Microgrid with CPLs is constructed using the Brayton and Moser equations. The authors then formulate specific criteria that lead to asymptotic stability of the system in a large-signal sense. The control analysis of parallel DC/DC converters was investigated in [121], providing tuning guidelines to improve the system damping under the effect of the CPLs. A Lyapunov based analysis is provided in [122] to prove the system asymptotic stability under the proposed control scheme, consisting of a nonlinear disturbance observer and a backstepping controller. Other approaches include the investigation of an AC Microgrid stability properties using the Popov criterion [123], employing tools from the robust parametric control literature [124], solving linear matrix equations to obtain sufficient stability conditions [125], or eigenvalue analysis of the resulting Jacobian matrix [126].

Despite the effort to provide an extensive theoretic analysis on the effect of CPLs on the network, there is still room for improvement. Many studies do not consider the dynamic modelling of the system or adopt some form of reduced model to simplify the analysis. Other studies formulate the stability conditions on the basis of a passive load effect assumption; this is commonly enforced by assuming larger effect of the “Z” and “I” components of the “ZIP” load compared with the “P” component, raising the question of how to achieve similar results when only constant power demand is present.

2.7 Constraint-Based Operation

Apart from a desire for strong stability guarantees, Microgrids are also required to satisfy operational constraints in order to avoid damages to the various electronic components. This is commonly referred to as “overcurrent” or “overvoltage” protection of the converters. This refers to protection of the converters in instances, where a larger than the intended electric current or voltage occurs in some parts of the converter, generating excessive heat and damaging the equipment. The first part of this section will provide an overview of constraint-based techniques regarding Microgrid systems, in an effort to highlight the gaps in the literature and the current open challenges. Then, the latter part will present the constraint-based techniques that commonly adopted in the wider literature of control theory. The purpose of this is to identify the areas for improvement in order to allow the extension of constraint-based techniques to Microgrid applications.

2.7.1 Constraint-Based Operations in Microgrid Literature

In order to limit the current flowing through a converter to the desired operating values, traditional techniques involve elements such as fuses and circuit breakers. However, due to the fact that these usually cause an interruption to the converter operation, a significant interest is noticed in embedding the constraint demand within the control design process and indirectly enforce bounded operation [127]. Control schemes that achieve overcurrent protection by transitioning to a “fault mode” have been proposed in [128, 129, 130, 131]. However, when multiple cascaded loops are employed, the transition between the “fault” and “normal” modes may lead to closed-loop instability, while a concise stability analysis is difficult to be established [70]. In particular, the authors of [70] also demonstrate how these techniques can lead to latch-up and integrator windup cases degrading the overall performance of the network. Similarly, overvoltage protection of Microgrids is studied in [132], where the authors propose an overvoltage monitoring system based on a neural network model. An optimal control approach was presented in [68] to avoid cascading during an overvoltage instance, however the computation burden in both studies is significantly large.

2.7.2 Constraint-Based Operations in Control Theory Literature

As mentioned above, the ability to satisfy constraints is particularly appealing in the context of Microgrid regulation, since the system is required to operate within

a predefined operating range. This can be translated to the form of constraints on both the current and the voltage of each DC/DC converter. One of the most popular and effective techniques for achieving control in the presence of constraints is Model Predictive Control (MPC) [133]. There are two important MPC categories one needs to consider when designing a Microgrid control scheme: robust and distributed MPC. The former is mainly required to counteract the effect of the external disturbances and model uncertainties, while the latter improves the flexibility and scalability of the Microgrid when this spans over large geographical areas.

There is a rich literature behind robust MPC approaches, the majority of which follow a Tube MPC formulation. The term Tube MPC refers to a collection of control approaches that bound the trajectories of the uncertain system within a sequence of sets and regulate this sequence to desired terminal sets [134]. One of the most famous approaches dates back to the work of [135], which standardized the Tube MPC for linear systems. First, the uncertain system is decomposed into nominal and error dynamics, then an approximation of the minimum robust positive invariant (mRPI) set is calculated to bound the error, while the uncertain system is driven by regulating the nominal state trajectory in conjunction with feedback control on the error dynamics. Calculation of the mRPI set approximation requires an explicit form of the integral flow of the system, *i.e.* the solution of the ordinary differential equation describing the system dynamics, [136]. A few approaches have focused on the nonlinear case, for example in [137] a linearisation around each point in the horizon was proposed, while a feedback linearisation was utilized in [138]. A tube nonlinear MPC was proposed in [139], however the calculation of the “restricted” nominal constraints is carried out through simulations and lacks an analytic approach. The Contraction Theory is used to construct the tubes in [140] for a design of a distributed nonlinear MPC for dynamically decoupled subsystems. A method to optimize the tube size online was proposed in [141] by exploiting the structure of the adopted boundary layer sliding controller. An approach that constructs positive invariance sets for globally Lipschitz systems was proposed in [142], where the control action relies in computing a quadratic Lyapunov function for the system. However, imposing a globally Lipschitz condition restricts the scope of possible applications of this control method and may result in a conservative controller. It is evident from the literature that a robust nonlinear MPC scheme is a subject open for investigation, and is often reliant on the specific structure of the dynamics.

The Distributed MPC approaches were initially conceptualised by adopting a Tube MPC and considering the system interactions as external disturbances [143, 144]. However, these techniques were developed for linear systems and re-

quire a “weak” interaction term among the subsystems, *i.e.* to be able to omit the coupling from the local model without causing a large error in the local system state trajectory. This is a particularly strong assumption that is not applicable in Microgrid systems, since the local dynamics are heavily affected by the coupling term. A distributed MPC scheme is proposed in [145] for nonlinear systems using the alternative direction method of multipliers. The proposed method solves local optimisation problems, however communication between the local controllers is carried through a central entity. The authors of [146] propose a DMPC scheme that deals with global system constraints in a distributed manner. An algorithm is proposed to guarantee recursive feasibility of the optimal control problem (OCP), which includes coupled constraints but only considers uncoupled subsystems. A robust DMPC approach is presented in [147], wherein the authors show that recursive feasibility of the OCP is guaranteed in the presence of inexact optimisation. By exploiting the linearity of the system dynamics, the system constraint sets are tightened in order to deal with inexactness of the optimal solution. Similarly in [148], the construction of tightened constraint sets for linear systems is performed through a computation of robust positive invariant sets. The authors propose time varying RPI sets in order to enlarge the region of attraction of the OCP, however this is shown to require a form of centralised computations and relies on reduced subsystem coupling.

It is evident from the literature that the computation of RPI sets is a popular approach. This relies on the computation of reachable sets, *i.e.* the set of states that the system trajectory can be steered from a specific initial state. In the case where the systems adopts a linear structure, this computation is reduced to a set of matrix operations. However, this can be proved to be an arduous task in a nonlinear setting, where the computation of reachable sets requires the existence of an explicit solution of a differential equation. Another issue that may arise in the nonlinear MPC is the design of a Lyapunov function for the terminal dynamics. A few approaches have been proposed to address this but the majority rely on linearisation around the terminal state, see for example [149]. In order to account for linearisation errors, this often leads to conservative terminal sets.

2.8 Gaps in the Literature

The beginning of this chapter presented the conventional droop controller and outlined its drawbacks, focusing on the display of poor power sharing accuracy, existence of circulating currents and deviation of the voltage and current from their respective rated values. Then, a plethora of droop and droop-free control varia-

2.8. GAPS IN THE LITERATURE

tions were presented that improve the overall system performance. Nevertheless, the literature review revealed the following three major shortcomings

- Lack of a concise theoretic analysis and an analytic stability proof in cases of nonlinear loads
- Many studies are case-specific, investigating a specific network topology, and/or require strong assumptions such as knowledge of the load voltage or system passivity
- Inability to guarantee equipment protection without compromising the system stability margin or disrupting the Microgrid operation

A few studies have been devoted in addressing one or more of the above issues. An overview of the works addressing the stability issue was presented in Section 2.6, showing that there is still ample room for improvement, either in regards to the invoked assumptions, or the analytic investigation of the nonlinear load effect on the network behaviour.

Furthermore, a distinct trend is identified towards the development of distributed control techniques for Microgrids [150]. In combination with the need to satisfy constraints and the recent developments in optimisation solving algorithms [94], this opens an avenue for the adoption of MPC techniques in Microgrid regulation [78, 76]. However, Section 2.7.2 showed that general nonlinear distributed MPC approaches display a high degree of conservativeness and/or require strong assumptions on the structure of the dynamics. In addition, the literature on nonlinear DMPC schemes for systems with strong coupling, neighbour-to-neighbour communication and local optimization objectives is limited. Therefore, the extension and adoption of similar control techniques in Microgrid applications is not straightforward, especially in the presence of nonlinear loads. This requires careful investigation of the network dynamical model in an effort to design an adequate control law that bridges the gap between the two fields. Another advantage is that investigating this particular case of nonlinear dynamics allows for a less conservative robust DMPC approach to be developed, since it is not necessary to adopt an approach for generic nonlinear dynamics with simplifying assumptions. Finally, further requirements such as coupled constraint satisfaction, which in the case of Microgrids may take the form of thermal constraints on the transmission lines, are also not thoroughly studied in the case of neighbour-to-neighbour communication and usually require a centralised computation of the control action.

Chapter 3

Distributed Constrained-Based Control of DC Microgrids

One of the most vital aspects of Microgrid control is in regards to constraint satisfaction. These constraints come in the form of actuator limits or protecting the electronic components from damages, and in some cases are necessary to guarantee tight regulation of the dynamics. The presence of loads in the network amplifies the necessity for this property, since the load demand is, in the majority of cases, unknown and takes the form of an external disturbance to the system. Motivated by this problem, this chapter will present a two-layer constraint-based control scheme for DC Microgrids that guarantees closed loop stability of the network dynamics. Contrary to the literature, instead of employing saturation units, the proposed controller is formulated by considering the dynamic behaviour of the closed loop system, while the system constraints are included in the control design procedure. Therefore, the problems associated with saturation devices, such as instability and performance degradation, are avoided. The proposed controller adopts a hierarchical structure. At the primary level, a nonlinear control law is proposed that uniformly bounds the system trajectory in a ball set centred at the origin. The main control objective at this level is ensure an overvoltage protection of the power converter from sudden changes in the load demand. Then, at the supervisory level, an optimisation-based approach is formulated that allows the satisfaction of constraints in the form of bounding the line currents, as well as bounding the local node voltage within a desired range of the rated operating voltage. The control scheme can be operated in two settings; either in a decentralised mode, where a uniform bound for each converter output voltage is guaranteed, or in a distributed mode that improves power sharing, reduces unnecessary circulating currents and guarantees coupled constraint satisfaction in the form of thermal limitations on the transmission lines. In order to minimise the dependence of the control scheme on

the communication among the nodes, the distributed mode adopts a neighbour-to-neighbour communication framework, where an exchange of information occurs once per sampling interval. Analytic conditions of the control parameters are provided such that the desired network behaviour is achieved in both cases where linear and nonlinear loads are present. In order to broaden the range of possible applications of the proposed controller, the control design is based upon a generic meshed network, while both the analytic conditions to be satisfied by the control parameters and the control law do not require explicit knowledge of the network parameters such as filters, line inductances etc.

In Section 3.1, the modelling of the investigated dynamics is provided. Sections 3.2 and 3.3 respectively formulate the control scheme and present the boundedness results of the node dynamics. Then, Sections 3.4 and 3.5 present the supervisory control level. More specifically, Section 3.4 suggests a target voltage computation for the network dynamics that satisfies the desired constraint sets. Then, Section 3.5 is split in two parts; Section 3.5.1 examines the recursive feasibility properties of the optimal control problem and Section 3.5.2 proves the stability of the closed-loop dynamics and establishes analytic conditions on the tuning parameters such that the desired behaviour is achieved. Finally, Sections 3.6 and 3.7 respectively demonstrate the controller properties in a simulation scenario and provide a few concluding remarks on the established results.

3.1 System Modelling

Consider a DC Microgrid consisting of resistive lines, which are commonly assumed in low-voltage DC Microgrids, and a set of $\mathcal{M} = [1, 2, \dots, n_x]$ nodes, each connected to a local load, see Fig. 3.1. Each node represents a DER unit interfaced to the network by a DC power converter. It is common in the literature to assume a time-scale separation of the dynamics, where the time constant of the inner current dynamics is significantly smaller than the one of the output voltage, see for example [151] or [152]. This allows one to consider the inner current as a control input to the node voltage dynamics, and thus study the simplified node circuit depicted in Fig. 3.2.

Employing the simplified representation of the power converter and applying the Kirchhoff laws, results in the dynamic model of the i^{th} node voltage

$$C_i \frac{dv_i}{dt} = i_i - i_{o,i}, \quad (3.1)$$

where C_i is the local output capacitance and (v_i, i_i) are the converter node voltage and input current. In addition, $i_{o,i}$ represents the output current of each node

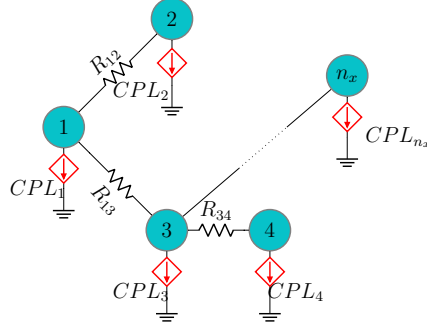


Figure 3.1: Generic meshed Microgrid consisting of DER units and local loads.

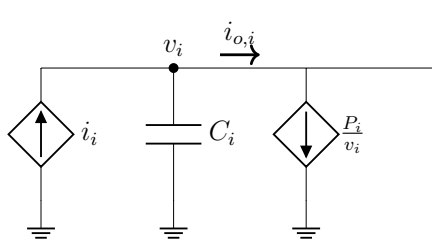


Figure 3.2: Simplified node circuit of a power converter connected to a local load and the common DC bus. The input takes the form of a controlled current source.

represented as a sum of the current consumed by the load and the current flowing through the transmission line of edge $\varepsilon = (i, j)$. In the case where the local load is a constant power load, then it is modelled as a controlled current source. Then, the local output current is given by the relation

$$i_{o,i} = i_{load,i} + i_{T,i} = \frac{P_i}{v_i} + \sum_{j \in \mathcal{N}_i} \mathcal{L}_{ij}(v_i - v_j), \quad (3.2)$$

where $P_i \in \mathbb{R}$ is the local load demand, \mathcal{N}_i denotes the set of neighbours of the i^{th} node, *i.e.*

$$\mathcal{N}_i := \{j \in \mathcal{M} : \mathcal{L}_{ij} \neq 0, i \neq j\}, \quad (3.3)$$

and \mathcal{L}_{ij} is the i - j component of the Laplacian matrix of the network $\mathcal{L} = \mathcal{B}^\top r^{-1} \mathcal{B}$, with r^{-1} the line admittance matrix. As it was shown in [153], considering an equilibrium node voltage \hat{v}_i corresponding to a constant load \bar{P}_i , the admittance matrix of the network can be computed as $Y = \mathcal{L} + D$, where $D = \text{diag} \left\{ -\frac{\bar{P}_i}{\hat{v}_i^2} \right\}$.

3.2 Primary Control Design

The aim of the primary control is to regulate the node voltage to a setpoint \hat{v}_i that achieves proportional power sharing among the units. As it was highlighted in the literature review, the calculation of the voltage setpoint is traditionally achieved

3.2. PRIMARY CONTROL DESIGN

via the droop control that introduces a virtual impedance on the converter output,

$$\hat{v}_i = \bar{v}_i - m_i i_{o,i}, \quad (3.4)$$

where \bar{v}_i is the rated operating voltage of the converter and $m_i \leq 1$ is the droop coefficient. Then, the conventional approach employs a PI controller to track this setpoint and achieve local stability of the dynamics. This approach however, ignores the inherent operational limitations of the converters, as the high transients caused by sudden changes in the power demand can damage the electronic components. In light of this issue, we propose a simplified version of the state-limiting PI controller [154] that ensures stability of the dynamics and overvoltage protection of the power converter. The droop control expression (3.4) is incorporated in the proposed control law, which is formulated as

$$\begin{aligned} i_i &= -k_{p,i} v_i + M_i \sigma_i, \\ \frac{d\sigma_i}{dt} &= \frac{k_{I,i}}{M_i} (1 - \sigma_i^2) (\bar{v} - m_i i_{o,i} - v_i + u_i), \end{aligned} \quad (3.5)$$

where $k_{p,i}$, $k_{i,i}$ and M_i are the tuning parameters. Therefore, applying the above control law in (3.1) results in the closed loop voltage dynamics

$$\begin{aligned} C_i \frac{dv_i}{dt} &= -k_{p,i} v_i + M_i \sigma_i - i_{o,i}, \\ \frac{d\sigma_i}{dt} &= \frac{k_{I,i}}{M_i} (1 - \sigma_i^2) (\bar{v} - m_i i_{o,i} - v_i + u_i), \end{aligned} \quad (3.6)$$

An additional integrator state σ_i is introduced, wherein the dynamics of the input from the supervisory level u_i shifts the equilibrium point $(\hat{v}, \hat{\sigma}_i)$ to a desired value which is later shown to improve the power sharing and minimise the unnecessary line currents. The overvoltage protection of the converter is proven in the following proposition, where an ultimate bound on the node voltage dynamics is established, following an appropriate tuning parameters choice. It is noted that u is a voltage shifting term computed according to the control policies introduced in the following sections, however no specific properties of this term are required for the following proposition to hold true.

Proposition 3.1 (Boundedness of Primary Dynamics). *Considering the closed-loop voltage dynamics in (3.6), then for all $i \in \mathcal{M}$ the set $\mathbb{V}_i \setminus \{0\}$, with*

$$\mathbb{V}_i = [-v_{\max,i}, v_{\max,i}] \times [-1, 1],$$

is positive invariant under the solution of the dynamics, where $v_{\max,i} = \frac{M_i}{k_{p,i}}$ and it is assumed that for any pair of nodes $i, j \in \mathcal{M}$ it holds that $v_{\max,i} = v_{\max,j}$.

3.2. PRIMARY CONTROL DESIGN

Proof. The strategy for proving the invariance of $[-v_{\max,i}, v_{\max,i}] \times [-1, 1]$ involves, first, showing that the integrator state σ_i is contained within $[-1, 1]$ for all positive time, and, later, to show that the boundedness of σ_i implies that node voltages remain within $[-v_{\max,i}, v_{\max,i}]$. The former is addressed by contradiction. By construction, the solutions of the differential equations defining the state $\sigma_i(\cdot)$ is unique and continuous around the points $\sigma_i = 1$ and $\sigma_i = -1$. Suppose now that $\sigma_i(0) \in [-1, 1]$ and there exists $\tau > 0$ such that $\sigma_i(\tau) \notin [-1, 1]$. By continuity, this implies the existence of $0 < \tau_1 < \tau$ such that $|\sigma_i(\tau_1)| = 1$; As a consequence, there exists $\delta > 0$ and $\epsilon > 0$ such that $|\sigma_i(\tau_1 + \delta)| > 1 + \epsilon$ and $|\sigma_i(\tau_1 - \delta)| < 1 - \epsilon$, *i.e.* the state trajectory enters and leaves the set $[-1, 1]$ in finite time. It is noted that the local integrator state $\sigma_i \in \mathbb{R}$ is scalar, *i.e.* the evolution of $\sigma_i(\cdot)$ is confined on the line of the real numbers. Furthermore, both points on the boundary of the set $[-1, 1]$ are equilibrium points for (3.6), therefore these have the property to either attract or repel the state trajectory $\sigma_i(\cdot)$. This leads to a contradiction as it is impossible for the state to escape this set and therefore $\sigma_i(t) \in [-1, 1]$ for all $t \geq 0$.

The second part is associated with the boundedness of $v_i(\cdot)$. Here, the energy function of the capacitor, *i.e.* $W_i = \frac{1}{2}C_i v_i^2$, is used where the respective time derivative yields

$$\dot{W}_i = -k_{p,i}v_i^2 + v_i M_i \sigma_i - v_i i_{o,i}. \quad (3.7)$$

The analysis is bifurcated into two cases: (a) $v_i i_{o,i} > 0$ and (b) $v_i i_{o,i} \leq 0$. For the former, $\dot{W}_i \leq -k_{p,i}v_i^2 + |v_i| M_i$. Using ultimate boundedness, see [155, Theorem 4.18], the condition $|v_i(0)| \leq \frac{M_i}{k_{p,i}}$ implies that $v_i(t)$ is ultimately bounded by $\frac{M_i}{k_{p,i}}$ for every $t \geq 0$, *i.e.* $|v_i(t)| \leq \frac{M_i}{k_{p,i}}, \forall t \geq 0$. For case (b), the condition $v_i i_{o,i} \leq 0$ implies that

$$P_i + v_i \sum_{j \in \mathcal{N}_i} \mathcal{L}_{ij}(v_i - v_j) \leq 0,$$

therefore there exists a node $j \in \mathcal{M}$ such that it feeds the i^{th} load, *i.e.* $v_j \geq v_i$. Considering a choice of the network tuning parameters such that $v_{\max,j} = v_{\max,i}$, then converter j falls in case (a), *i.e.* $v_j \leq v_{\max,j} = v_{\max,i}$ which implies $v_i \leq v_{\max,i}$. Therefore the tuning parameters M_i and $k_{p,i}$ can be chosen to establish an appropriate converter voltage bound $v_{\max,i} = \frac{M_i}{k_{p,i}}, \forall i \in \mathcal{M}$. \square

The above results demonstrates that in the case where the one does not employ the supervisory controller, *i.e.* when $u_i = 0$, the local node operated in a decentralised mode where the controller guarantees upper boundedness of the voltage solution $v(\cdot)$ in a desired set. Hence, an overvoltage protection of the converter is guaranteed without the use of saturation devices, even during transients. Furthermore, the following sections will formulate a condition on the controller gain $k_{p,i}$

such that stability of the closed loop system is also guaranteed. However, the primary controller ignores the fact that the point $v_i = 0$ is a singularity of the dynamics and does not guarantee that a voltage drop to $v_i = 0$ can always be avoided. Therefore, a supervisory controller should be incorporated in order to provide an input u such that the voltage is bounded around the desired rated operating voltage, as opposed to the origin, and ensure that this constraint set is never violated. Finally, it is noted that this chapter does not consider limitations on the input current and assumes that the desired input current can always be provided. This could be a limiting factor in the application of the proposed control scheme and therefore is addressed in the following chapters.

3.3 Supervisory control structure

The following sections describe the formulation and theoretical analysis of the supervisory controller. The use of a supervisory controller allows a more sophisticated operation, such as coupled constraint satisfaction, boundedness of the solution around a desired range of the rated voltage and inclusion of input constraints. These constraints are accounted for in the supervisory control, which is composed of two parts. First, an upper layer computes economic steady state targets $z^t = (x^t, u^t)$ according to the load demand, where x collects the states of the system into a single variable, *i.e.* $x = (v, \sigma)$. Then, at the lower layer, a local finite horizon distributed NMPC, denoted as NMPC- i , is employed to drive the system to the provided targets. The target z_i^t is updated each time a “significant” change in load demand occurs; this is further explained in Remark 3.1. Then, the local NMPC- i is solved at every sampling instant, denoted as $k \in \mathbb{N}$. The exchange of information follows a non-iterative, neighbour-to-neighbour framework. This is formalised in the following assumption.

Assumption 3.1 (Communication framework). *At each time step $k \in \mathbb{N}$, each local node receives the voltage v_j from the neighbouring nodes $j \in \mathcal{N}_i$ and assumes $v_j = \text{constant}$ until $k + 1$.*

For the following results, a discrete time approximation of system (3.6) is considered. By compactly representing (3.6) as $\dot{x}_i = f_i(x_i, u_i, i_{o,i})$, a discrete model through Euler approximation can be derived as

$$x_i(k+1) = x_i^+ = x_i + \Delta T_i f_i(x_i, u_i, i_{o,i}) = H_i(x_i, u_i, i_{o,i})$$

with a sufficient small sampling period $\Delta T_i \in \mathbb{R}_{\geq 0}$ that captures the dynamics. The variable of the input current $i_{o,i}$ in the discrete model can be substituted by a

3.4. UPPER LEVEL - TARGET COMPUTATION

state-dependent disturbance function $w_i: \mathbb{R} \rightarrow \mathbb{R}$. This function is a summation of the load current $i_{load,i}$ and a term consisting of the interactions with the neighbour voltages, *i.e.*

$$w_i(v_i) = \frac{P_i}{v_i} + d_i, \quad (3.8)$$

where $d_i = -\sum_{j \in \mathcal{N}_i} \mathcal{L}_{ij} v_j$ represents the transmitted information to the i^{th} node.

3.4 Upper Level - Target Computation

The computation of the network voltage setpoints considers the line current limitations, as well as the network load demand. In order to perform this, information needs to be gathered from the entire network, thus requiring a centralised setup. First, it is noted that, due to the adopted primary controller, the equilibrium map of (3.6) is given by

$$\begin{aligned} \hat{v} &= \text{sat}\left((I_n + mY)^{-1}\bar{v} + u, v_{\max}\right), \\ \hat{\sigma} &= \text{sat}\left(M^{-1}(k_p + Y)\left((I_n + mY)^{-1}\bar{v} + \hat{u}\right), 1\right), \end{aligned} \quad (3.9)$$

where $\text{sat}(\cdot)$ is the saturation function and $I_n \in \mathbb{R}^{n \times n}$ is the identity matrix. Then, the steady state optimisation problem can be formulated as

$$\begin{aligned} z^t &= \arg \min_z \ell_{\text{eco}}(z) \\ &\text{s.t. (3.9),} \\ &z \in (\mathbb{X}(P) \cap \mathbb{X}_L) \times \mathbb{U}, \end{aligned}$$

where $\ell_{\text{eco}}(\cdot)$ is a strictly convex function, $\mathbb{X}(P)$ translates the line current and economic constraints to polytopic constraints on the network voltage. Furthermore, the set $\mathbb{X}_L \subseteq \mathbb{V}$ are the local state constraints which enforce strictly positive values of the voltage. Finally, \mathbb{U} denotes the desired input constraint set regarding the voltage shifting term u . The function ℓ_{eco} can be chosen according to the desired network behaviour; examples of these are solving an optimal power flow problem, where ℓ_{eco} computes target states by minimising the DC power flow equation, or minimising deviation from a rated voltage. The latter case would result in a quadratic cost function e.g. $\ell_{\text{eco}} = z^\top W z$, where $W \in \mathbb{R}^{n \times n}$ is a positive definite weight matrix. The only requirement for ℓ_{eco} is strict convexity. The usefulness of this assumption is twofold: first strict convexity implies a unique minimum within a compact set and, secondly, strict convexity implies dissipativity with respect to a trivial storage function.

Remark 3.1. *In a real world application, the load demand may arbitrary change between the time steps, which would result in the need to constantly recalculate the*

steady state targets. This can be overcome by setting an event-triggered optimisation steady state computation, where the decision to update the target states is made only when a defined threshold on the load demand changes is exceeded. It is noted that computation of optimal steady state targets is an active topic in the literature and partially falls beyond the scope of this study. Here, emphasis is given in the challenge of designing a distributed local controller, thus a relatively simple representation for the upper-level is used with the sole purpose of providing a target state to facilitate the analysis of the lower-level supervisory controller.

3.5 Lower-Level distributed control

In this section, the lower-level distributed controller will be presented. An local NMPC- i is adopted for the lower level of the supervisory control. The NMPC- i uses predictions of the system evolution over a horizon N to calculate an optimal control sequence that minimises the cost function. In order to realise a distributed operation, each local controller, at sampling instant $k \in \mathbb{N}$, constructs the disturbance term w_i from the received information d_i and the local measurements of the load P_i . This is included in the state predictions of the NMPC at every sampling instance k as an N -length sequence

$$\mathbf{w}_i(k) = \{w_i(0|k), \dots, w_i(N-1|k)\}, \quad (3.10)$$

where, due to the adopted communication framework from Assumption 3.1, both the load demand and the interaction term are kept constant over the horizon. Therefore, for any $c = 0, \dots, N-1$ it holds that the respective disturbance sequence element is given by

$$w_i(c|k) = \frac{\bar{P}_i}{v_i(c|k)} - \sum_{j \in \mathcal{N}} \mathcal{L}_{ij} \bar{v}_j \quad (3.11)$$

where $v_i(c|k)$ denotes the respective c^{th} element of the state prediction sequence at sampling instant k . In order to simplify the notation, it will be assumed that the disturbance sequence and its elements are always parametrised by the respective state predictions, without explicitly stating this. Therefore, the local NMPC- i computes the local state trajectory predictions assuming constant external inputs over the horizon. Before proceeding to the optimisation problem formulation, the state constraints need to be formally defined. Let $\mathcal{E}_i \subset \mathcal{E}$ denote the set of edges connected to node $i \in \mathcal{M}$ i.e. ,

$$\mathcal{E}_i := \{\varepsilon = (i, j) \in \mathcal{E} : j \in \mathcal{N}_i\}.$$

Each line current $i_{T,ij}$ flowing to edge $\varepsilon \in \mathcal{E}_i$ can be analytically expressed as

$$i_{T,ij} = \mathcal{L}_{ij}(v_i - v_j), \quad \forall j \in \mathcal{N}_i. \quad (3.12)$$

3.5. LOWER-LEVEL DISTRIBUTED CONTROL

The requirement is that each line current is uniformly bounded by some maximum line current I_j^{max} , as $|i_{T,ij}| \leq I_{ij}^{max}$, or equivalently restricted within a compact set $i_{T,ij} \in \mathbb{I}_i \subset \mathbb{R}$. Considering Assumption 3.1, the neighbouring voltage is locally perceived as a piecewise constant signal. Thus, it follows from (3.12) that the line current constraint can be expressed as a collection of time varying constraints on the local voltage v_i parametrised by the available information at each sampling time, *i.e.* $v_i \in \mathbb{X}_i(d_i)$. Furthermore, is assumed that both the network node voltages and inputs are also subjected to uncoupled constraint sets

$$\begin{aligned}\mathbb{X}_L &= \prod_{i \in \mathcal{M}} \mathbb{X}_{L,i} := \{v_i \in \mathbb{R} : v_{lb,i} \leq v_i \leq v_{ub,i}\}, \\ \mathbb{U} &= \prod_{i \in \mathcal{M}} \mathbb{U}_i := \{u_i \in \mathbb{R} : u_{lb,i} \leq u_i \leq u_{ub,i}\}.\end{aligned}\tag{3.13}$$

However, at each sampling instant k , the local NMPC- i computes state predictions considering a constant external inputs. This can lead to problems regarding the feasibility of the optimisation problem, since the time-varying nature of these parameters is ignored. As it will be shown later, the monotonic descent property of the NMPC value function can be used to guarantee that the true state remains within the constraint set despite this induced uncertainty.

In order to ensure regularity and convexity of the optimal control problem, the following assumption is invoked on the structure of the constraint sets.

Assumption 3.2 (Regularity of the constraint sets). *The sets \mathbb{I}_i , \mathbb{X}_L and \mathbb{U} are compact, convex and \mathbb{U} contains the origin in its non-empty interior.*

This assumption is required to obtain a necessary condition on the optimality of the minimisation problem and allows consideration of a uniformly continuous value function [133, Appendix C.2]. Each local subproblem NMPC- i incorporates the sequence $\mathbf{w}_i(k)$ in the prediction model, as well as in the parametrisation of the state constraints. This is formulated as,

$$\begin{aligned}J_i^o(x_i(0), z_i^t, \mathbf{w}_i) &= \\ \min_{\mathbf{u}_i, z_i^s} &\sum_{n=0}^{N-1} \ell_i(z_i(n) - z_i^s) + \ell_{o,i}(z_i^s - z_i^t) \\ \text{s.t.} & \\ x_i(0) &= x_i(0|k) \\ x_i^+(n) &= H_i(x_i(n|k), u_i(n|k), w_i(n|k)), \\ z_i &\in (\mathbb{X}_{L,i} \cap \mathbb{X}_i(w_i(n|k))) \times \mathbb{U}_i, \\ z_i^s &\in (\mathbb{X}_{L,i} \cap \mathbb{X}_i(w_i(n|k))) \times \mathbb{U}_i\end{aligned}\tag{3.14}$$

$$\forall n \in 0, \dots, N - 1$$

where $z_i = (v_i, \sigma_i, u_i)$. The solution of (3.14) generates the optimal control sequence $\mathbf{u}_i^o = \{u_i^o(0|k), u_i^o(1|k), \dots, u_i^o(N-1|k)\}$. As it was highlighted in [133, Section 6.3.4], the presence of coupled constraints necessitates a centralised calculation of the target states z^t . From the local controller point of view, this may result in the i^{th} target z_i^t being outside the constraint set at some time step k . This is because the targets are calculated based on steady state network voltages, while each node's constraint set is parametrised by the current value of the neighbour voltages. To account for this a strictly convex offset function $\ell_{o,i}(\cdot)$ is added to the stage cost, which can be thought as incorporating a steady state target optimiser into the optimisation problem. The addition of an offset cost function further ensures recursive feasibility under changing target points. Let $z_i^t(\tau_1)$ and $z_i^t(\tau_2)$ denote the target points for two consecutive times with $\tau_1 < \tau_2$ and the set $\mathcal{R}_N(x)$ denote the set of states that can be steered to x in N steps. Assuming that the system has converged to $z_i^t(\tau_1)$, it is not necessarily true that $z_i^t(\tau_1)$ belongs to $\mathcal{R}_N(z_i^t(\tau_2))$. As shown in [156], the offset function allows the system to converge to the closest state to $z_i^t(\tau_2)$, while the system state trajectory will eventually enter $\mathcal{R}_N(z_i^t(\tau_2))$ due to the recursive update of the optimal control action. At every step k , the i^{th} node transmits its state value to the neighbouring nodes $j \in \mathcal{N}_i$, the optimal problem (3.14) is solved, the first element of the resulting optimal control sequence \mathbf{u}_i is used as an input to the system, *i.e.*, $u_i = u_i^o(0|k)$, and the process is repeated again at $k + 1$, thus realising a receding horizon formulation.

3.5.1 Recursive Feasibility

This section investigates the feasibility and stability properties of the proposed control scheme. As it was described in the previous section, the system evolves according to the discrete model,

$$x_i^+ = H(x_i, u_i, w_i) \tag{3.15}$$

It is important to note that, generally, the discrete state x_i^+ is not equal to the state resulting from the continuous solution map $x_i(t + \Delta T)$. In this study, it is implicitly assumed that the errors induced by the Euler discretization are small enough and can be omitted in the analysis. While this can be argued to increase the conservativeness of this approach, it can be justified from the already-present necessity for a small sampling time.

Traditionally, the recursive feasibility proof of the NMPC uses the tails of the resulting optimal sequences and relies on the existence of terminal penalties and

3.5. RECURSIVE FEASIBILITY

constraints. In view of the absence of terminal ingredients of (3.14), the following analysis exploits the property of the optimisation solution to spend a significant amount of time “close” to the desired setpoint. This property is termed “turnpike”, where its original definition can be found in [157]. This definitions is slightly adjusted here to better accommodate this specific problem setting.

Definition 3.1 (Turnpike property in OCP). *Let the optimal control problem (3.14) be strictly dissipative with respect to the setpoint $x_i^s = (v_{eq,i}, \sigma_{eq,i})$ and x_i^s be locally controllable. Then, $|Q| \leq \Psi$ for some $\Psi \in \mathbb{N}$ and*

$$Q = \{k \in [0, 1, 2, \dots, N]: \mathbf{x}_i^o(k) \notin \mathcal{B}_\epsilon(x_i^s)\}, \quad (3.16)$$

where $\mathcal{B}_\epsilon(x_i^s)$ is a ball of radius ϵ centred on x_i^s .

Essentially, the turnpike property describes that the time the optimal solution spends outside of a ball $\mathcal{B}_\epsilon(x^s)$ is finite and bounded. In addition, the longer the horizon N is, the more time the optimal solution stays closer to x_i^s . As it was denoted in [158], in order for a system to have the turnpike property it is required to be dissipative and locally controllable. It will be shown that the proposed control system satisfies both requirements, starting by the dissipativity one. Strict dissipativity requires the following inequality to be satisfied [159],

$$\lambda(x_i^+) - \lambda(x_i) \leq s(x_i, u_i) - \theta(\|x_i - x_i^s\|) \quad (3.17)$$

where $\lambda(\cdot)$ denotes the energy saved to the system, $s(\cdot, \cdot)$ is the supply rate function and θ is a \mathcal{K}_∞ function.

Lemma 3.1 (Dissipativity of the NMPC). *The NMPC- i problem (3.14) is strictly dissipative with respect to the setpoint x_i^s for any strictly convex cost function $\ell(\cdot)$.*

Proof. The stage cost function satisfies $\ell(0, 0) = 0$ for $(x_i, u_i) = (x_i^s, u_i^s)$. Extending what was shown in [157], by considering a supply rate $s(x_i, u_i) = \ell(x_i - x_i^s, u_i - u_i^s) + \ell_o(x_i^s - x_i^t) - (\ell(0, 0) + \ell_o(x_i^s - x_i^t))$ and storage function $\lambda \equiv 0$ the inequality (3.17) takes the form,

$$\ell(x_i - x_i^s, u_i - u_i^s) \geq \theta(\|x_i - x_i^s\|) \quad (3.18)$$

which is satisfied for any strictly convex function ℓ with extreme point x_i^s . \square

The second requirement of the existence of turnpikes in the NMPC- i is the local controllability of the system (3.15). This is shown in the following.

Lemma 3.2 (Local controllability of the network dynamics). *The network closed loop dynamics are locally controllable in the set $\text{int}(\mathbb{V})$.*

3.5. RECURSIVE FEASIBILITY

Proof. The proof starts by writing the network system, with individual subsystems' model given in 3.6, in the control affine form,

$$\dot{x} = f(x) + g(x)u$$

where,

$$\begin{aligned} f(x) &= \begin{pmatrix} f_1 \\ f_2 \\ \vdots \\ f_{2n_x} \end{pmatrix} (x) \\ &= \begin{pmatrix} C^{-1}(-k_p + Y)v + M\sigma \\ M^{-1}k_I (I_{n_x} - \text{diag}(\sigma^2)) (\bar{v} - (I_{n_x} + mY)v) \end{pmatrix}, \\ g(x) &= \begin{pmatrix} \tilde{g}_1 & 0_{2 \times 1} & \dots & 0_{2 \times 1} & 0_{2 \times 1} \\ 0_{2 \times 1} & \tilde{g}_2 & \dots & 0_{2 \times 1} & 0_{2 \times 1} \\ \vdots & \vdots & \ddots & \vdots & \vdots \\ 0_{2 \times 1} & 0_{2 \times 1} & \dots & \tilde{g}_{n_x-1} & 0_{2 \times 1} \\ 0_{2 \times 1} & 0_{2 \times 1} & \dots & 0_{2 \times 1} & \tilde{g}_{n_x} \end{pmatrix} (x), \end{aligned}$$

where $\tilde{g}_i(x)$ is the respective vector of each node dynamics,

$$\tilde{g}_i(x_i) = \begin{pmatrix} 0 \\ -\frac{k_{I,i}}{M_i}(1 - \sigma_i^2) \end{pmatrix}.$$

In order for the system to be controllable, the columns of the controllability matrix

$$\mathcal{C} = \left(g_1(x), g_2(x), \dots, g_{n_x}(x), [f, g_1](x), [f, g_2](x), \dots, [f, g_{n_x}](x) \right), \quad (3.19)$$

need to be linearly independent, where $g_i, i \in \mathcal{M}$ is the respective column of matrix $g(x)$ and $[f, g](x)$ denotes the Lie bracket¹ between the vector fields $f : \mathbb{R}^{2n_x} \rightarrow \mathbb{R}^{2n_x}$ and $g : \mathbb{R}^{2n_x} \rightarrow \mathbb{R}^{2n_x}$. As the columns of $g(x)$ are linearly independent, it suffices to investigate the linear independence of the columns of \mathcal{C} collected in the reduced matrix $\mathcal{A}_{\mathcal{C}}$, where

$$\mathcal{A}_{\mathcal{C}} = \left(g_1(x), [f, g_1](x) \right).$$

Expanding, this results in,

$$\mathcal{A}_{\mathcal{C}} = \begin{pmatrix} 0 & C_1 k_{I,1} (1 - \sigma_1^2) \\ -\frac{k_{I,1}}{M_1} (1 - \sigma_1^2) & 2 \frac{k_{I,1}}{M_1} \sigma_1 f_2(x) \end{pmatrix}$$

where the columns are linearly independent for $|\sigma_1| < 1$. Combined with the fact that \mathbb{U} is compact, it can be concluded that the system is locally controllable within the set $\text{int}(\mathbb{V})$. \square

¹The Lie bracket of two vector fields $X, Y : \mathbb{R}^n \rightarrow \mathbb{R}^n$ is defined by $[X, Y](x) = \frac{\partial Y}{\partial x} X - \frac{\partial X}{\partial x} Y$.

3.5. RECURSIVE FEASIBILITY

Essentially, Lemma 3.2 in combination with Proposition 3.1 describe the existence of ball $\mathcal{B} := \{\sigma \in \mathbb{R}^{n_x} : |\sigma| \leq 1\}$ such that no state can be steered to the boundary $\partial\mathcal{B}$ nor exit it in the case of $\sigma_i(0) = 1$ for any $i \in \mathcal{M}$. Nevertheless, the dynamics are continuous around the point $|\sigma| = 1$, hence, if any state satisfies $|\sigma_i(0)| < 1$, then it can be steered in finite time to any state in $\text{int}(\mathcal{B})$ but not outside \mathcal{B} . As it will be shown now, satisfaction of the turnpike property can be used to guarantee recursive feasibility of the optimisation problem. First, the simple scenario is investigated, where the external inputs of the disturbance remain unchanged between the sampling intervals, with feasibility set $\mathcal{X}_N(w_i) := \{x_i \in \mathbb{X}_i(w_i) : \mathcal{U}_N(x_i, w_i) \neq \emptyset\}$. This will be later exploited in the analysis of recursive feasibility under perturbations of the external inputs between sampling times.

Proposition 3.2 (Recursive feasibility of nominal NMPC without terminal ingredients). *Let the NMPC- i have the turnpike property with respect to the setpoint x_i^s and $w_i(k+1) = w_i(k)$, then $x_i \in \mathcal{X}_N(w_i)$ implies $x_i^+ \in \mathcal{X}_N(w_i^+)$.*

Proof. Define the solution $\mathbf{x}_i^o = \{x_i^o(1|k), \dots, x_i^o(N-1|k)\} \in \mathcal{X}_N(w_i)$ at time k , that corresponds to the control sequence $\mathbf{u}_i^o(w_i)$. At time $k+1$, denote the predicted control sequence $\mathbf{u}_i^o(w_i^+)$ corresponding to the respective state predictions sequence. Then, consider that the turnpike property implies the existence of time instants κ_1 and κ_2 , such that the resulting state trajectory \mathbf{x}_i^o respectively enters and leaves a neighbourhood $\mathcal{B}_\epsilon(x_i^s)$ of the setpoint x_i^s . Local controllability of the dynamics imply the existence of a local control action sequence $\tilde{\mathbf{u}}_i \in \mathbb{U}_i$ such that $\tilde{\mathbf{x}}_i^+ = H(\mathbf{x}_i, \tilde{\mathbf{u}}_i, \mathbf{w}_i^+) \in \mathcal{B}_\epsilon(x_i^s) \subset \mathbb{X}_i(w_i)$ for the interval $[\kappa_1, \kappa_2]$. Utilising the fact that the external inputs P_i and d_i remain constant between the sampling times k and $k+1$, then the lack of uncertainty implies that $v_i(1|k) = v_i(0|k+1)$ and $w_i(1|k) = w_i(0|k+1)$. Therefore, the resulting trajectory $\mathbf{u}_i^o(w_i^+)$ is the tail of $\mathbf{u}_i^o(w_i)$ in the time intervals $[0, \kappa_1)$ and $(\kappa_2, N-1]$. This yields,

$$\begin{aligned} \mathbf{u}_i^o(w_i^+) = \{ & u_i^o(1|k), u_i^o(2|k), \dots, \\ & u_i^o(\kappa_1 - 1|k), \tilde{\mathbf{u}}_i, u_i^o(\kappa_2 + 1|k), \dots, \\ & u_i^o(N - 2|k), u_i^o(N - 1|k)\} \in \mathcal{U}_N(x_i^+, w_i^+). \end{aligned} \quad (3.20)$$

and resulting state sequence,

$$\begin{aligned} \mathbf{x}_i^o = \{ & x_i^o(1|k), x_i^o(2|k), \dots, \\ & x_i^o(\kappa_1 - 1|k), \tilde{\mathbf{x}}_i, x_i^o(\kappa_2 + 1|k), \dots, \\ & x_i^o(N - 2|k), x_i^o(N - 1|k)\} \in \mathcal{X}_N(w_i^+). \end{aligned} \quad (3.21)$$

3.5. RECURSIVE FEASIBILITY

Therefore, the respective future control and state sequences are feasible, when the external inputs remain constant. \square

The recursive feasibility of the NMPC- i in the case of unchanging external inputs is shown, with the state entering a neighbourhood $\mathcal{B}_\epsilon(x_i^s)$ of the setpoint. In fact, it can be shown that the cost decreases outside of $\mathcal{B}_\epsilon(x_i^s)$ and the state sequence converges to this neighbourhood of the setpoint, see [160, Proposition 2]. In addition, for a sufficient large finite horizon N , it can be shown that $\mathcal{B}_\epsilon(x_i^s)$ shrinks to $\{x_i^s\}$ and thus convergence to the setpoint is established. The proofs for these two statements are omitted here since many studies are dedicated to showing the above; the interested reader is referred to [161] or [162] for discrete time case and [160] for a continuous time study. This work is dedicated to extending these results in the scenario where some parameters of the disturbance sequence are subject to bounded perturbations. The local supervisory controller considers the sequence $w_i(k)$ constant in the prediction model, however $w_i(k)$ evolves according to the neighbour voltages $v_j(k)$ and the load demand P_i ; this is ignored by the prediction model. Therefore, the question arises of how to ensure the robustness of the NMPC- i in perturbations of the disturbance sequence and thus ensure that the problem remains recursively feasible. The following assumption on the continuity of the OCP value function is a direct result of choosing ingredients that ensure regularity and convexity of the optimisation problem.

Assumption 3.3 (K-Continuity of value function). *The value function J_i^o is class- \mathcal{K} continuous on the constraint sets and satisfies*

$$|J_i^o(z_1) - J_i^o(z_2)| \leq \mathcal{F}(|z_1 - z_2|),$$

with \mathcal{F} a class- \mathcal{K} function.

The above assumption is required to ensure that the value function of the optimal control problem is continuous, a property that facilitates the following robustness analysis. This assumption is less restrictive than requiring Lipschitz continuity, however it is still a reasonable source of conservativeness of the proposed approach. While this is easily satisfied in the presence of linear dynamics, there are examples where the continuity property can be compromised in some case of nonlinear systems [163]. Nevertheless, one can argue that the studied system behaviour is “similar enough” to a linear system, making the adoption of such assumptions reasonable.

Furthermore, it is assumed that the load perturbations are bounded between the sampling intervals.

Assumption 3.4 (Bounded load demand). *The maximum load demand is uniformly bounded in $P_i \in \mathbb{D}_i$, where $\mathbb{D}_i = \{P_i \in \mathbb{R}_{\geq 0} : P_i \leq P_i^{max}\}$.*

3.5. RECURSIVE FEASIBILITY

Therefore, the error of the prediction sequences between two consecutive time steps can be characterised as

$$|\mathbf{w}_i^+ - \mathbf{w}_i| = |w_i^+ - w_i| |\mathbb{1}_N|,$$

where $\mathbb{1}_N$ is an all-ones vector of N elements. This leads to

$$|\mathbf{w}_i^+ - \mathbf{w}_i| = \left| \frac{P_i^+}{v_i^+} - \frac{P_i}{v_i} + \sum_{j \in \mathcal{N}_i} \mathcal{L}_{ij} (v_j^+ - v_j) \right| \sqrt{N},$$

substituting for the discrete time model (3.15), and formulating a worst-case scenario for the current drawn by the load at each sampling interval, yields

$$|\mathbf{w}_i^+ - \mathbf{w}_i| \leq \left| \frac{P_i^{\max}}{v_{lb,i}} + \sum_{j \in \mathcal{N}_i} \mathcal{L}_{ij} \Delta T_i \hat{f}_j(v_j, u_j, w_j) \right| \sqrt{N}.$$

where $\hat{f}_j(\cdot)$ is the voltage dynamics of the j^{th} node. Due to the continuity of the dynamics over the constraint set and the fact that v_j and u_j lie in bounded sets, there exists a bound $\hat{f}_j(v_j, u_j, w_j) \leq B_j$ introduced by the NMPC- j that depends on the constraint sets. Therefore, a bound can be deduced for the error $\delta w_i = w_i^+ - w_i$ between the elements of the two consecutive disturbance sequences as,

$$|\delta w_i| \leq e_i^{\max},$$

$$\text{with } e_i^{\max} = \left(\left| \frac{P_i^{\max}}{v_{lb,i}} \right| + \Delta T_i \sum_{j \in \mathcal{N}_i} |\mathcal{L}_{ij}| |B_j| \right) \sqrt{N}.$$

Remark 3.2. *The uncertainty error can be reduced by either choosing a short sampling period, which is already a requirement for systems with fast dynamics, or appropriately choosing the input constraint set \mathbb{U}_i . This way a smaller error bound can be achieved.*

Assumption 3.5 (Bounded Disturbance perturbation). *The maximum disturbance error δw_i satisfies*

$$e_i^{\max} \leq \mathcal{F}^{-1}((\rho_i - \gamma_i)\beta_i), \quad (3.22)$$

with $\rho_i \in (\gamma, 1)$, $\gamma_i \in (0, 1)$ and positive constant β_i such that it defines a level set of the value function $\Omega_\beta = \{x_i: J_i^o(x_i, \mathbf{w}_i) \leq \beta_i\}$.

In the following, the convergence property of the value function from Prop. 3.2 is exploited to ensure recursive feasibility of the optimisation problem under changing disturbance sequences. Thus, a degree of robustness is introduced to the proposed control scheme, provided that the perturbations in the disturbance sequence evolution $w_i^+ = w_i + \delta w_i$ satisfy $\delta w_i \in \mathbb{D}_i \oplus \mathcal{DW}_i$ with $\mathcal{DW}_i = \{\delta w_i \in \mathbb{R}: |\delta w_i| \leq e_i^{\max}\}$. This is demonstrated in the next result.

3.5. RECURSIVE FEASIBILITY

Theorem 3.1 (Robustness to disturbance perturbations). *Suppose Assumptions 3.2-3.5 hold. Then, for any initial state satisfying $x_i \in \Omega_{\alpha,i} = \{x_i : J_i^o(x_i, w_i) \leq \alpha_i\} \subset \mathcal{X}_N(w_i)$ for some $\alpha_i > \beta_i > 0$, there exists a finite horizon length N^* , such that for all $N \geq N^*$ the set $\Omega_{\alpha,i}$ is positive invariant for the closed loop system (3.15) and $x_i^+ \in \mathcal{X}_N(w_i^+)$.*

Proof. Consider a state $x_i \in \Omega_{\alpha,i}$, then combining Proposition 3.2 with [161] wherein practical stability of MPC with turnpikes is shown, the following inequality is satisfied,

$$J_i^o(x_i^+, w_i) \leq \gamma J_i^o(x_i, w_i) + \mu_i(N) \quad (3.23)$$

where $\mu_i(N) : \mathbb{N} \rightarrow [0, \infty)$ and $\mu_i(N) \rightarrow 0$ as $N \rightarrow \infty$. Then, for a sufficient large N , it holds that $\mu_i(N) \leq \alpha_i(1 - \rho_i)$. Applying the continuity property of Assumption 3.3 results in

$$\begin{aligned} J_i^o(x_i^+, w_i^+) - J_i^o(x_i^+, w_i) &\leq \mathcal{F}(|w_i^+ - w_i|) \\ J_i^o(x_i^+, w_i^+) &\leq \mathcal{F}(|w_i^+ - w_i|) + J_i^o(x_i^+, w_i) \\ &\leq (\rho_i - \gamma_i)\alpha_i + \gamma_i J_i^o(x_i, w_i) + \mu_i(N) \end{aligned}$$

Using the fact that $J^o(x_i, w_i) \leq \alpha_i$ and Assumption 3.5,

$$\begin{aligned} J_i^o(x_i^+, w_i^+) &\leq (\rho_i - \gamma_i)\alpha_i + \gamma_i\alpha_i + \mu_i(N) \\ &\leq \alpha_i. \end{aligned}$$

Therefore, the value function remains within the set $\Omega_{\alpha,i}$, and thus $\Omega_{\alpha,i}$ is positive invariant for the composite dynamics,

$$\begin{aligned} x_i^+ &= H(x_i, u_i, w_i), \\ w_i^+ &\in \{w_i\} \oplus \mathbb{D}_i \oplus \mathcal{D}\mathcal{W}_i. \end{aligned}$$

Therefore, $x_i^+ \in \mathcal{X}(w_i^+)$ and applying this result recursively for all future states implies that the problem remains recursively feasible. \square

The decreasing property of the value function $J_i^o(\cdot, \cdot)$ is preserved provided that a large horizon N is chosen and the disturbance is bounded as described in Assumption 3.5. Essentially, in the absence of terminal ingredients, one requires a large prediction horizon N such that the monotonic decrease property of the value function is preserved. The disadvantage of this method is that the size of N is dependant on the specific case study parameters, however Theorem 3.1 guarantees the existence of a positive invariant set for the composite state trajectory. Furthermore, it is noted that one may choose the level set $J_i^o(x_i, w_i) \leq \alpha_i$ as the largest level set that satisfies the disturbance bound. It is important to highlight that the

resulting network voltage trajectory is not optimal. Indeed, this is the price one has to pay for adopting a distributed control scheme. Nevertheless, the above result shows robustness with respect to the update rate of the available information can be ensured and the value function inherits similar monotonic descent properties with an optimal trajectory resulting from solving the problem in a centralised fashion.

3.5.2 Stability of the Closed-Loop Dynamics

The stability analysis of the dynamics will follow the common principle of utilising the recursive feasibility property of the NMPC- i and using the value function as a Lyapunov function to drive the system trajectories to a neighbourhood of the desired setpoints. Then, the properties of the primary controller are exploited to establish convergence to the network setpoint x^s . This is demonstrated in the following result, where a local condition on the control parameters of each subsystem is derived to guarantee stability of the closed loop system under the proposed control scheme.

Theorem 3.2 (Stability of the closed loop dynamics). *Considering a setpoint $x_i^s = (\hat{v}_i, \hat{\sigma}_i)$ and a fixed power demand \bar{P}_i , the closed loop system is asymptotically stable with respect to x_i^s , if*

$$k_{p,i} > \frac{\bar{P}_i}{\hat{v}_i^2},$$

and

$$m_i < \frac{\hat{v}_i^2}{\bar{P}_i}$$

hold for all $i \in \mathcal{M}$.

Proof. The proof is split in two parts to distinguish whether the state is within the neighbourhood of the setpoint $\mathcal{B}_\epsilon(x_i^s)$ or not.

Case 1. $x_i \notin \mathcal{B}_\epsilon(x_i^s)$.

Following Theorem 3.1 the value function $J_i^o(\cdot, \cdot)$ satisfies

$$\begin{aligned} \theta_1(\|x_i - x_i^s\|) &\leq J_i^o(x_i, w_i) \leq \theta_2(\|x_i - x_i^s\|), \\ J_i^o(x_i^+, w_i^+) &\leq J_i^o(x_i, w_i) - \theta_3(\|x_i - x_i^s\|), \end{aligned}$$

for $\theta_1, \theta_2, \theta_3$ class \mathcal{K}_∞ functions. Then, following [155, Theorem 4.1], the value function is a Lyapunov function for the system with respect to the region $\mathcal{B}_\epsilon(x_i^s)$.

Case 2. $x_i \in \mathcal{B}_\epsilon(x_i^s)$.

In this case the properties of primary controller are exploited to show asymptotic stability of the states given a setpoint x^s . In the following, k_p, m, k_I, M, C are diagonal matrices with each (i, i) element being the respective parameter of the

3.5. STABILITY OF THE CLOSED-LOOP DYNAMICS

i^{th} node. Considering a steady state point $(\hat{v}, \hat{\sigma})$, with elements $\hat{v}_i \in (0, v_{\max})$ and $\hat{\sigma}_i \in (-1, 1)$, the Jacobian matrix of the overall system around this point can be computed as

$$J = \begin{pmatrix} C^{-1}(-k_p - Y) & C^{-1}M \\ -M^{-1}k_I (I_n - [\hat{\sigma}^2]) (I_{n_x} + mY) & 0_{n \times n} \end{pmatrix}.$$

The characteristic polynomial of the Jacobian can be reformulated into the form

$$|\lambda - J| = |\lambda^2 + \lambda A + B| = 0, \quad (3.24)$$

where

$$\begin{aligned} A &= C^{-1}(k_p + \mathcal{L} + D), \\ B &= C^{-1}k_I (I_n - [\hat{\sigma}^2]) (I_n + m(D + \mathcal{L})). \end{aligned}$$

The above is left multiplied by

$$\left| (I_n - [\hat{\sigma}^2])^{-1} k_I^{-1} C \right|$$

which results in

$$\left| (I_n - [\hat{\sigma}^2])^{-1} k_I^{-1} C \lambda^2 + \lambda \bar{A} + \bar{B} \right| = 0, \quad (3.25)$$

with

$$\begin{aligned} \bar{A} &= (I_n - [\hat{\sigma}^2])^{-1} k_I^{-1} (k_p + \mathcal{L} + D), \\ \bar{B} &= (I_n + m(D + \mathcal{L})). \end{aligned}$$

It is noted that according to Lemma A.2, the matrix \bar{A} is diagonalizable as it is the product of two positive definite matrices. Therefore, there exist a unitary matrix P such that $\bar{A} = P\Lambda P^{-1}$ holds, with Λ a diagonal matrix containing the eigenvalues of \bar{A} . Substituting in (3.25), this yields

$$\left| (I_n - [\hat{\sigma}^2])^{-1} k_I^{-1} C \lambda^2 + \lambda P \Lambda P^{-1} + \bar{B} \right| = 0. \quad (3.26)$$

Multiplying in left by P^{-1} and in right by P and using the fact that P is unitary results in the quadratic eigenvalue problem

$$\left| P^{-1} (I_n - [\hat{\sigma}^2])^{-1} k_I^{-1} C P \lambda^2 + \lambda \Lambda + P^{-1} \bar{B} P \right| = 0. \quad (3.27)$$

Then, according to Lemma A.1, in order for the eigenvalues of the Jacobian matrix to be negative, the matrix coefficients of (3.27) need to be positive-definite. The matrix $(I_n - [\hat{\sigma}^2])^{-1} k_I^{-1} C$ is indeed positive definite as it is a product of diagonal matrices with positive elements. The remaining coefficients are investigated separately:

3.5. STABILITY OF THE CLOSED-LOOP DYNAMICS

1. From the properties of the Laplacian matrix from Lemma A.4, its eigenvalues satisfy $\lambda_1 = 0 < \lambda_2 \leq \dots \leq \lambda_n$. As k_p , \mathcal{L} , and D are symmetric matrices and $\lambda_{\min}(\mathcal{L}) = 0$, the following necessary scalar condition can be derived to enforce positive definiteness of Λ and respectively \bar{A} ,

$$k_{p,i} > \frac{\bar{P}_i}{\hat{v}_i^2}.$$

2. In order for $\bar{B} \succ 0$ the following must hold,

$$I_n + mD + m\mathcal{L} \succ 0$$

Again, using Lemma A.4, the above can be translated into the scalar condition

$$m_i \frac{\bar{P}_i}{\hat{v}_i^2} < 1$$

or equivalently,

$$m_i < \frac{\hat{v}_i^2}{\bar{P}_i}.$$

□

It is clear from the proof of Theorem 3.2, that the monotonic decent property of the value function is required to deduce convergence of the nodal state to a ball around the setpoint, *i.e.* $x_i \in \mathcal{B}_\epsilon(x_i^s)$. Therefore, it is necessary for Theorem 3.1 to hold in order to establish asymptotic stability of the closed loop dynamics. A point of careful consideration is whether an existence of the solution to the optimisation problem (3.14) exists. As highlighted before, one needs to guarantee that a solution does in fact exist. The analysis demonstrated here is required to achieve this property, where one then is simply required to follow the tuning condition formulated in this section and choose a strictly convex nodal cost function $\ell_i(\cdot)$ in (3.14) to ensure existence of a unique minimum extreme point. The following proposition shows that the properties of the proposed control scheme ensure satisfaction of the coupled constraints, see Fig. 3.3.

Proposition 3.3 (Coupled constraint satisfaction). *Consider the pair of neighbouring nodes (v_i, v_j) with $j \in \mathcal{N}_i$ and denote the coupled constraint of the edge $\epsilon = (i, j)$ as \mathbb{X}_ϵ . If, at some sampling time k , the states satisfy $(v_i, v_j) \in \mathcal{B}_\zeta \subseteq \mathbb{X}_\epsilon$, with \mathcal{B}_ζ a ball of radius $\zeta \geq 0$, then applying the proposed control law implies that at time $k + 1$ it holds that $(v_i^+, v_j^+) \in \mathbb{X}_\epsilon$.*

Proof. As a consequence of Theorem 2, the distance of a state $x_{0,i}$ from the setpoint $x_{s,i}$ is bounded from below by zero and upper bounded by $d(x_{0,i}, x_i^s)$, where $d(\cdot)$

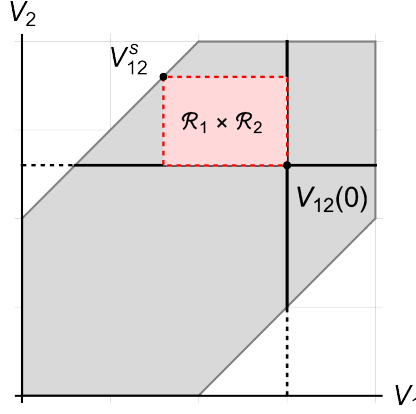


Figure 3.3: Coupled constraint and reachability sets for a two-node system. The product of the resulting two reachability sets is always within the constraint set.

denotes the euclidean distance function. In addition, the one-step reachable set of the i^{th} local dynamics, for some initial state $x_{0,i}$ and current disturbance value w_i , is given by

$$\mathcal{R}_i(x_{i,0}) = \{x_i \in \mathbb{R} : x_i = H(x_{i,0}, u_i, w_i^+), u_i \in \mathbb{U}_i, w_i^+ \in \{w_i\} \oplus \mathbb{D} \oplus \mathcal{D}\mathcal{W}_i\}$$

For the two neighbouring nodes of an edge $\varepsilon = (i, j)$, the Cartesian product of their respective one-step forward reachable sets $\mathcal{R}_i(x_{i,0})$ and $\mathcal{R}_j(x_{j,0})$ forms a two-dimensional trapezoid $\mathcal{T}_\varepsilon = \mathcal{R}_i \times \mathcal{R}_j$ on the voltage subspace. Due to the monotonic decent property of the state trajectory with respect to the voltage setpoint $v_{s,i}$, the trapezoid is characterised by the vertices $p_1 = (v_i^s, v_j^s)$, $p_2 = (v_i^s, v_{0,j})$, $p_3 = (v_{0,i}, v_j^s)$ and $p_4 = (v_{0,i}, v_{0,j})$. Therefore, feasibility of the setpoint $v_{s,i}$ implies that $\mathcal{T}_\varepsilon \subseteq \mathbb{X}_\varepsilon$ and the problems remains recursively feasible. This completes the proof. \square

The proof of Proposition 3 reveals that the proposed control architecture guarantees satisfaction of the time varying coupled constraints at all times $t > 0$. This result is demonstrated in Fig. 3 where the constraint set is depicted by the gray shaded area. Consider two neighbouring nodes, denoted by v_1 and v_2 respectively. For a initial state $v_{12}(0)$ and a setpoint v_{12}^s , the local constraint set of node 1, \mathbb{X}_1 , is depicted by the horizontal black solid line and the local constraint set of node 2, \mathbb{X}_2 , by the vertical solid line. Due to the monotonic descend property of the value function, the distance between the initial state and the terminal state is decreasing and thus the one step forward reachability set of each node is all points contained in the subspace defined by the coupled constraint set X_ε of the edge $\varepsilon = (i, j)$.

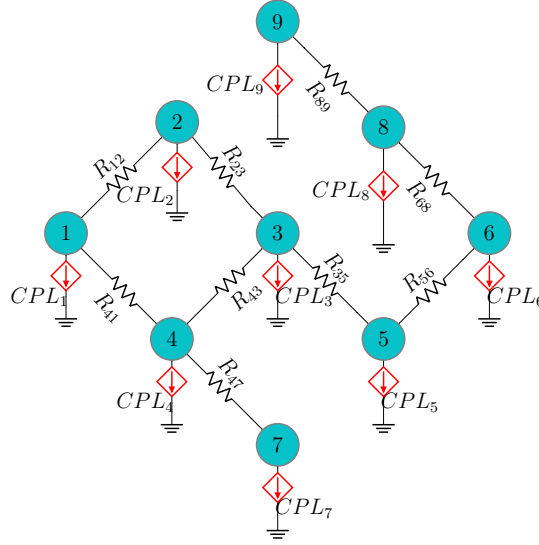


Figure 3.4: A MG network with nine converters and seven local loads

3.6 Simulation Results

This case study considers a MG with topology depicted in Fig. 3.4 with set of edges

$$\mathcal{E} := \{(\mathcal{V}_1, \mathcal{V}_2), (\mathcal{V}_1, \mathcal{V}_4), (\mathcal{V}_2, \mathcal{V}_3), (\mathcal{V}_3, \mathcal{V}_4),$$

$$(\mathcal{V}_3, \mathcal{V}_5), (\mathcal{V}_4, \mathcal{V}_7), (\mathcal{V}_5, \mathcal{V}_6), (\mathcal{V}_6, \mathcal{V}_8), (\mathcal{V}_8, \mathcal{V}_9)\}.$$

The aim of the control system is to keep the voltages close to the rated voltage $\bar{v} = 100V$ and the converter currents below $i_{\max} = 10A$, while satisfying the local power demand. This translates into $\ell_{\text{eco}} = (v - \bar{v})^T (v - \bar{v})$ and $\mathbb{S}(P) = \{v \in \mathbb{R}^n : Y(P)v \leq i_{\max}\}$. These requirements imply that each converter can maintain its voltage equal to the rated when the load demand is equal or below $P_i = 1000W$. The upper supervisory layer computes the setpoints according to these economic criteria, while the lower layer drives the closed loop system to these setpoints without violating the line power constraints, see Fig. 3.5.

The voltage evolution changes according to the power demand in order to satisfy each continuously changing local load as depicted in Fig. 3.6. This is done either by solely using the local converter or utilising neighbouring converters when this is required. At time $t = 0.05s$ both CPL_1 and CPL_3 power demands exceed the threshold of $P_i = 1000W$ and thus require input currents from the neighbouring nodes. As a result nodes 2 and 3 increase their voltage, while node 1 voltage drops. Then, at time $t = 0.35s$ the load demand of CPL_9 exceeds the rated power of the ninth node and the setpoints are adjusted accordingly to alleviate the necessary portion of the power demand from the neighbouring node. At $t = 0.55s$ the line between node 1 and 2 operates at maximum power capacity and the voltages evolve

3.7. CONCLUSIONS

Parameter	Value
C [μF]	{200, 150, 100, 140, 150, 100, 140, 150, 100}
L [mH]	{10, 15, 11, 6, 8, 10, 9, 10, 11}
$R_{ij}[\Omega], (i, j) \in \mathcal{E}$	{1, 1.5, 0.5, 0.6, 0.5, 0.6, 0.5, 0.9, 1}
m_i	0.42
$k_{p,i}$	200
M_i	$21 \cdot 10^3$
$k_{I,i}$	$2 \cdot 10^7$

Table 3.1: Network component and control parameter values.

to new setpoints in order to avoid constraint violation. The line powers and the respective bounds are depicted in Fig. 3.7 showing that the coupled constraints are satisfied at all times. Hence, the theoretical analysis of the proposed hierarchical control approach is validated, maintaining the node voltages and line currents within the required ranges at all times. In addition, following the results of Section 3.3, the closed loop behaviour is independent of the number of nodes in the network, which ensures the depicted results can be extended to topologies with additional nodes. The network component values are provided in Table 3.1.

It can be seen from Fig. 3.5 that each voltage trajectory follows close to its respective reference, which is a result of the requirement for a small sampling time to accommodate the distributed setting. This is a source of conservativeness in this proposed approach, stemming from the requirement to bound the disturbance error according to equation (3.22). In order to practically ensure that the effect of the error does not affect the descent of the value function, the sampling time must be chosen sufficiently small. This computational burden is partially alleviated in the following chapters by adopting a separate control design to counteract the effect of the load.

3.7 Conclusions

A detailed framework for developing and analysing a hierarchical control scheme for DC Microgrids subject to coupled constraints was proposed in this chapter. A primary control level controller was presented that introduces boundedness and local stability properties to the closed loop dynamics. Then, a supervisory controller was formulated to achieve economic operation of the network. This was presented in two layers. The upper layer computes the feasible economic targets by considering the desired constraint sets. Then, in the lower layer, a distributed NMPC approach

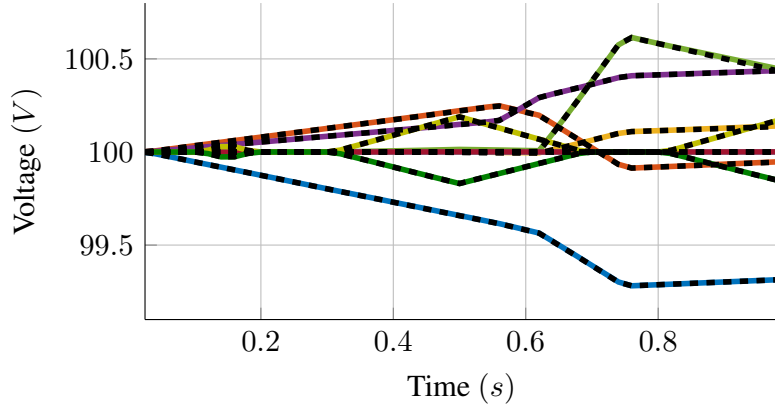


Figure 3.5: Converter voltage trajectories of Node 1 (—), Node 2 (—), Node 3 (—), Node 4 (—), Node 5 (—), Node 6 (—), Node 7 (—), Node 8 (—), Node 9 (—), and setpoints (---) of all converter subsystems with the use of the proposed control scheme.

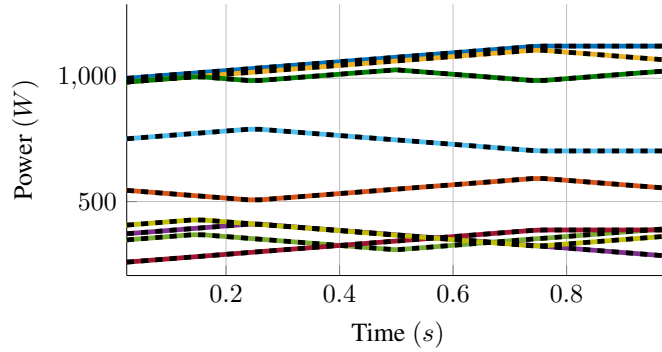
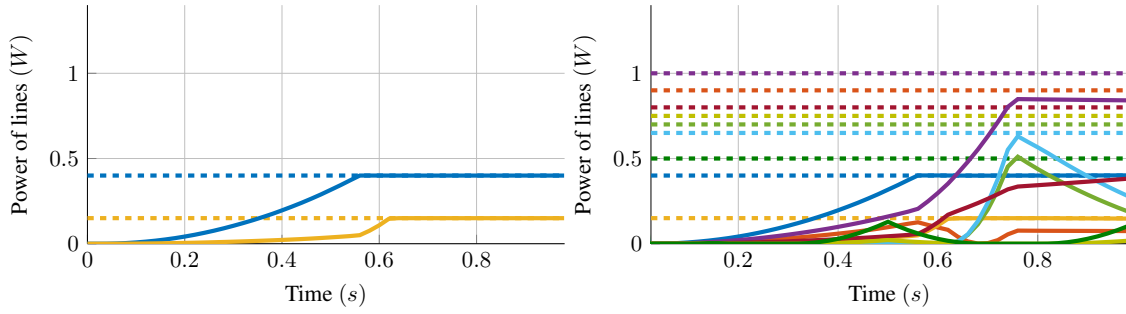


Figure 3.6: Power supply to CPL_1 (—), CPL_2 (—), CPL_3 (—), CPL_4 (—), CPL_5 (—), CPL_6 (—), CPL_7 (—), CPL_8 (—), CPL_9 (—) and respective power demands (---)

was proposed to drive the system trajectories to the economic targets computed in the upper layer. In Sections 3.5.1 and 3.5.2, analytic condition on the tuning parameters, and the setup of the optimisation problem, were provided such that the optimal control problem remains recursively feasible and the closed loop system admits asymptotically stable equilibrium points. Furthermore, it was shown that adoption of the proposed distributed NMPC scheme leads to guaranteed satisfaction of the coupled constraints among the neighbouring subsystems. The theoretic results of the proposed control scheme were illustrated in a simulated scenario consisting of an isolated DC Microgrid with nine nodes, where a CPL was connected in parallel to each local node.

3.7. CONCLUSIONS



(a) Lines operating at maximum power capacity

(b) All lines among the nodes

Figure 3.7: Line power trajectories and the respective boundaries for $Line_{12}$ (—), $Line_{23}$ (—), $Line_{34}$ (—), $Line_{41}$ (—), $Line_{35}$ (—), $Line_{56}$ (—), $Line_{47}$ (—), $Line_{68}$ (—), $Line_{89}$ (—).

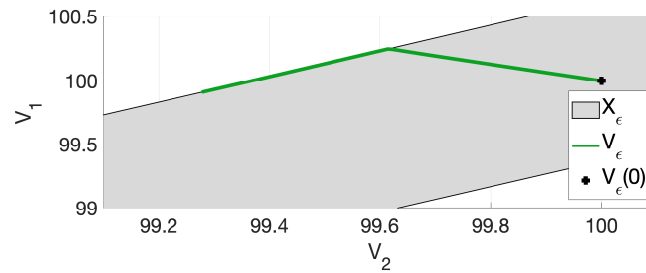


Figure 3.8: Trajectory evolution of node 1 and node 2 voltages within the coupled constraint set.

Chapter 4

Tube-based Control of DC Microgrids

A substantially limiting factor in the development of a distributed Microgrid control scheme is the need for frequent communication exchange among the individual subsystems. As it was demonstrated in the previous chapter, the communication requirement can be reduced to a non-iterative, neighbour-to-neighbour structure, by leveraging the inherent robustness properties of the nominal MPC framework. However, by including load demand in the rate-of-change bound of the disturbance term, the dependence on inherent robustness can result in a rather conservative requirement, limiting the range of possible applications. In order to overcome this problem, the analytic properties of the load model need to be exploited in the control design process. More specifically, by studying the induced geometric behaviour of the load on the network dynamics, a robust positive invariant set can be constructed, such that the state trajectory is bounded within this set at all times. In addition, as it will be shown in this chapter, the centre of this set lies upon a generated prediction trajectory, termed “nominal” due to its independence from the load demand fluctuations. This ultimately leads to a tube-like behaviour, where the state trajectories are uniformly bounded in a compact set, the centre of which follows a desired path in the state space. Guaranteeing this, allows the development of a supervisory distributed control scheme, where the error bound between two consecutive prediction trajectories only relies upon the information exchange among the network nodes. Therefore, this leads to a less conservative assumption regarding the effect of the external inputs on the closed loop dynamics and the error bound between the predicted and true state trajectory.

This chapter considers the Microgrid network as an uncertain system, where the uncertainty rises from the unknown perturbations of the load demand, and proposes a control scheme that demonstrates the aforementioned desired properties.

In particular, the effect of the CPL behaviour is analysed to propose a control law for the uncertain nodal dynamics, such that the state is guaranteed to remain close to a generated nominal trajectory. This nominal trajectory is shown to be the solution of a nominal system, where the CPL demand is kept at a constant value. Regulation of the nominal system is carried out through an MPC scheme, that guarantees constraint satisfaction of the uncertain nodal dynamics. Ultimately, the main contribution of this chapter is the development of a Tube NMPC for a particular class of nonlinear dynamics. This fills the gap between similar approaches that address different types of nonlinear systems, such as [164, 165], and reduces possible conservativeness that can arise from adopting a Tube NMPC approach that has been developed for generic nonlinear dynamics, e.g. [142, 166]. Furthermore, it is noted that even though this approach is developed for the case of DC Microgrids, the proposed controller can be adopted for nonlinear systems with similar model structure, where the uncertainty enters in a parametric way, *i.e.* the system model is of the form

$$\dot{x} = Ax + Bu + \frac{w}{x},$$

where $A, B \in \mathbb{R}^{n \times n}$ and w is the exogenous disturbance.

In the following, Section 4.1 formally defines the problem and outlines the proposed control scheme structure. This approach considers both the output voltage and inner current states of the converter, providing a unified constrained-based control scheme. To this aim, the inner current controller is proposed in Section 4.2, while Section 4.3 formulates the voltage controller and analyses the theoretic properties of the closed loop system. By employing control Lyapunov functions, Section 4.4 proves the asymptotic stability of the cascaded voltage-current dynamics and provides a region-of-attraction estimation of the respective equilibrium points. In Section 4.5, the theoretic properties of the proposed control scheme are illustrated in a simulated scenario, while Section 4.6 provides some concluding remarks on the results of this chapter.

4.1 Problem Statement

Similar to the previous chapter, the problem of an islanded meshed DC Microgrid is considered, see Fig. 4.1. The network is composed of n number of power converters, where each i^{th} converter is connected to local CPL, with $i \in \mathcal{M} = [1, 2, \dots, n]$. The main control objectives are introducing system robustness with respect to load demand fluctuations and ensuring that the system dynamics are restricted in a predefined operational range.

In order to achieve a unified control approach, the original buck converter dy-

4.1. PROBLEM STATEMENT

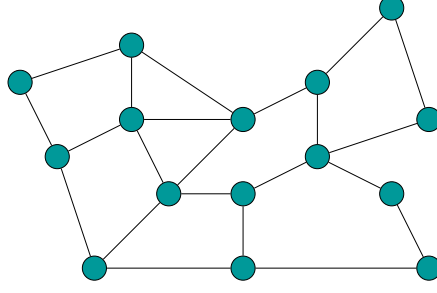


Figure 4.1: Network topology of a meshed islanded DC MicroGrid.

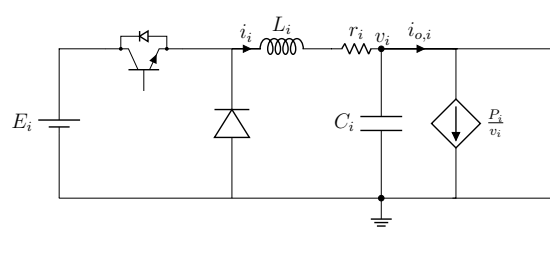


Figure 4.2: Node circuit modelled as a DC/DC Buck converter connected in parallel to a local constant power load.

namics are considered, with circuit diagram depicted in Fig. 4.2. Following this, the Kirchhoff model of the network dynamics is given by

$$L \frac{di}{dt} = \nu E - ri - v, \quad (4.1a)$$

$$C \frac{dv}{dt} = i - i_o. \quad (4.1b)$$

The capacitance and inductance of each node are collected into diagonal matrices $L \in \mathbb{R}^{n \times n}$ and $C \in \mathbb{R}^{n \times n}$ respectively, $r \in \mathbb{R}^{n \times n}$ denotes a diagonal matrix collecting the node parasitic resistances, and $E \in \mathbb{R}^{n \times n}$ denotes the input voltage of the converters. The states of the system are the capacitor voltage $v \in \mathbb{R}^n$ and the inductor current $i \in \mathbb{R}^n$, while the duty ratio of the switching mechanism $\nu \in \mathbb{R}^n$, with $\nu_i \in [0, 1]$, is regarded as the input of the system. Contrary to the previous chapter, in this case the inner converter current model is included in the studied system, where the aim is to propose a unified control scheme that guaranteed constraint satisfaction for both the voltage and current states.

The connection between the nodes of the graphs can be represented by the weighted adjacency matrix $A(R) \in \mathbb{R}^{n \times n}$, where $a_{ij} = R_{ij}^{-1}$, with R_{ij}^{-1} the admittance of the line between nodes i and j , and $a_{ij} = 0$ if the edge (i, j) is not incident. The full topology of the network is represented by the Laplacian matrix $\mathcal{L} = [A(R)\mathbf{1}_n] - A(R)$. Therefore, the output network current can be modelled as

$$i_o = \mathcal{L}v + [v]^{-1}P, \quad (4.2)$$

4.1. PROBLEM STATEMENT

where $P \in \mathbb{R}^n$ is the power demand vector. To facilitate the development of a robust control strategy, the maximum load demand is assumed to be bounded. This is formalised in the following assumption.

Assumption 4.1. *The load demand lies in a polytopic set, i.e. $P \in \mathbb{P} \subset \mathbb{R}^n$, where $0 \in \text{int}(\mathbb{P})$.*

In addition, the system is subjected to operational constraints, *i.e.* desired regions of voltage and current operation, denoted as \mathbb{X} and \mathbb{I} respectively. In order to ensure a smooth region of operation, the following assumption is invoked.

Assumption 4.2. *The constraint sets \mathbb{X} , \mathbb{I} are polytopic and compact sets, where $0 \in \text{int}(\mathbb{I})$.*

It is common to require the inner current and output voltage of a converter to operate in a predefined range, usually in the form of a bounded deviation from a rated value. The above assumptions translate this requirement into a mathematical notion, as well as ensure that the load demand acquires a finite maximum value. This property is used to ensure convexity of the optimization problem that is introduced in later sections. In addition, a consequence of this assumption is that the origin is not included in the voltage constraint set. Thus, the voltage dynamics are smooth over the constraint set, which allows the consideration of the respective state subspace as a Riemannian manifold M embedded in \mathbb{R}^n . Compactness of the constraint set also implies that any closed subset of \mathbb{X} is also compact. As a result, any subspace of the metric space (\mathbb{X}, d_R) has the Heine-Borel property, *i.e.* the metric space is compact and complete. This is a particularly useful property that will assist the following sections to establish convergence of the system flow.

Linearity of the load model in (4.2) with respect to the load demand P , allows for the separation of the load current into a nominal current, depending on an a-priori known nominal load \bar{P} , and an uncertain one parametrised by a deviation, *i.e.* $\delta P = P - \bar{P}$. Then, the set of deviations from the nominal load demand is defined as a disturbance set

$$\mathbb{W} := \{\delta P \in \mathbb{R}^n : \bar{P} + \delta P \in \mathbb{P}\} \quad (4.3)$$

In addition, as a consequence of Assumption 4.1, the disturbance set \mathbb{W} inherits the same properties of \mathbb{P} .

Following this problem formulation, the aim now becomes introducing system robustness with respect to fluctuations of the load demand δP from the known, constant value \bar{P} . To achieve this, a state-limiting PI controller is employed for the regulation of the current dynamics, which introduces boundedness of each converter

inner current state i_i in a desired set. Then, the uncertain voltage dynamics are “split” into a nominal subsystem, where the load demand attains a constant value \bar{P} at all times, and an error subsystem, characterising the error between the uncertain and the nominal subsystems. Finally, conditions on the choice of the tuning parameters are introduced, such that the distance between the nominal and the uncertain voltage trajectories is bounded, the network satisfies the desired operational constraints and the stability of the overall system is guaranteed.

4.2 Inner Current Control

The current controller regulates the input current to a desired setpoint by adjusting the duty ratio ν in (4.1a). It is common in the literature to use some form of a saturated controller in order to achieve overcurrent protection of each power converter. To this aim, the state-limiting PI of the previous chapter is adopted, in order to ensure smoothness of the dynamics and avoid performance degradation or instabilities caused by traditional saturated controllers. Moreover, the properties of this controller facilitates an analytic procedure to tune the control parameters, such that the closed-loop system obtains a desired behaviour. The parametrisation of the duty ratio is given by

$$\begin{aligned}\nu &= (v - k_p i + D\sigma)E^{-1} \\ D\dot{\sigma} &= k_I(\mathbb{1}_n - \sigma^2)(\hat{i} - i).\end{aligned}\tag{4.4}$$

resulting in closed loop current dynamics,

$$\begin{aligned}L\frac{di}{dt} &= -(k_p + r)i + D\sigma \\ D\dot{\sigma} &= k_I(\mathbb{1}_n - \sigma^2)(\hat{i} - i).\end{aligned}\tag{4.5}$$

where \hat{i} is the reference current, D , k_p , $k_I \in \mathbb{R}^{n \times n}$ are the tuning parameters and σ is the controller introduced integrator state. As shown in the following proposition, this control parametrization restricts the flow of the closed loop system in a positive invariant subset of the constraint set $\mathbb{C} \subseteq \mathbb{I}$.

Proposition 4.1 (Current limitation). *For each node $i \in \mathcal{M}$, the set*

$$\mathbb{C} = [-I_{\max}, I_{\max}] \times [-1, 1],\tag{4.6}$$

with $I_{\max, i} = \frac{D_i}{k_{p, i}}$, is positive invariant for the current dynamics (4.5).

Proof. Similar to the proof of Proposition 3.1. □

Therefore, the desired behaviour of the inner current loop can be achieved by adjusting the tuning parameters according to the desired bound $I_{\max,i} = \frac{D_i}{k_{p,i}}$. It is noted that the choice of the inner current bound needs to be made according to the required voltage constraint set \mathbb{X} , in order to satisfy the inherent requirement $v_i \in (0, 1)$ from (4.4) for all $(i_i, \sigma_i) \in \mathbb{C}_i$ and $v_i \in \mathbb{X}_i$.

4.3 Voltage Control

This section formulates the robust control scheme for the voltage node dynamics. The original system is “split” into a nominal and an error subsystem. The nominal subsystem assumes a time-invariant load demand \bar{P} , but *time-varying* load current $i_{load}(v) = [v]^{-1}\bar{P}$, while the error subsystem captures the difference between the nominal and the true voltage trajectories. In the following, it will be shown that the uncertain part of the dynamics can be bounded within a robust positive invariant set, by leveraging the geometric properties of the closed loop error subsystem. Then, the nominal dynamics act as a driving subsystem, regulating the true system to some desired reference behaviour. The notion of positive invariant sets will be used to guarantee constraint satisfaction of the nominal subsystem, which, by an appropriate parametrization of the constraint sets, ensures constraint satisfaction of $\mathbb{Y} = \mathbb{X} \times \mathbb{C}$ by the uncertain dynamics. In this chapter, it is assumed that the current operates in a faster time-scale than the voltage. As it was mentioned in the previous chapter, this is a common assumption in the literature as it allows to study each of the dynamic components separately and thus significantly simplifies the analysis. This leads to a cascaded structure, where the input current in (4.1b) represents a piecewise constant reference and is considered as the input to the voltage dynamics. Following [167, Theorem 4.4] and [168, Appendix A] the reachability, and consequently convergence, properties are preserved under the replacement of integrable smooth controls with piecewise constant controls. Following the boundedness of the inner current solution from Prop. 4.1, the time-scale separation assumption can be formally defined.

Assumption 4.3 (Time-scale separation). *The network parameters satisfy*

$$\max_{i \in \mathcal{M}} \left\{ \frac{L_i}{k_{p,i} + r_i}, \frac{k_{p,i}}{k_{I,i}} \right\} \ll \min_{i \in \mathcal{M}} \left\{ \frac{C_i P_i}{(I_{\max,i})^2} \right\}$$

Remark 4.1. *As a consequence of Assumption 4.1, the local load demand P_i is bounded and thus one can enforce the time-scale separation of the node dynamics by an appropriate selection of the tuning parameters, as shown in Assumption 4.3, where the explicit time constants are derived using singular perturbation analysis. The interested reader is referred to [155, Chapter 11] for a detailed analysis.*

4.3.1 Formulation and boundedness of the error dynamics

Following Assumption 4.3, the node voltage dynamic can be written as

$$C\dot{v} = -\mathcal{L}v - [v]^{-1}\bar{P} - [v]^{-1}\delta P + \hat{i}. \quad (4.7)$$

Then, in order to separate the nominal part of the dynamics from the uncertain, an error term is defined as $e = v - z$. The objective is to use the nominal state z as a driving state of the system's flow $\phi_v(\cdot)$, while restricting the effect of the disturbance such that the distance between the flow of the uncertain system and the nominal satisfy $d_R(\phi_v, \phi_z) \leq \varepsilon$ for some $\varepsilon > 0$. To this aim, the proposed control policy is

$$\hat{i}(e) = -Ke + u \quad (4.8)$$

where K is a scalar matrix of the form $K = kI_n$ for some scalar gain $k \in \mathbb{R}_{>0}$, and u is the nominal positive input that will be formally defined later. Then, isolating the nominal part of (4.7), results in

$$C\dot{z} = -\mathcal{L}z - [z]^{-1}\bar{P} + u. \quad (4.9)$$

Therefore, the evolution of the error dynamics can be described by the ordinary differential equation

$$C\dot{e} = -\mathcal{L}e - Ke - [e + z]^{-1}\bar{P} + [z]^{-1}\bar{P} - [e + z]^{-1}\delta P. \quad (4.10)$$

The above can be compactly expressed by the vector field map $\gamma: M \rightarrow TM$,

$$C\dot{e} = \gamma(e; z) \quad (4.11)$$

where for a constant power demand deviation $\delta\hat{P}$ and converged nominal dynamics to some point \hat{z} , yields

$$\gamma(\hat{e}; \hat{z}) = 0. \quad (4.12)$$

In order to simplify the notation of the following sections, the parameter dependence of the vector field $\gamma(e; z)$ on the nominal state z will be implicitly assumed by simply writing $\gamma(e)$. Many studies have been focused on the existence of real solutions for the voltage equilibrium map usually deriving a necessary condition to be satisfied by the system parameters, see for example [118]. Therein, it is shown that if the necessary conditions are met, the equilibrium map is a diffeomorphism where a high and a low voltage solution exist, see [169] or [64]. Note that $\gamma(\hat{e}) = 0$ is the result of the state transformation $v = e + z$, similar results with the voltage v equilibrium map can be obtained for $\hat{e} = \gamma^{-1}(0)$. Therefore, the discontinuity of the true voltage dynamics is translated to the critical point $e = -z$ of the error state space. The

4.3. FORMULATION AND BOUNDEDNESS OF THE ERROR DYNAMICS

second solution of $\gamma(\hat{e}) = 0$ is then the steady state displacement caused by the load demand perturbations δP between the true voltage trajectory and the nominal. In the following, the imposed properties of the vector field $\gamma(\cdot)$ in an area around the origin are used to restrict the error flow ϕ_e in a positive invariant set. Considering the solution of $\hat{e} = \gamma^{-1}(0)$ closest to the origin, the maximum displacement due to the load demand can be found by

$$e^m = \max_{\delta P \in \mathbb{W}} \left(\|\gamma^{-1}(0)\| \right). \quad (4.13)$$

Next, one can define the polytopic set

$$N := \{e \in M : Ae \leq \xi(e^m)\} \quad (4.14)$$

where $A = [I_n - I_n]^\top$ and $\xi(e^m) = [\mathbf{1}_n e^m \mathbf{1}_n e^m]^\top$, that is the set N is a n -dimensional “box” around the origin. A question now arises; Under which conditions does the system guarantee the desired theoretic properties, *i.e.* existence of a unique solution of the error dynamics in N , as well as positive invariance of N ? The former is addressed in the following result.

Lemma 4.1 (Lipschitz continuity). *Consider the error dynamics given in (4.10) and bounded positive nominal voltage $\underline{z} \leq z \leq \bar{z}$. Given a constant power load demand $\hat{P} \in \{\bar{P}\} \oplus \mathbb{W}$ and a scalar positive definite matrix K , the map $\gamma(\cdot)$ is Lipschitz continuous on N , with Lipschitz constant*

$$\mathcal{K} = \left| \lambda_{\max} \left(-K + [-\mathbf{1}_n e^m + \underline{z}]^{-2} [\hat{P}] \right) \right|.$$

Proof. The gradient derivative of $\gamma(\cdot)$ for a constant load demand $\hat{P} \in \{\bar{P}\} \oplus \mathbb{W}$ yields

$$\nabla \gamma = -(\mathcal{L} + K) + [e + \hat{z}]^{-2} [\hat{P}].$$

Due to the fact that \underline{z} and e^m are positive values, the matrix ℓ^2 – norm is given by

$$\begin{aligned} \|\nabla \gamma\|_{\ell^2} &= \sup_{e \in N} \|\nabla \gamma\|_{\ell^2} \\ &= \left\| -(\mathcal{L} + K) + [-\mathbf{1}_n e^m + \underline{z}]^{-2} [\hat{P}] \right\|_{\ell^2} \\ &\leq \left\| -(\mathcal{L} + K) + [-\mathbf{1}_n e^m + \underline{z}]^{-2} [\hat{P}] \right\|_{\ell^2}. \end{aligned}$$

Let $\mathcal{K} = \left\| -(\mathcal{L} + K) + [-\mathbf{1}_n e^m + \underline{z}]^{-2} [\hat{P}] \right\|_{\ell^2}$, where it is noted that the resulting matrix within the norm is symmetric. Then, for a symmetric matrix the largest singular value is given by its spectral radius, *i.e.*

$$\mathcal{K} = \left| \lambda_{\max} \left(-(\mathcal{L} + K) + [-\mathbf{1}_n e^m + \underline{z}]^{-2} [\hat{P}] \right) \right|.$$

4.3. FORMULATION AND BOUNDEDNESS OF THE ERROR DYNAMICS

By the properties of the Laplacian matrix, it holds that $\lambda_n \geq \dots \geq \lambda_2 \geq \lambda_1 = 0$ and thus $\lambda_{\max}(-\mathcal{L}) = 0$. The above takes the form,

$$\mathcal{K} = \left| \lambda_{\max} \left(-K + [-\mathbf{1}_n e^m + \underline{z}]^{-2} [\hat{P}] \right) \right|.$$

This establishes the desired upper bound on the norm of the gradient, *i.e.* $\|\nabla\gamma\|_{\ell^2} \leq L$. Therefore, for two infinitesimally different $e_1, e_2 \in N$ and a $\xi \in (e_1, e_2)$, an application of the mean value theorem [170, Section 12.11] states

$$\begin{aligned} \|\gamma(e_1) - \gamma(e_2)\|_{\ell^2} &= \|\nabla_{\xi}\gamma\|_{\ell^2} \|e_1 - e_2\|_{\ell^2} \\ &\leq \mathcal{K} \|e_1 - e_2\|_{\ell^2}. \end{aligned}$$

Therefore, the vector field is Lipschitz continuous on N with Lipschitz constant \mathcal{K} . \square

Having established the Lipschitz continuity of the system flow inside N , the stability properties of the equilibrium $\hat{e} \in N$ can now be investigated. It can be shown that the equilibrium point bounds any voltage trajectory with initial state within N . This is demonstrated in the following result.

Proposition 4.2 (Stability and Positive Invariance of the error dynamics). *For bounded local nominal dynamics $\underline{z}_i \leq z_i \leq \bar{z}_i$, the error dynamics of every node $i \in \mathcal{N}$, admit an asymptotically stable equilibrium point in N , if the local feedback gain satisfies*

$$K_{ii} > \max \left\{ \frac{\bar{P}_i}{\underline{z}_i e^m}, \frac{P_i^m}{(\underline{z}_i - e^m)^2} \right\}$$

with $P_i^m = \max(|\bar{P}_i + \delta P_i|)$ and $\delta P_i \in \mathbb{W}_i$. In addition, the set N is positive invariant under the flow of the system $\phi_e(e^0, t)$, for all $t > 0$ and $e^0 \in N$.

Proof. For any equilibrium point $\hat{e} \in N$ and respective constant load demand \hat{P} , the resulting Jacobian matrix takes the form

$$J = -(\mathcal{L} + K) + [(z + \hat{e})^2]^{-1} \hat{P}.$$

In order for the equilibrium point \hat{e} to be stable, the respective Jacobian matrix J needs to be Hurwitz, *i.e.* to have negative eigenvalues. Since J is also a symmetric matrix, using the fact that $\lambda_{\max}(-\mathcal{L}) = 0$, the largest eigenvalue $\lambda_{\max}(J)$ is given by

$$\lambda_{\max}(J) = \lambda_{\max}(-K + [(z + \hat{e})^2]^{-1} \hat{P}).$$

Hence, it suffices to show that $\lambda_{\max}(J) < 0$, *i.e.*

$$-K_{ii} + \frac{\hat{P}_i}{(z_i + \hat{e})^2} < 0.$$

4.3. FORMULATION AND BOUNDEDNESS OF THE ERROR DYNAMICS

In order to ensure that a similar condition holds for any $\hat{e} \in N$ and any $\hat{P} \in \mathbb{P}$, it is noted that

$$\frac{P_i^m}{(\underline{z}_i - e^m)^2} \geq \frac{\hat{P}_i}{(z_i + \hat{e}_i)^2},$$

holds for all $\hat{e} \in N$. Therefore, a condition on a worst-case scenario can be formulated as

$$K_{ii} > \frac{P_i^m}{(\underline{z}_i - e^m)^2},$$

where the nominal voltage is bounded as $\underline{z}_i \leq z_i \leq \bar{z}_i$, with $\underline{z}_i > 0$. Following the definition of N , for some point at ∂N it follows that $e_i = e^m$ for $i \in \mathcal{M}$ and $e_j \leq e^m$ for $j \neq i$. Now, considering a quadratic function of the state $V(e) = \frac{1}{2}e^\top C e$, the aim becomes showing that its time derivative $\dot{V}(e)|_{e \in \partial N}$ is negative outside the set N . Since $e_i \leq e^m$ for all $i \in \mathcal{M}$, it suffices to show $\dot{V}_i|_{e_i \in \partial N_i}$ is non-positive in both cases of $e_i = e^m$ and $e_i = -e^m$, *i.e.* it is required for

$$\begin{aligned} \dot{V}|_{e_i \in \partial N} &= e_i \gamma_i(e_i) \\ &= e_i \left(-(\mathcal{L}_{ii} + K_{ii})e_i - \sum_{j \in \mathcal{N}_i} \mathcal{L}_{ij}e_j + \frac{\bar{P}_i}{z_i} - \frac{P_i}{e_i + z_i} \right) \end{aligned}$$

to be non-positive. The analysis is bifurcated into two cases: (a) $e_i = e^m$ and (b) $e_i = -e^m$. In case of (a) the term inside the parenthesis needs to be negative. Since $e^m \geq e_j$, the diagonal Laplacian term dominates the off-diagonal elements. Comparing the lower bound of the feedback K_{ii} , it can be seen that when the gain obtains its lower value, it is not necessarily true that $-K_{ii}e_i + \frac{\bar{P}_i}{z_i} \leq 0$, unless the deviation between the maximum load demand and the nominal is “large enough”. In order to ensure that the desired result holds in every case, an additional condition on the feedback gain needs to be imposed, *i.e.*

$$K_{ii} > \max \left\{ \frac{\bar{P}_i}{\underline{z}_i e^m}, \frac{P_i^m}{(\underline{z}_i - e^m)^2} \right\}.$$

Then, the desired inequality $\dot{V}_i|_{e_i=e_i^m} \leq 0$ holds as the expression inside the parenthesis is a summation of strictly negative elements. In case of (b), it is noted that, by construction, at the point $e = -\mathbf{1}_n e^m$ the velocity is given by

$$\underbrace{\mathcal{L}_{ii}e^m + \sum_{j \in \mathcal{N}_i} \mathcal{L}_{ij}e^m + K_{ii}e^m}_{=0} + \frac{\bar{P}_i}{\underline{z}_i} - \frac{P_i^m}{-e^m + \underline{z}_i} = 0,$$

when K_{ii} , z_i obtain their respective lower bound and the load demand P_i is maximized. Then, for any $e_j \geq -e^m$, $P_i \leq P_i^m$ and $z_i \geq \underline{z}_i$, the above yields

$$\underbrace{\mathcal{L}_{ii}e^m - \sum_{j \in \mathcal{N}_i} \mathcal{L}_{ij}e_j}_{\geq 0} + K_{ii}e^m + \frac{\bar{P}_i}{z_i} - \frac{P_i}{-e^m + z_i} \geq K_{ii}e^m + \frac{\bar{P}_i}{\underline{z}_i} - \frac{P_i^m}{-e^m + \underline{z}_i}$$

and therefore the desired inequality immediately follows,

$$\mathcal{L}_{ii}e^m - \sum_{j \in \mathcal{N}_i} \mathcal{L}_{ij}e_j + K_{ii}e^m + \frac{\bar{P}_i}{z_i} - \frac{P_i}{-e^m + z_i} \geq 0,$$

which ensures $\dot{V} \leq 0$. Therefore, the convex nature of set N implies that the velocity vector assigned to every point $e \in \partial N$ by the map $\gamma: N \rightarrow TN$ is sub-tangential to the set N and by direct application of the Nagumo's theorem, the set N is positive invariant under the flow of the error dynamics with $\phi_e: N \rightarrow N$. \square

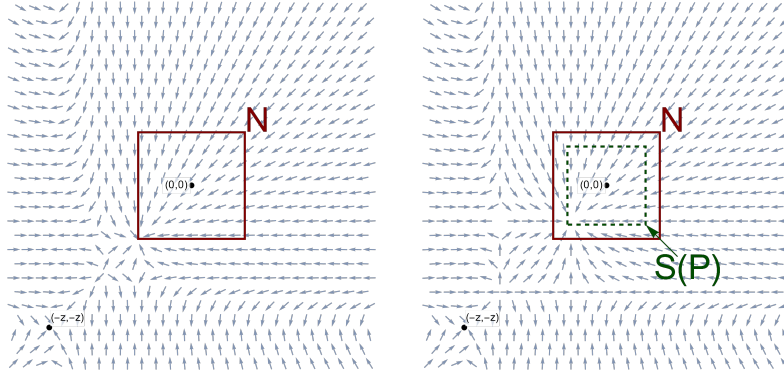
The invariance of set N combined with the asymptotic stability of every equilibrium point in N implies the following result.

Corollary 4.1. *The set N is within the region of attraction of system (4.10).*

Remark 4.2. *The above results reveal the immediate effect of the feedback gain K on the degree of conservativeness of N . Higher values of K result in higher magnitudes of the velocity introduced by the linear part and therefore a decrease in the maximum displacement of the equilibrium point from the origin. Therefore, there exists a subset of N parametrized by K , $\tilde{N}(K) \subset N$, such that \tilde{N} is positive invariant and contains the limit of the flow for any $e_0 \in N$, i.e. $\lim_{t \rightarrow \infty} \phi_e(e_0, t) \in \tilde{N}(K)$. However, while a high feedback gain would diminish the effect of the load demand on the voltage dynamics, this has a negative effect on the converter current steady state, as can be seen by the reference current parametrization $\hat{i} = -Ke + u$. Higher values of the feedback introduce larger deviations of the reference current \hat{i} from the desired reference u , revealing an inherent trade-off on the choice of the system parameters.*

The results are illustrated in Fig. 4.3, where the set $S(P)$ is a polytope similar to N but parametrized by an equilibrium point corresponding to some load demand with $P_i < P_i^m$. It is seen that the vector field drives the flow on the boundary of $S(P)$, while N is positive invariant. The above results also suggests that the set $\Omega = N \oplus \hat{z}$ is positive invariant for the uncertain system. A question that arises is that under which conditions, the uncertain state flow ϕ_v , parametrized by the control input \hat{i} , is driven in Ω , while $v \in \mathbb{X}$ is satisfied at all times. One way to guarantee this is to prove the existence of a robust positive invariant set (RPI) for the uncertain voltage dynamics within the constraint set. To this end, the following definition from [171] is adapted to this setting.

Definition 4.1 (Robust Positive Invariant Set). *The set \mathcal{R} is said to be robust positive invariant for the system (4.7), if there exists a control $\hat{i} \in \mathbb{C}$ such that for all initial states $v^0 \in \mathcal{R}$ and any $w \in \mathbb{W}$ the flow of the system satisfies $v = \phi(v^0, \hat{i}, w, T) \in \mathcal{R}$, for all $T > 0$.*



(a) Given a constant power demand P^m , any solution starting in N will remain in N and converge to ∂N

(b) For a power demand $P \in \mathbb{P}$ the region of the dynamic mapping shrinks within the set $S(P) \subset N$

Figure 4.3: Vector field and positive invariant set N for a two node system.

Using this notion of RPI sets, it is necessary that the terminal set is entirely contained within a positive invariant set, which in turn is entirely contained within the constraint set \mathbb{X} , *i.e.*

$$\Omega \subseteq \mathcal{R} \subseteq \mathbb{X}.$$

This would imply that since the uncertain state cannot leave \mathcal{R} , then it is also impossible to violate the constraint set \mathbb{X} . Following the previous analysis, recall that $\Omega = N \oplus \hat{z}$, where N is a positive invariant set. Therefore, the above question can be formulated in the nominal setting, by defining the nominal constraint sets as

$$\mathbb{Z} := \mathbb{X} \ominus N, \quad \mathbb{U} := \mathbb{C} \ominus (-K)N. \quad (4.15)$$

The above indicates that the input constraint set is “shrinking” with larger choices of the control gain K , while on the other hand the nominal state constraint set \mathbb{Z} approaches the size of the original constraint set \mathbb{X} . As it was also discussed in Remark 4.2, this is the expected trade-off that needs to be considered when choosing the tuning parameter K . The aim of this interplay is to proportionally distribute the high-transients effect of the CPL between the current and the voltage trajectories, in order to satisfy the operational constraints.

Furthermore, it is noted that the computation of the positive invariant set can be done offline and only utilizes the information regarding the bound on the load demand; this significantly simplifies the development of a control scheme for the nominal voltage dynamics and substantially reduces conservativeness stemming from the need of instantaneous load measurements during operation.

4.3.2 Formulation of the nominal voltage controller

The problem now becomes of choosing references within the nominal constraint set, *i.e.* $\hat{z} \in \mathbb{Z}$, and proving the existence of a positive invariant set for the nominal dynamics. While the former can be trivially satisfied, the latter requires the association of a control policy with the candidate positive invariant set. A common way to resolve this, is by employing an MPC control scheme. In MPC, the control policy is generated by solving a finite horizon optimal control problem subject to the system constraints and dynamics. The cost function is often adopted as a quadratic function penalizing the deviation of the system current state from a reference point, thus achieving regulation of the flow to a desired equilibrium. At each time instant, a sequence of control actions is generated and the first element is used as an input to the system, while the rest of the sequence is discarded. This process is repeated in the next time instant, thus achieving the receding horizon implementation. Efficient techniques have been developed to solve the continuous-time counterpart of the optimal control problem that usually involve an approximation of the solutions using a numerical solver. Some of the most commonly adopted techniques are the interior point method (IPM) or sequential quadratic programming (SQP), see [172, Chapter 10] for a detailed analysis.

One way to achieve a stabilizing and recursively feasible controller is by adopting a positive definite cost, compact constraint sets and invariant terminal ingredients [135], [149]. Following Assumption 4.2, it is straightforward to satisfy the first two requirements. However, the CPL destabilizes every fixed point $\hat{z} \in \mathbb{Z}$. To overcome this, the nominal control input is defined as

$$u = -K_z z + \eta^o, \quad (4.16)$$

where η^o is the optimal control policy generated by solving the MPC problem and K_z is the feedback gain of the nominal control input. Thus, the nominal dynamics take the form

$$C\dot{z} = -(\mathcal{L} + K_z)z - \frac{\bar{P}}{z} + \eta^o. \quad (4.17)$$

A way to guarantee recursive feasibility of the MPC optimisation problem is by employing positive invariant terminal ingredients. To this aim, the following result formulates a condition on the nominal feedback gain K_z , such that the stability of the terminal dynamics, *i.e.* beyond the prediction horizon of the MPC, is guaranteed.

Proposition 4.3 (Stability of the terminal dynamics). *Considering the nominal system (4.17), there exists a $\delta > 0$ such that the fixed point \hat{z} is an asymptotically*

4.3. FORMULATION OF THE NOMINAL VOLTAGE CONTROLLER

stable equilibrium with region of attraction $\mathcal{A} = \{z \in M: \|z - \hat{z}\| \leq \delta\}$, if and only if,

$$K_{z,i} > \frac{\bar{P}_i}{\hat{z}_i^2},$$

for all $\hat{z}_i \in \mathbb{Z}_i$.

Proof. To investigate the stability of the fixed point \hat{z} the nominal dynamics (4.17) are linearised around this point. The resulting Jacobian matrix is then

$$J = \nabla_{z=\hat{z}} \dot{z} = C^{-1}(-\mathcal{L} + [\hat{z}^2]^{-1} \bar{P} - K_z).$$

The point \hat{z} is asymptotically stable if and only if the Jacobian is a Hurwitz matrix. Exploiting the properties of the Laplacian matrix a worst-case scenario is defined at $\lambda_{\max}(-\mathcal{L}) = 0$. Then, the fact that the rest of the terms are symmetric matrices yields the condition

$$-K_{z,i} + \frac{\bar{P}_i}{\hat{z}_i^2} < 0$$

Which results in the required inequality

$$K_{z,i} > \frac{\bar{P}_i}{\hat{z}_i^2},$$

for all $\hat{z}_i \in \mathbb{Z}_i$. Shifting the axes to the desired point \hat{z} the new dynamics can be described by

$$\dot{\tilde{z}} = J\tilde{z} + g(\tilde{z})$$

where $\tilde{z} = z - \hat{z}$ and for some $\varepsilon > 0$ and $\delta > 0$, $g(\tilde{z})$ satisfies $\|g(\tilde{z})\| \leq \varepsilon \|\tilde{z}\|$ in some neighbourhood of the origin, *i.e.* $\|\tilde{z}\| \leq \delta$. Then, let $V(\tilde{z}) = \tilde{z}^\top \mathcal{P} \tilde{z}$ be a Lyapunov candidate function, where \mathcal{P} is a solution of $\mathcal{P}J + J^\top \mathcal{P} = -Q$ with $Q \succ 0$. Note that existence and uniqueness of \mathcal{P} is guaranteed due to J being a Hurwitz matrix [155, Theorem 4.6]. Using the fact that $\|g(\tilde{z})\| \leq \varepsilon \|\tilde{z}\|$ and $\tilde{z}^\top Q \tilde{z} > \lambda_{\min}(Q) \|\tilde{z}\|^2$, the time derivative of $V(\cdot)$ results in,

$$\dot{V} = \tilde{z}^\top \mathcal{P} (J\tilde{z} + g(\tilde{z})) + (\tilde{z}^\top J^\top + g^\top(\tilde{z})) \mathcal{P} \tilde{z} \quad (4.18)$$

$$= -\tilde{z}^\top Q \tilde{z} + 2\tilde{z}^\top \mathcal{P} g(\tilde{z}) \quad (4.19)$$

$$\leq (\lambda_{\min}(Q) + 2\|\mathcal{P}\| \varepsilon) \|\tilde{z}\|^2. \quad (4.20)$$

Now, for $\varepsilon < \frac{\lambda_{\min}(Q)}{2\|\mathcal{P}\|}$, the function $V(\tilde{z}) = \tilde{z}^\top \mathcal{P} \tilde{z}$ is a Lyapunov function for the shifted system as $\dot{V} \leq 0$ and thus there exists a $\delta > 0$ such that the region of attraction of \hat{z} is $\mathcal{A} = \{z \in M: \|z - \hat{z}\| \leq \delta\}$. \square

Corollary 4.2. Any level set \mathbb{Z}_0 satisfying $\mathbb{Z}_0 = \beta \mathcal{A}$ for $0 \leq \beta \leq 1$ is positive invariant for the dynamics (4.17).

4.3. FORMULATION OF THE NOMINAL VOLTAGE CONTROLLER

Following the above result above, the optimization problem can be formally defined as

$$J^o(z(0), \hat{z}, \hat{\eta}) = \min_{\eta} \int_{t_0}^{t_f} \ell(z - \hat{z}, \eta - \hat{\eta}) dt + J_f(z_f - \hat{z}) \quad (4.21)$$

subject to the constraints,

$$\begin{aligned} z(0) - z &\in N, \\ C\dot{z} &= -(\mathcal{L} + K_z)z - [z]^{-1}\bar{P} + \eta, \\ (z, \eta) &\in \mathbb{Z} \times \mathbb{U} \oplus K_z\mathbb{Z}, \quad z_f \in \mathbb{Z}_f, \end{aligned} \quad (4.22)$$

where $\ell(\cdot)$ is a positive definite function. The continuous time optimal control problem can be solved by a multiple shooting method [173], which discretizes the state trajectory over the prediction horizon to a predefined number of steps and employs numerical solvers to approximate the true solution between consecutive sampling intervals. Then, the resulting control can be applied in a receding horizon fashion, where at some time, or step, t_1 the first element of the resulting optimal control sequence is used as input to the system and the process is repeated at the next sampling instant $t_2 = t_1 + T$. Note that a direct consequence of Proposition 4.3 and Corollary 4.2, is that choosing $\mathbb{Z}_f = \mathbb{Z}_0$ and $J_f = \frac{1}{2}(z_f - \hat{z})^\top \mathcal{P}(z_f - \hat{z})$ leads to recursive feasibility of (4.21) provided that the problem is feasible at some initial time t_0 . In addition, any sublevel set of the stabilizing terminal cost function is positive invariant for the nominal dynamics. This is a well-established result in the literature, however, for completeness purposes, a sketch of the recursive feasibility result is provided here and the interested reader is referred to [172, Chapter 5] for a detailed analysis.

Proposition 4.4 (Recursive Feasibility of OCP). *Let the problem (4.21) be feasible at some initial state z_0 and time $t_0 > 0$. Then, the problem remains feasible for all $t > t_0$.*

Proof. Let $\mathbf{z}(z_0, t_0)$ and $\boldsymbol{\eta}(z_0, t_0)$ denote the feasible solutions of the optimal control problem respectively, with initial state z_0 and time t_0 . In addition, let $\mathbf{z}(\phi_z(z_0, t_0 + T), t_0 + T)$ and $\boldsymbol{\eta}(\phi_z(z_0, t_0 + T), t_0 + T)$ be the candidate state and control sequences at the next immediate sampling instant, *i.e.* at time $t_0 + T$. Assuming no additive uncertainties to the system, following Proposition 4.3 and Corollary 4.2, the candidate solutions at time $t_0 + T$ are formulated as the tails of the ones at time t_0 where the predicted state at the end of the horizon satisfies $z_f(t_0 + T + t_f) \in \mathbb{Z}_f$. Positive invariance of \mathbb{Z}_f implies that $\mathbf{z}(\phi_z(z_0, t_0 + T), t_0 + T)$ and $\boldsymbol{\eta}(\phi_z(z_0, t_0 + T), t_0 + T)$ are feasible and the problem is recursively feasible for all $t > t_0$. \square

The optimisation problem in (4.21) is recursively feasible provided that the initial state satisfies the constraints. Following the results of the previous chapter, the above nominal problem can also be formulated in a distributed manner, where the maximum allowed prediction error between the sampling intervals from (3.22) is reduced to

$$e_i^{\max} = \Delta T_i \sum_{j \in \mathcal{N}_i} |Y_{ij}| |B_j| \sqrt{N}. \quad (4.23)$$

Therefore, the prediction accuracy of the distributed optimisation problem no longer depends on the load demand term. Ultimately, the control designer has two choices; either solve the optimisation problem by including terminal ingredients as in (4.21), or rely on the turnpike property to establish recursive feasibility of the MPC, as shown in Chapter 3. On the one hand, the use of terminal ingredients usually requires smaller prediction horizon, and thus can reduce the computation time. On the other hand, it involves more steps during the control design process and the feasibility set of the MPC, *i.e.* the set of initial states for which the optimisation problem is recursively feasible, relies on the size of the terminal constraint set. The size of the feasibility set is, arguably, the main concern when making this choice. Enlarging this set effectively guarantees recursive feasibility for a larger set of initial states, thus reducing the overall conservativeness of the controller. Therefore, choosing whether to make use of terminal ingredients should prioritise the method that results in a larger feasibility set, the interested reader is referred to [174] for more details. In the linear case, this can be analytically known a priori, by computing the constrained image of the solution of the dynamics, see [175]. In the nonlinear case this process can be more involved and requires some form of numerical approximation of the solutions, which falls beyond the scope of this study.

4.4 Stability analysis of the cascaded dynamics

Following the analysis of the previous sections, the problem has been shifted to regulating the following cascaded dynamics,

$$L \frac{di}{dt} = -(k_p + r)i + D\sigma \quad (4.24a)$$

$$D \frac{d\sigma}{dt} = k_I (\mathbb{1}_n - \sigma^2)(u - Ke - i) \quad (4.24b)$$

$$C \frac{dz}{dt} = -\mathcal{L}z - [z]^{-1} \bar{P} - u \quad (4.24c)$$

$$C \frac{de}{dt} = -\mathcal{L}e - Ke - [e + z]^{-1} \bar{P} + [z]^{-1} \bar{P} - [e + z]^{-1} \delta P. \quad (4.24d)$$

4.4. STABILITY ANALYSIS OF THE CASCADED DYNAMICS

To better state the overall control scheme, the following algorithm outlines the required actions to achieve the desired operation.

Control Algorithm: Cascaded operation of the controllers

1. Outer nominal voltage loop computes control input u according to (4.16), by employing an MPC scheme to calculate the optimal control action η^o .
 2. The reference inner converter current is provided by the control law (4.8) and used as a reference input to the inner current loop (4.5).
 3. The duty ratio of the converter switching device is then computed according to (4.4).
-

The stability of a cascaded structure has been thoroughly investigated in the literature, see [176]. The conventional procedure is to separate the dynamics into a driving subsystem and a driven one, where the state of the former is considered an input to the latter. Then, asymptotic stability of the overall dynamics follows from asymptotic stability of the driving subsystem and asymptotic stability or some form of boundedness of the driven dynamics. Given a desired reference nominal voltage z^{ss} , the equilibrium set for (4.24) with state vector $x = (i, \sigma, z, e)$ is defined as

$$\mathcal{E} := \{\hat{i}, \hat{\sigma}, \hat{z}, \hat{e} \in \mathbb{R}^n : \hat{i} = u - K\hat{e}, \hat{\sigma} = D^{-1}(k_p + r)\hat{i}, \hat{z} = z^{ss}, \hat{e} \in N\}. \quad (4.25)$$

First, the asymptotic stability of the inner current dynamics is shown.

Theorem 4.1 (Lyapunov stability of the driving dynamics). *For every node $i \in \mathcal{M}$, the \mathcal{C}^1 function $\mathcal{W}_i: \mathbb{R} \times \mathbb{R} \rightarrow \mathbb{R}$,*

$$\begin{aligned} \mathcal{W}_i(i_i, \sigma_i) = & \frac{1}{2}L_i(i_i - \hat{i}_i)^2 + \frac{D_i^2 - D_i(k_{p,i} + r_i)\hat{i}_i}{k_{I,i}} \ln \frac{1}{1 - \sigma_i^2} + \\ & + \frac{D_i(k_{p,i} + r_i)\hat{i}_i}{k_{I,i}} \ln \frac{1}{1 + \sigma_i}, \end{aligned} \quad (4.26)$$

is a Control Lyapunov Function for the subsystem (4.24a), (4.24b), and the subsystem is asymptotically stable with equilibrium point described by (4.25) and region of attraction $\mathbb{C}_i = [-I_{\max}, I_{\max}] \times [-1, 1]$.

Proof. Following the definition of \mathcal{W} , it can be seen that it is positive definite. Therefore, all we need to show is negative definiteness of the first derivative. Following the assumption on the time scale separation of the dynamics, the input

4.5. SIMULATIONS

current is constant, *i.e.* $\hat{i}_i = \bar{i}_i$. Then, the time derivative of \mathcal{W}_i results in

$$\begin{aligned}\dot{\mathcal{W}}_i &= L_i \frac{di_i}{dt} (i_i - \bar{i}_i) + \frac{D_i^2 - D_i(k_{p,i} + r_i)\bar{i}_i}{2k_{I,i}} \frac{2\sigma_i}{1 - \sigma_i^2} \frac{d\sigma_i}{dt} \\ &\quad - \frac{D_i(k_{p,i} + r_i)\bar{i}_i}{k_{I,i}(1 + \sigma_i)} \frac{d\sigma_i}{dt} \\ &= - (k_{p,i} + r_i)(i_i - \bar{i}_i)^2,\end{aligned}$$

where

$$\dot{\mathcal{W}}_i = -(k_{p,i} + r_i)(i_i - \bar{i}_i)^2 \leq 0$$

for $k_{p,i}, r_i > 0$. Following La Salle's invariance theorem and noting that the derivative vanishes only at $i \in \mathcal{E}$, the driving subsystem is asymptotically stable with respect to the equilibrium set \mathcal{E} . In addition, following Prop. 4.1 the set \mathbb{C}_i is within the region of attraction for the current equilibria. \square

The next Theorem combines the aforementioned results to establish the stability of the cascaded dynamics under the proposed control scheme.

Theorem 4.2 (Asymptotic stability of the cascaded dynamics). *The cascaded dynamics (4.24) are asymptotically stable with $\lim_{t \rightarrow \infty} \phi(x, u, w, t) \in \mathcal{E}$.*

Proof. Asymptotic stability of the driving subsystem follows from Theorem 4.1. In addition, following Proposition 4.4, the dynamics described by (4.24c) are also asymptotically stable, where the proof follows the common approach of exploiting the recursive feasibility properties of the optimal control problem and using the cost function as a Lyapunov function for the system. Finally, boundedness of (4.24d) follows from Proposition 4.2. Thus, the cascaded dynamics are an interconnection of Lyapunov stable driving subsystems (4.24a), (4.24b), (4.24c) and a bounded driven subsystem (4.24d). Then, according to [176], the equilibrium points in (4.25) are asymptotically stable for the cascaded dynamics (4.24). \square

4.5 Simulations

In this section, the operation of the proposed control scheme is demonstrated in a simulated scenario comprising of a seven node meshed network, see Fig. 4.4. The control objective is for the nominal voltage to converge to desired reference values, while satisfying the “tighter” version of the original constraint sets. As it is demonstrated, this enforces the uncertain voltage to always remain within the original constraint set, denoted in this scenario as $\mathbb{X}_i = \{v_i \in \mathbb{R}^n : 97.9 \leq v_i \leq 102.6\}$. The rated voltage of each converter is chosen as $v^* = 100V$, while the maximum allowed inner converter current is $I_{\max,i} = 17A$. Furthermore, the

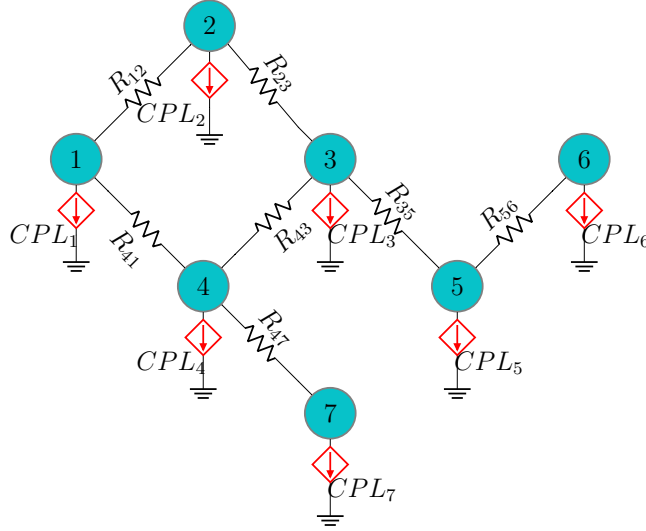


Figure 4.4: Network topology of a meshed islanded MicroGrid.

nominal power demand is $\bar{P}_i = 500W$, where the maximum deviations from this value are bounded in $|\delta P_i| \leq 500W$. A quadratic cost functional is chosen of the form $\ell(z - \hat{z}, \eta - \hat{\eta}) = \|z - \hat{z}\|^2 + \|\eta - \hat{\eta}\|^2$ and the problem is solved using the SQP solver and “ICLOCS” MATLAB toolbox provided by [177].

The node voltage evolution is depicted in Fig. 4.5, where at time $t = 0s$ the nominal voltage references are changed to $\{101, 100, 101.5, 102, 99, 98, 102.5\}$. Then, three changes to the reference value occur at times $t = 0.01s$, $t = 0.02s$ and $t = 0.03s$. The power demand deviations from the nominal value \bar{P} of the load in Node 1 is depicted in Fig. 4.7. Despite the constant load fluctuations, the network voltages are contained within the respective positive invariant set N_i , while also satisfying the desired state constraint \mathbb{X}_i . In addition, the current trajectories of Node 1, 3 and 7, along with the respective generated references, are shown in Fig. 4.6. It is seen that both the trajectories and the references are contained within the desired constraint set, validating the analysis developed in the previous sections. In addition, it is noted that the fluctuations of the current references are a result of the varying load demand which also affects the error dynamics. Here, the choice to allow larger current fluctuations was made, however, as it was demonstrated by the previous sections, one may choose to limit the fluctuations of the input currents by enlarging the set N_i , hence allowing larger deviations between the nominal and uncertain node voltages. The explicit values of the tuning and system parameters are given in Table 4.1.

4.6. CONCLUSIONS

Parameter	Value
C [μF]	{200, 150, 100, 140, 150, 100, 140}
L [mH]	{10, 15, 11, 6, 8, 10, 9, 10, 11}
R_{ij} [Ω], $(i, j) \in \mathcal{E}$	{1, 1.7, 0.4, 0.7, 0.5, 0.8, 0.5}
r_i [Ω]	2
$k_{p,i}$	$600 \cdot 10^5$
D_i	$102 \cdot 10^7$
$k_{I,i}$	$6 \cdot 10^{13}$
K_i	50
$K_{z,i}$	4

Table 4.1: Network component and control parameter values.

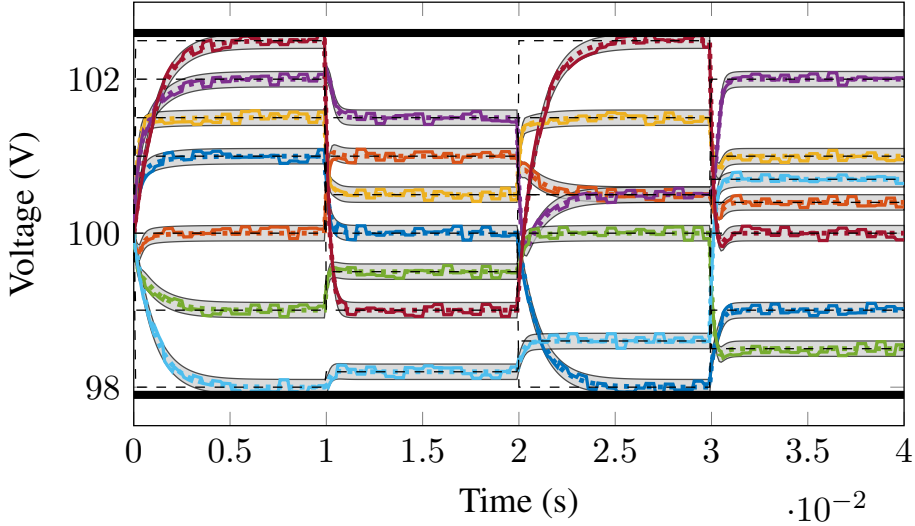


Figure 4.5: Voltage and nominal voltage trajectories for Node 1(—,····), Node 2(—,····), Node 3(—,····), Node 4(—,····), Node 5(—,····), Node 6(—,····) and Node 7(—,····) respectively. The constrained region is represented with black solid lines (—) and the voltage references by black dashed lines (---). The voltage trajectories are within the respective \mathcal{S}_i (□) at all times.

4.6 Conclusions

In this chapter, a robust control scheme for meshed DC Microgrids was proposed that ensures stability of the closed loop system in the presence of fluctuating CPL load demand. It was initially shown that a “tube” behaviour naturally arises from the interplay of the proposed control policy with the rest of the dynamics. Then, in the later sections, it was established that this result in combination with the

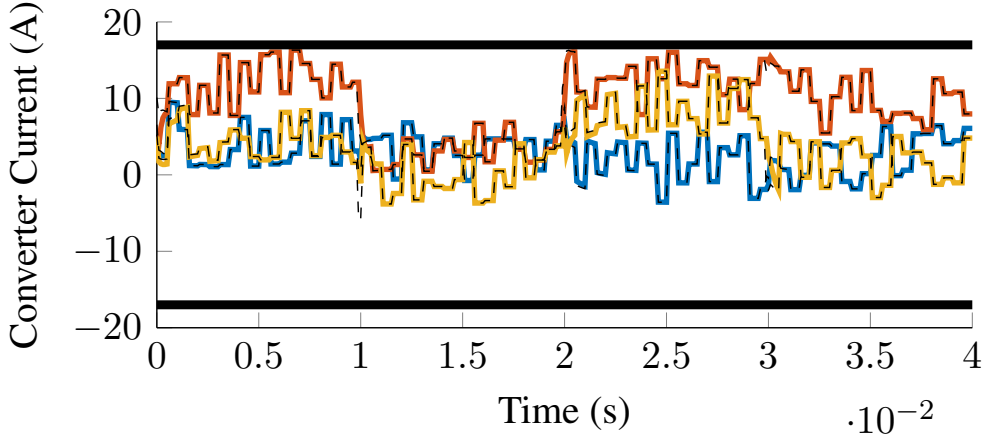


Figure 4.6: Converter Current trajectories for Node 1(—), Node 3(—) and Node 7(—) respectively. The constrained region \mathbb{C} is represented by black solid lines (—) and the current references \hat{i}_i by black dashed lines (---).

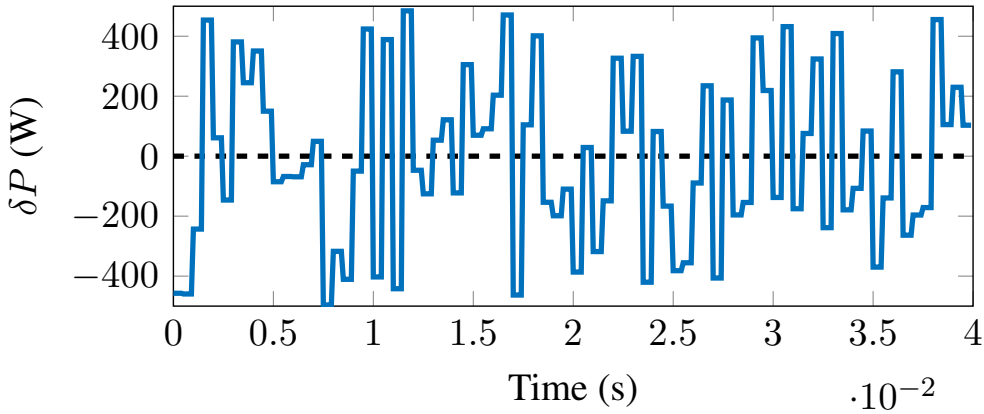


Figure 4.7: Load fluctuations around the nominal value \bar{P} for Node 1. A similar load profile is shared among the rest of the Nodes.

proposed analytic conditions of the controller tuning parameters, facilitates the boundedness of the uncertain system trajectory within a predefined positive invariant set. Furthermore, the presented theoretical analysis revealed an inherent trade-off between the choice of the tube size and the availability of the inner currents that reside within the operational constraints and satisfy the load demand. As it was discussed, arbitrary large values of the feedback gain should be avoided and it was suggested that a choice can be made by considering both the proposed lower bound and the desired maximum magnitude of input current fluctuations.

A characterisation of the appropriate nominal control actions to achieve feasible uncertain trajectories was attained by a discrete approximation of the nominal control sets. It was shown that if the control vector was chosen large enough, then the rest of the dynamics would follow the desired behaviour and a positive

4.6. CONCLUSIONS

invariant set is guaranteed to exist within the state constraint set. To achieve this behaviour an MPC scheme was adopted in order to include the constraint sets within the control design process. To ensure recursive feasibility of the receding horizon optimization problem, the nominal control action was parametrized by a feedback gain that ensures positive invariance of the terminal ingredients. Finally, demonstration of the results was given by a simulation scenario on a seven node network with local constant power loads.

Chapter 5

Dynamic tube control scheme for islanded DC Microgrids

The use of tube-based approaches has long been used in the literature to address the problem of designing a control scheme in the presence of an unknown external input. While a plethora of studies have been devoted in solving this task for linear systems, extending these for a general nonlinear system is difficult. A few studies have been developed by assuming Lipschitz continuity of the system and designing the tube using the respective Lipschitz constant. However, this can result in an overly conservative approach, since one attempts to bound changes in the value function by a single, uniform constant and additionally this constant is fairly large for a wide range of systems. In order to achieve more applicable results, the explicit nonlinear form of the dynamics can be utilized for each specific case. This was demonstrated in the previous chapter, where it was shown that a feedback control law can be used to establish the existence of a positive invariant set under the solution of the dynamics. This approach assumed a worst-case scenario for both the external input, *i.e.* the load demand, and the nominal voltage in order to deduce a lower bound on the tuning parameter such that the closed loop system achieves the desired behaviour and admits asymptotically stable equilibria. As it was shown, the magnitude of the feedback gain also affected the size of the positive invariant set, where smaller values of the controller gain resulted in a larger set. Since this set is used to “tighten” the nominal constraint sets, some degree of conservativeness was introduced by having an unnecessarily large lower bound on the feedback gain. This problem can be overcome by exploiting the fact that the nominal voltage is a state of the system, thus the controller determines its dynamical evolution. This chapter will demonstrate how the nominal voltage can be incorporated in the theoretical analysis of the error dynamics and investigate under which conditions the Microgrid achieves a similar, but improved, behaviour with the previous chapter.

It will be shown that inclusion of the nominal voltage trajectory in the analysis of the error dynamics can result in a time-varying, positive invariant set, reducing the conservativeness stemming from assuming a worst-case scenario. In addition, conditions on the nominal voltage trajectory will also be derived such that the continuity of the original dynamics is preserved.

In the following, Section 5.1 formally defines the problem. Then, Section 5.2 presents the theoretical analysis on the error dynamics such that the system achieves the desired behaviour. Section 5.3 formulates the controller of the nominal subsystem and Section 5.4 establishes the recursive feasibility and stability of the optimisation problem and the closed loop system respectively. Finally, the theoretic results are demonstrated in a simulated scenario in Section 5.5, and Section 5.6 draws conclusions on the results.

5.1 Problem Formulation

Similar to the previous chapter, the case of an isolated, meshed, DC Microgrid is considered with n number of nodes, where each node is locally connected to a constant power load. The aim is to introduce robustness of the network to perturbations of the load demand and guarantee restriction of the dynamics in a predefined operational range, while also reducing the conservativeness of the tube. In order to build upon the results of the previous chapter, the investigated problem will also be briefly presented here. It is, therefore, reminded that the node voltage dynamics are formulated as

$$C_i \frac{dv_i}{dt} = i_{in,i} - i_{o,i}, \quad (5.1)$$

where C_i is the capacitance of the output capacitor, $i_{in,i}$ is the control input current and $i_{o,i}$ is the output current flowing in the lines of the network and into the local CPL. The connections among the nodes of the graph can be represented by the weighted adjacency matrix $A(R) \in \mathbb{R}^{n \times n}$, where $a_{ij} = R_{ij}^{-1}$, with R_{ij}^{-1} the admittance of the line between nodes i and j , and $a_{ij} = 0$ if the edge (i, j) is not incident. The full topology of the network is represented by the Laplacian matrix $\mathcal{L} = [A(R)\mathbf{1}_n] - A(R)$. Therefore, the output network current can be modelled as

$$i_{o,i} = \frac{P_i}{v_i} + \mathcal{L}_{ii}v_i + \sum_{j \in \mathcal{N}_i} \mathcal{L}_{ij}v_j, \quad (5.2)$$

where P_i represents the load demand and is assumed to be bounded in a compact set as $P_i \in \mathbb{P}_i \subset \mathbb{R}$. Then, considering a nominal constant power demand $\bar{P}_i \in \mathbb{P}_i$, the network dynamics can be rewritten with respect to the deviation from the nominal

load as

$$C_i \frac{v_i}{dt} = i_{in,i} - \mathcal{L}_{ii} v_i - \sum_{j \in \mathcal{N}_i} \mathcal{L}_{ij} v_j - \frac{\bar{P}_i}{v_i} - \frac{\delta P_i}{v_i}, \quad (5.3)$$

Following the load boundedness assumption $P_i \in \mathbb{P}$, the load perturbations satisfy $\delta P_i \in \mathbb{W}_i$, where $\{\bar{P}_i\} \oplus \mathbb{W}_i \subseteq \mathbb{P}_i$. Furthermore, the system is required to operate in a predefined operational range. This is formulated as state and input constraint sets on the node voltages and input currents, denoted \mathbb{X}_i and \mathbb{C}_i respectively, where the aim is to guarantee that $v_i \in \mathbb{X}_i$ and $i_{in,i} \in \mathbb{C}_i$ at all times. The constraints are formally defined in the following assumption, where the assumption on the set structure ensures regularity of the optimisation problem defined in the next section.

Assumption 5.1. *The input constraint set $\mathbb{C}_i \subset \mathbb{R}$ and the state constraint set $\mathbb{X}_i \subset \mathbb{R}$ are compact, closed and $\mathbb{C}_i \subset \mathbb{R}$ contains the origin within its non-empty interior.*

In this chapter, it is further assumed that there are no coupling constraints between the nodes, *i.e.* we can represent the network constraint sets as,

$$\mathbb{X} = \prod_{i \in \mathcal{M}} \mathbb{X}_i, \quad (5.4a)$$

$$\mathbb{C} = \prod_{i \in \mathcal{M}} \mathbb{C}_i. \quad (5.4b)$$

In the cases where this assumption cannot be made, then a similar approach to the one in Chapter 3 can be adopted to guarantee satisfaction of the coupled constraints.

5.2 Voltage dynamics and boundedness analysis

In this section, the original, uncertain voltage dynamics are “split” into a nominal voltage and an error component, describing the difference between the nominal and the uncertain state. The aim is to exploit the structure of the dynamics and the analytical behaviour of the load, in order to design a control law that implicitly “enforces” the existence of a positive invariant set under the solution of the uncertain dynamics. Furthermore, the size of this set will be allowed to be time-varying by considering the nominal voltage as a control input to the error dynamics. This the main difference with the previous chapter, where a worst-case scenario was assumed by perceiving the nominal voltage constant at the lower-bound value. This way, the conservativeness of the control law can be reduced, allowing for a larger number of available control actions during the nominal optimisation problem. First, the error is defined as

$$e_i = v_i - z_i, \quad (5.5)$$

where z_i is the nominal state with dynamical evolution,

$$C_i \dot{z}_i = u_i - \mathcal{L}_{ii} z_i - \sum_{j \in \mathcal{N}_i} \mathcal{L}_{ij} z_j - \frac{\bar{P}_i}{z_i} \quad (5.6)$$

with $u_i \in \mathbb{R}$ the input to the nominal dynamics, which is to be computed by the nominal optimisation problem. In addition, the control law of the uncertain dynamics 5.3 is defined as

$$\dot{i}_{in,i} = -K_i e_i + u_i, \quad (5.7)$$

where $K_i \in \mathbb{R}_{>0}$ is a constant control parameter. Then, using the representation of the dynamics in (5.3) and substituting the input current with (5.7), the error dynamics are given by

$$C_i \dot{e}_i = -(\mathcal{L}_{ii} + K_i) e_i - \sum_{j \in \mathcal{N}_i} \mathcal{L}_{ij} e_j - \frac{\bar{P}_i}{e_i + z_i} + \frac{\bar{P}_i}{z_i} - \frac{\delta P_i}{e_i + z_i}, \quad (5.8)$$

The ultimate aim is formulating conditions on K_i and z_i , such that the error will always be bounded in a robust positive invariant set, by perceiving z_i and δP_i as, respectively known and unknown, external inputs to the system. Doing so, the nominal dynamics can act as a driving subsystem, determining the behaviour of the network, while the uncertain state will always remain close to the nominal one. Observing the form of the dynamics in (5.8), it can be seen that the disturbance δP_i enters the system as a parametric disturbance where the magnitude of its effect also depends on the states e_i and z_i respectively. Now, consider the quadratic energy-like function

$$V_i = \frac{1}{2} C_i e_i^2, \quad (5.9)$$

with time derivative

$$\dot{V}_i = -(\mathcal{L}_{ii} + K_i) e_i^2 - \sum_{j \in \mathcal{N}_i} \mathcal{L}_{ij} e_j e_i + \frac{\bar{P}_i}{z_i} e_i - \frac{\bar{P}_i}{e_i + z_i} e_i - \frac{\delta P_i}{e_i + z_i} e_i. \quad (5.10)$$

In order to show the existence of a robust positive invariant set for the error dynamics in (5.8), there needs to exist a set \mathcal{S}_i , such that in the complement of \mathcal{S}_i the above eq. (5.10) satisfies $\dot{V}_i \leq 0$, $\forall e_i \notin \mathcal{S}_i$. Therefore, the derivative of the energy function is non-positive outside \mathcal{S}_i , effectively “trapping” the error trajectory evolution within this set. This is translated in investigating the ultimate boundedness of the dynamics, therefore it suffices to investigate the behaviour of the points on the boundary of this set. At these boundary points, there exists a subgraph $\mathcal{G}_b \subseteq \mathcal{G}$, with node set $\mathcal{M}_b \subseteq \mathcal{M}$, where for the nodes $i \in \mathcal{M}_b$, it holds that $|e_i| \geq |e_j|$, for all $j \in \mathcal{M}$. Investigating the behaviour of the node dynamics in \mathcal{M}_b , and enforcing boundedness of their respective state trajectories, implicitly bounds the node

trajectories of the entire network. This is a particularly useful property, since it allows the decoupling of the analysis and the resulting stability problem. The reason for this is that the inequality $|e_i| \geq |e_j|$ implies that for every node $i \in \mathcal{M}_b$, the diagonal component of the Laplacian matrix dominates the sum of the off-diagonal components. Combined with the fact that $\delta P_i \in \mathbb{W}_i$, this allows the bound of (5.10) as

$$\dot{V}_i \leq g(e_i, z_i), \quad \forall i \in \mathcal{M}_b \quad (5.11)$$

where

$$g(e_i, z_i) = -K_i e_i^2 + \frac{\bar{P}_i}{z_i(e_i + z_i)} e_i^2 + w_i \frac{|e_i|}{e_i + z_i}, \quad (5.12)$$

with

$$w_i = \max \|\delta P_i\|. \quad (5.13)$$

In the following, the analysis will focus on investigating the behaviour of the nodes in the subgraph of the original network. First, in order to investigate the analytical properties of the bound (5.12), the focus shifts on the choice of control parameters such that (5.12) admits real roots. This will later be helpful to establish the existence of a closed RPI set around the origin.

Proposition 5.1. *Consider the bound on the time derivative in (5.12), if the feedback gain and the nominal state satisfy respectively*

$$K_i > \frac{\sqrt{(\bar{P}_i + 4w_i)^2 - 12w_i^2} - 2\sqrt{w_i(\bar{P}_i + w_i)}}{\bar{P}_i + 4w_i}$$

and

$$z_i \geq \beta_i$$

where

$$\beta_i = \sqrt{\frac{2\bar{P}_i K_i + 4K_i w_i + 4K_i \sqrt{w_i(\bar{P}_i + w_i)}}{2K_i^2}},$$

then (5.12) admits two negative and one positive non-zero real roots.

Proof. For now, it is assumed that the nominal voltage is strictly greater than the error and thus $g(e_i, z_i)$ is continuous. However, conditions will later be provided such that property is guaranteed. The non-zero roots of (5.12) are given by solving the polynomial

$$K_i z_i |e_i| e_i + |e_i| (K_i z_i^2 - \bar{P}_i) - z_i w_i = 0. \quad (5.14)$$

Two cases are distinguished: (a) $e_i > 0$ and (b) $e_i < 0$. For (a) the above yields

$$\Delta_1 = \frac{-(K_i z_i^2 - \bar{P}_i) + \sqrt{(K_i z_i^2 - \bar{P}_i)^2 + 4K_i z_i^2 w_i}}{2K_i z_i}$$

$$\Delta_2 = \frac{-(K_i z_i^2 - \bar{P}_i) - \sqrt{(K_i z_i^2 - \bar{P}_i)^2 + 4K_i z_i^2 w_i}}{2K_i z_i}.$$

Note that $(K_i z_i^2 - \bar{P}_i)^2 + 4K_i z_i^2 w_i$ is always positive as it is a summation of positive terms. In order to show that $\Delta_1 > 0$, it is required that

$$\left| \sqrt{(K_i z_i^2 - \bar{P}_i)^2 + 4K_i z_i^2 w_i} \right| > \left| (K_i z_i^2 - \bar{P}_i) \right|,$$

always holds. This results in the necessary inequality

$$4K_i z_i^2 w_i > 0$$

which is indeed true, since every term is strictly positive. Hence, $\Delta_1 > 0$. Similarly, it can be shown that $\Delta_2 < 0$ which contradicts the assumption $e_i > 0$ and therefore is discarded as a root of the polynomial. Then, in the second case (b), the roots are given by

$$\begin{aligned} \Delta_3 &= \frac{-(K_i z_i^2 - \bar{P}_i) + \sqrt{(K_i z_i^2 - \bar{P}_i)^2 - 4K_i z_i^2 w_i}}{2K_i z_i} \\ \Delta_4 &= \frac{-(K_i z_i^2 - \bar{P}_i) - \sqrt{(K_i z_i^2 - \bar{P}_i)^2 - 4K_i z_i^2 w_i}}{2K_i z_i}. \end{aligned}$$

In this case, it is not necessarily true that the roots are always non-complex values, *i.e.* that the term under the square root is non-negative. Guaranteeing the existence of real roots yields the condition

$$(K_i z_i^2 - \bar{P}_i)^2 - 4K_i z_i^2 w_i \geq 0,$$

or

$$K_i^2 z_i^4 - z_i^2 (2\bar{P}_i K_i + 4K_i w_i) + \bar{P}_i^2 \geq 0.$$

The largest root of the above exists and is given by,

$$\beta_i = \sqrt{\frac{2\bar{P}_i K_i + 4K_i w_i + 4K_i \sqrt{w_i (\bar{P}_i + w_i)}}{2K_i^2}}$$

which results in the desired condition for the bound on the nominal state z_i . Now, considering the special case where $z_i = \beta_i$, then the requirement of negative roots, since in this case $e_i < 0$, yields

$$\frac{-K_i \beta_i^2 + \bar{P}_i}{2K_i z_i} < 0.$$

Solving the above with respect to K_i and substituting with the explicit form of β_i results in the necessary condition

$$K_i > \frac{\sqrt{(\bar{P}_i + 4w_i)^2 - 12w_i^2} - 2\sqrt{w_i (\bar{P}_i + w_i)}}{\bar{P}_i + 4w_i}.$$

Note that the nominator of the above is always positive. Then, similarly to case (a) it can be shown that both roots Δ_3 and Δ_4 are negative and $\Delta_4 < \Delta_3$. This completes the proof. \square

The proof of Prop.5.1 reveals the existence of one negative and one positive root of $g(e_i, z_i)$ around the origin given by the functions $\alpha_1, \alpha_2: [\beta_i, \infty) \rightarrow \mathbb{R}$, where

$$\alpha_1(z_i) = \frac{-(K_i z_i^2 - \bar{P}_i) + \sqrt{(K_i z_i^2 - \bar{P}_i)^2 + 4K_i z_i^2 w_i}}{2K_i z_i}, \quad (5.15a)$$

$$\alpha_2(z_i) = \frac{-(K_i z_i^2 - \bar{P}_i) + \sqrt{(K_i z_i^2 - \bar{P}_i)^2 - 4K_i z_i^2 w_i}}{2K_i z_i}. \quad (5.15b)$$

Using the above functions, one may obtain an explicit form of a candidate robust positive invariant set, *i.e.*

$$\mathcal{S}(z_i) := \{e_i \in \mathbb{R}^n : \alpha_2(z_i) \leq e_i \leq \alpha_1(z_i)\} \quad (5.16)$$

In the following result, the qualitative behaviour of the bounding functions $\alpha_1(\cdot)$ and $\alpha_2(\cdot)$ is investigated, where monotonic decrease and increase is revealed respectively. This property will be proven useful in establishing that (5.12) is strictly negative between inside \mathcal{S}_i , *i.e.* it obtains negative values between its roots around the origin.

Lemma 5.1. *For all z_i that satisfy Prop. 5.1, the upper bounding function (5.15a) is strictly decreasing, while (5.15b) is strictly increasing, and obtains a maximum, and respectively a minimum, at $z_i = \beta_i$.*

Proof. The derivative of (5.15a) is given by,

$$\frac{\partial \alpha_1(z_i)}{\partial z_i} = -\frac{(\bar{P}_i + K_i z_i^2) \left(-\gamma_i + \sqrt{\gamma_i^2 + 4K_i z_i^2 w_i} \right)}{2K_i z_i^2 \sqrt{\gamma_i^2 + 4K_i z_i^2 w_i}}. \quad (5.17)$$

where $\gamma_i = K_i z_i^2 - \bar{P}_i$. As it has already been shown in the proof of Prop.5.1, the second parenthesis of the nominator is always positive, hence the conclusion can be drawn that $\frac{\partial \alpha_1(z_i)}{\partial z_i} < 0$ and $\alpha_1(z_i)$ is a strictly decreasing in its domain. Therefore, it immediately follows that it obtains a maximum at $z_i = \beta_i$. Similarly, it can be shown that $\alpha_2(\cdot)$ is strictly increasing and obtains a minimum value when $z_i = \beta_i$. \square

The next step is to guarantee that the error trajectory is upper bounded by the nominal state and thus guarantee the continuity of (5.12) inside the candidate robust positive invariant set.

Lemma 5.2. *Consider the error (5.8) and nominal (5.6) dynamics respectively, if z_i satisfies Prop. 5.1 then the relation $z_i > e_i$ is guaranteed for all $e_i \in \mathcal{S}(z_i)$ and all $i \in \mathcal{M}$.*

Proof. Using Lemma 5.1, the necessary condition can be formulated by assuming a worst-case scenario, *i.e.*

$$z_i > -\alpha_2(\beta_i),$$

which yields the requirement

$$z_i > \frac{K_i\beta_i^2 - \bar{P}_i}{2K_i\beta_i}.$$

Using Prop. 5.1, at a worst-case scenario the nominal state satisfies $z_i = \beta_i$. Substituting in the above yields the relation

$$K_i\beta_i^2 > -\bar{P}_i.$$

This is always true since the right-hand side is strictly positive and the left-hand side strictly negative. Therefore, the relation $z_i + e_i > 0$ holds for all $e_i \in \mathcal{S}_i(z_i)$ and $z_i \geq \beta_i$, and the bound on the energy-like function (5.12) is uniformly continuous within $\mathcal{S}_i(z_i)$. \square

The main result of this chapter can now be presented. If the previously established conditions on the choice of tuning parameters are met, the set $\mathcal{S}(z_i)$ is a robust positive invariant set under the solution of the error dynamics. This is shown in the following.

Proposition 5.2. *The set $\mathcal{S}(z_i)$ is a robust positive invariant set for the error dynamics (5.8) for every node $i \in \mathcal{M}$ and $\delta P_i \in \mathbb{W}_i$.*

Proof. Using Prop. 5.1 and Lemma 5.2, first, the nominal term of (5.12) needs to be strictly negative. This will be proven by contradiction. Assume that for all $e_i \in \mathcal{S}(z_i)$ it holds that

$$-\left(K_i - \frac{\bar{P}_i}{z_i(e_i + z_i)}\right)e_i^2 > 0.$$

This implies that in $\mathcal{S}(z_i)$ it holds that

$$K_i - \frac{\bar{P}_i}{z_i(e_i + z_i)} < 0.$$

Note that the relation $z_i(e_i + z_i) > 0$ was proven in Lemma 5.2. Therefore, from the above it is implied that

$$e_i < \frac{\bar{P}_i - K_i z_i^2}{K_i z_i}.$$

Substituting for the bounding function (5.15b) yields

$$\frac{-(K_i z_i^2 - \bar{P}_i) + \sqrt{(K_i z_i^2 - \bar{P}_i)^2 - 4K_i z_i^2 w_i}}{2K_i z_i} < \frac{-\bar{P}_i - K_i z_i^2}{K_i z_i}.$$

Gathering every term on the one side and simplifying the expression results in

$$K_i z_i^2 - \bar{P}_i + \sqrt{(K_i z_i^2 - \bar{P}_i)^2 - 4K_i z_i^2 w_i} < 0.$$

It is noted that substituting $z_i = \beta_i$, the relation $K_i z_i^2 - \bar{P}_i > 0$ immediately follows. This leads to a contradiction as the left hand side of the inequality is a strictly positive quantity. Therefore, the nominal term of (5.12) is negative for all $e_i \in \mathcal{S}(z_i)$. Furthermore, it is straightforward to show that the derivative of (5.12) does not vanish at the boundary points. Finally, using with the fact that the third summand of (5.12) containing the disturbance is non-negative, it is concluded that $\mathcal{S}(z_i)$ is a robust positive invariant set for the error dynamics and for all $e(0) \in \mathcal{S}(z_i)$ the solution satisfies $\lim_{t \rightarrow \infty} e(t) \in \mathcal{S}(z_i)$. This completes the proof. \square

One advantage of the proposed technique is that the bound on the local error dynamics depends solely on locally available information at the i^{th} node. This implies that it can be applied with the same effect in both cases, where either a distributed or a centralized approach is adopted for the regulation of the nominal dynamics.

5.3 Regulation of the Nominal Dynamics

In the previous section, it was established that adopting the proposed control law leads to bounded error dynamics. Furthermore, the bounding functions depend on the nominal state, thus it is possible to establish a dynamic behaviour of the constraint set and reduce possible conservativeness stemming from assuming a constant nominal state. In this section, the results of Section IV will be used to design a control scheme for the nominal dynamics that is able to satisfy a modified dynamic version of the constraints. More specifically, the “tightened” constraints for the nominal dynamics can be formulated using the control law $i_{in,i} = -K_i e_i + u_i$ as

$$\mathbb{Z}(z) = \prod_{i \in \mathcal{M}} \mathbb{X}_i \ominus \mathcal{S}_i(z_i), \quad (5.18a)$$

$$\mathbb{U}(z) = \prod_{i \in \mathcal{M}} \mathbb{C}_i \ominus (-K_i) \mathcal{S}_i(z_i). \quad (5.18b)$$

It is noted that in both (5.18a) and (5.18b), the constraints are parametrised by a time-varying error set. This is where the conservativeness of the previous chapter is addressed. Instead of assuming the largest variant of $\mathcal{S}(z_i)$, the set is permitted to change in size, thus a larger set of control actions and feasible states is available during the optimisation process. The problem now becomes of choosing a control

law $u_i(\cdot)$ such that the nominal system,

$$C_i \dot{z}_i = -\mathcal{L}_{ii} z_i + \sum_{j \in \mathcal{N}_i} \mathcal{L}_{ij} z_j - \frac{\bar{P}_i}{z_i} + u_i \quad (5.19)$$

is asymptotically stable and satisfies the modified constraint sets in (5.18). This problem is traditionally addressed by adopting an MPC control scheme that is able to incorporate the constraint sets in the control design process. In order to achieve this, similar to the previous chapter, the following finite horizon optimization problem is adopted

$$V(z(t_0)) := \min_{\mathbf{u}} J(z(t_0), \mathbf{u}) \quad (5.20a)$$

$$= \min_{\mathbf{u}} \int_{t_0}^{t_0+T} \ell(z - \hat{z}, u - \hat{u}) dt + \ell_f(z - \hat{z}) \quad (5.20b)$$

and, for all $t \in [t_0, t_0 + T]$, subject to

$$z(0; t_0) = z(t_0) \quad (5.20c)$$

$$C \dot{z} = -\mathcal{L}z - [z]^{-1} \bar{P} + u, \quad (5.20d)$$

$$z \in \mathbb{Z}(z) \cap \{z \in \mathbb{R}^n : z_i \geq \beta_i, \forall i \in \mathcal{M}\}, \quad (5.20e)$$

$$u \in \mathbb{U}(z), \quad (5.20f)$$

$$\mathbb{Z}(z) \subseteq \mathbb{X}, \mathbb{U}(z) \subseteq \mathbb{C}, \quad (5.20g)$$

$$z_f := z(t_0 + T; t_0) \in \mathbb{Z}_f(\hat{z}) \quad (5.20h)$$

where $[t_0, t_0 + T]$ is the optimization horizon, the pair (\hat{z}, \hat{u}) denotes the desired network operating point, $\ell(\cdot, \cdot)$ is the stage cost of the optimal control problem, and $\ell_f(\cdot, \cdot)$ is the terminal cost function. The calculation of the reference pair (\hat{z}, \hat{u}) can be carried out by either incorporating an additional optimization objective in (5.20), or solved as a separate optimization problem, *i.e.* by solving

$$J_e = \min_{\hat{z}, \hat{u}} \sum_{i \in \mathcal{M}} f_{e,i}(z_i^*, u_i^*) \quad (5.21a)$$

s.t.

$$\hat{z} \in \mathbb{Z}(\hat{z}) \cap \{\hat{z} \in \mathbb{R}^n : \hat{z}_i \geq \beta_i, \forall i \in \mathcal{M}\}, \quad (5.21b)$$

$$\hat{u} \in \mathbb{U}(\hat{z}) \quad (5.21c)$$

$$-\mathcal{L}\hat{z} - [\hat{z}]^{-1} \bar{P} + \hat{u} = 0_n \quad (5.21d)$$

where $f_e(\cdot)$ is a strictly convex function translating the desired network operation to a set of reference points. The following assumption on the structure of the stage cost is invoked to ensure convexity of the optimization problem in (5.20). This will also be used to establish monotonic descent of the optimal value function and stability of the nominal dynamics.

Assumption 5.2 (Convexity and lower boundedness of stage cost). *The stage cost is continuous and satisfies $\ell(0, 0) = 0$. In addition, there exists a class \mathcal{K}_∞ function $\theta_1(\cdot)$, such that for all $(z, u) \in (\mathbb{Z} \times \mathbb{U})(z)$,*

$$\theta_1(\|z - \hat{z}\|) \leq \ell(z - \hat{z}, u - \hat{u}).$$

In order to ensure recursive feasibility and convergence of the solution in an MPC setting, it is common to employ positive invariant terminal ingredients, see [133]. This involves the existence of a positive invariant set for the terminal dynamics, *i.e.* the evolution of the system beyond the optimization horizon, a local control Lyapunov function and constraint satisfaction. A plethora of studies have successfully addressed this issue in the linear setting, however the nonlinearity introduced by the CPL in (5.19) destabilizes every reference fixed point \hat{z} . Similarly to the previous chapter, the nominal control law is augmented with a feedback term in order to address this problem. This yields,

$$u = -K_u z + \nu^o \tag{5.22}$$

where K_u is a diagonal matrix representing the feedback gain and ν^o is now the new control action that is generated by the optimization problem in (5.20). The augmented control law in (5.22) provides additional damping to the dynamics such that the effect of the CPL at steady state is counteracted. In addition, it is now possible to construct suitable terminal ingredients such that (5.20) is recursively feasible. This is shown in the following result.

Proposition 5.3 (Stability of the terminal dynamics). *Considering the nominal system (5.19) and control law (5.22), there exists a $\delta > 0$ such that the fixed point \hat{z} is an asymptotically stable equilibrium with region of attraction $\mathcal{A} = \{z \in M : \|z - \hat{z}\| \leq \delta\}$, if and only if,*

$$K_{z,i} > \frac{\bar{P}_i}{(\hat{z}_i)^2},$$

for all $\hat{z} \in \mathbb{Z}(\hat{z})$.

Proof. Similar to the proof of Proposition 4.3. □

Corollary 5.1. *Any level set \mathbb{Z}_o of \mathcal{A} , such that $\mathbb{Z}_o = \beta\mathcal{A}$ with $\beta \in [0, 1]$, is control invariant for the nominal dynamics in (5.19).*

5.4 Stability and Recursive Feasibility

The previous sections established the conditions under which the error dynamics are bounded when the nominal state is perceived as an external input. Furthermore, the tools to construct a feasible MPC control scheme were also provided. In

this section, the obtained results are exploited to show that the cascaded system is asymptotically stable and the optimization problem of the previous section is recursively feasible. A direct consequence of Proposition 5.3 and Corollary 5.1 is that by using the augmented control law in (5.22) in combination with a terminal cost function $\ell_f = \|z - \hat{z}\|_{\mathcal{P}}$ and terminal set $\mathbb{Z}_f(\hat{z}) = \mathbb{Z}_o(\hat{z})$ in (5.20) yields recursive feasibility of the optimization control problem, provided that it is feasible at some initial state $z(t_0)$. This is a well-established result in the literature, where a sketch of the proof was provided in Proposition 4.4 of the previous chapter. Having established the recursive feasibility property of the optimal control problem, the value function of the optimisation problem can be shown to be a Control Lyapunov function for the closed loop system. This implies that, for every $\delta P \in \mathbb{W}$, there exist a continuous map to the equilibrium space, where each respective equilibrium is asymptotically stable. The stability of the nominal dynamics is shown in the following result.

Proposition 5.4. *For all $i \in \mathcal{M}$, the reference point \hat{z} is an asymptotically stable equilibrium point of the nominal dynamics (5.19).*

Proof. Let for simplicity $z = z(t_0)$ and $z^+ = \phi(z_0, t_0 + k)$, where $\phi(z_0, t_0 + k)$ is the trajectory map from initial state z_0 and after time $t_0 + k$. Then, optimality of $V(\cdot)$ yields

$$V(z^+) - V(z) \leq J(z, \mathbf{u}) - V(z).$$

The feasibility of the nominal optimisation problem in 5.20 implies that the control sequence at time $t_0 + k$ is the tail of the optimal control sequence at time t_0 . Therefore, at the next sampling time one has $u^+ = u^o(t_0 + k; t_0)$ and $z^+ = z(t_0 + k; t_0)$. By applying Assumption 5.2, the above yield

$$\begin{aligned}
 J(z, \mathbf{u}) - V(z) &\leq \\
 &\ell(z^o(t_0 + T; t_0) - \hat{z}, u^o(t_0 + T; t_0) - \hat{u}) \\
 &\quad - \theta_1(\|z - \hat{z}\|) \\
 &\quad + \ell_f(\phi(z^o(t_0 + N; t_0), t_0 + T + k)) \\
 &\quad - \ell_f(z^o(t_0 + N; t_0)).
 \end{aligned}$$

However, the stabilizing terminal control law implies

$$\begin{aligned}
 \ell_f(z^o(t_0 + N; t_0)) &\geq \\
 &\ell(z^o(t_0 + T; t_0) - \hat{z}, u^o(t_0 + T; t_0) - \hat{u}) \\
 &\quad + \ell_f(\phi(z^o(t_0 + N; t_0), t_0 + T + k)),
 \end{aligned}$$

therefore

$$V(z^+) - V(z) \leq -\theta_1(\|z - \hat{z}\|) \leq 0.$$

5.5. SIMULATIONS

Hence, the value function $V(\cdot)$ monotonically decreases for all $z \in \mathbb{Z}(z)$. Since $V(\cdot)$ is also positive definite by construction, the value function is a Control Lyapunov function for the system (5.19) and thus \hat{z} is an asymptotically stable equilibrium point. \square

In the sequel, the results of this chapter are collected in order to show the stability of the decomposed dynamics.

Theorem 5.1. *Let Assumptions 5.1 and 5.2 hold, then the cascaded dynamics given by*

$$\begin{aligned} C_i \dot{e}_i &= -(\mathcal{L}_{ii} + K_i)e_i - \sum_{j \in \mathcal{N}_i} \mathcal{L}_{ij}e_j + \frac{\bar{P}_i}{(e_i + z_i)z_i}e_i - \frac{\delta P_i}{e_i + z_i}, \\ C_i \dot{z}_i &= -\mathcal{L}_{ii}z_i + \sum_{j \in \mathcal{N}_i} \mathcal{L}_{ij}z_j - \frac{\bar{P}_i}{z_i} + u_i, \end{aligned}$$

admit asymptotically stable equilibrium point (\hat{e}, \hat{z}) in $\mathcal{S}(\bar{z}) \times \mathbb{Z}(\hat{z}) \subseteq \mathbb{X} \times \mathbb{C}$.

Proof. Boundedness of the error dynamics follows from Prop. 5.2, by considering the nominal state $z(t)$ as an exogenous input. Using Assumptions 5.1 and 5.2, Prop. 5.4 shows asymptotic stability of the equilibrium points of the nominal dynamics. Therefore, by applying [176, Theorem 10.3.1], it can be concluded that the equilibrium pair (\hat{e}, \hat{z}) is asymptotically stable for the cascaded dynamics. \square

5.5 Simulations

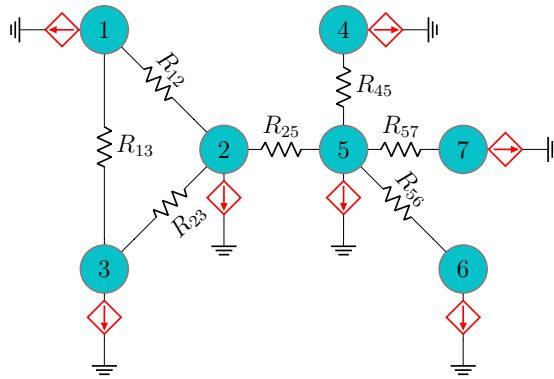


Figure 5.1: Meshed MG with seven nodes locally connected to a CPL.

In this section, the theoretic properties of the proposed control scheme are illustrated in a simulated scenario of a network with topology depicted in Fig. 5.1. The network voltages are required to operate in the range $22 V \leq v \leq 26V$, where

5.5. SIMULATIONS

the rated voltage is $24V$. This choice of voltage levels aids in a clearer illustration of this chapter’s theoretic results, since a large nominal voltage would result in a smaller difference between the dynamic tube and the rigid tube of the previous chapter. The inner current of the converter is also subjected to the constraint set $|i_{in}| \leq 15A$. Similar to the previous chapter, the state-limiting PI is adopted for the regulation of the inner current loop. The nominal load demand is chosen at $\bar{P}_i = 100W$, with maximum perturbations restricted as in $|\delta P| \leq 20W$. The tube upper and lower boundaries for each node is constructed according to Section 5.2, with feedback gain chosen as $K_i = 4$ and nominal feedback gain $K_{z,i} = 15$ for all $i \in \mathcal{M}$. The network voltage dynamics are subjected to a reference change at times $t = 0ms$, $t = 0.5ms$ and $t = 1ms$. Following the application of the MPC scheme, the nominal trajectories converge to their respective reference, while satisfying a “tightened” parametrisation of the state and input constraints. This is depicted in Fig. 5.5. In addition, Fig. 5.5 demonstrates that the true voltage is always contained in the dynamic tube, where the size of the tube depends on the distance between the nominal voltage and the lower bound of the constraint set. Furthermore, Fig. 5.6 shows that both the current references provided by the voltage controller and the current trajectories satisfy their respective constraints, validating the presented analysis. A clear demonstration of the controller properties can be seen in Fig. 5.2, depicting the state space of Node 1 from Fig. 5.1. Starting from initial state $x(t_0) = (v(t_0), i_{in}(t_0))$ the nominal trajectory defines the centre of the tube, where cross-sections at various time instances is shown by the rectangles. As it can be seen, the uncertain trajectory is always contained within the Cartesian product of the constraint sets. The dynamic transition of the tube size is clearly depicted in Fig. 5.3, where the cross-sections of the tube of Node 1 are plotted at times $t = 0s$ and $t = 15s$, *i.e.* at the times where the nominal voltage is closer to the lower bound and the upper bound of the constraint set respectively. It is seen that the closer the nominal trajectory is to the respective lower bound of the parametrised constraint set, the more conservative is the tube size. The ability to reduce the tube size conservativeness is a clear improvement over the approach presented in the previous chapter, since it implies a larger nominal input constraint set, *i.e.* availability of more control actions in the nominal control layer. In order to clearly demonstrate this, a comparison between the rigid tube approach and the dynamic tube are illustrated in Fig. 5.4. Therein, it is seen that with the same problem setup, same tuning parameters and same nominal voltage reference values, the dynamic tube avoids activation of the constraint set and results in a quicker response. On the other hand, the rigid tube approach demonstrates higher convergence time. Finally, it is important to mention the interaction between the

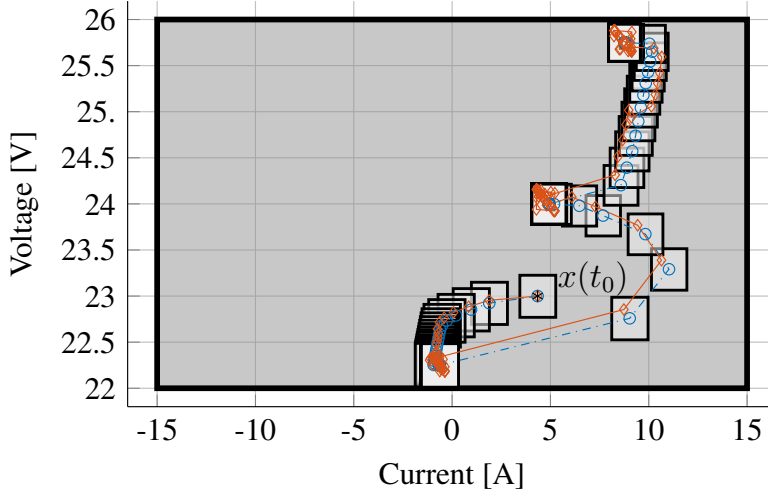


Figure 5.2: State space of Node 1. The constraint set $\mathbb{Y} = \mathbb{X} \times \mathbb{C}$ is depicted as \blacksquare and the tube cross-sections with \square . The nominal voltage defining the centre of the tube is depicted with $(- - -)$ and the uncertain trajectory with $(- - -)$.

feedback gain and the sizes of the voltage and current constraint sets. As it was also explained in Remark 4.2, higher values of the gain K result in a “less tightened” state constraint set, which, however, inversely affects the size of the input current constraint set. This can be seen by the constraint set parametrisation in (5.18). Therefore, the choice of the gain K needs to be made according to the each individual case-study specifications to achieve the desired result.

5.6 Conclusions

This chapter presented a dynamic tube-based control scheme for DC Microgrids with local CPLs connected in parallel to each node of the network. The behaviour of the CPL was characterised by constant fluctuations of the load demand. The presented theoretical analysis demonstrated that system robustness to this constant disturbance effect can be achieved by exploiting the structure of the node dynamics. In particular, the original uncertain dynamics were “split” into two subsystems; a nominal subsystem where the load demand is considered constant to a predefined value, and an error subsystem describing the difference between the nominal and the uncertain model. Then, Section 5.2 showed how a tube around the nominal voltage trajectory can be constructed, such that it is positive invariant under the solution of the uncertain dynamics. Analytic conditions on the tuning parameters were also provided to guarantee that the system exhibits the desired closed-loop behaviour. In addition, it was revealed that the size of the tube is dependent on the evolution of the nominal trajectory. This result was then used in the parametrization of the

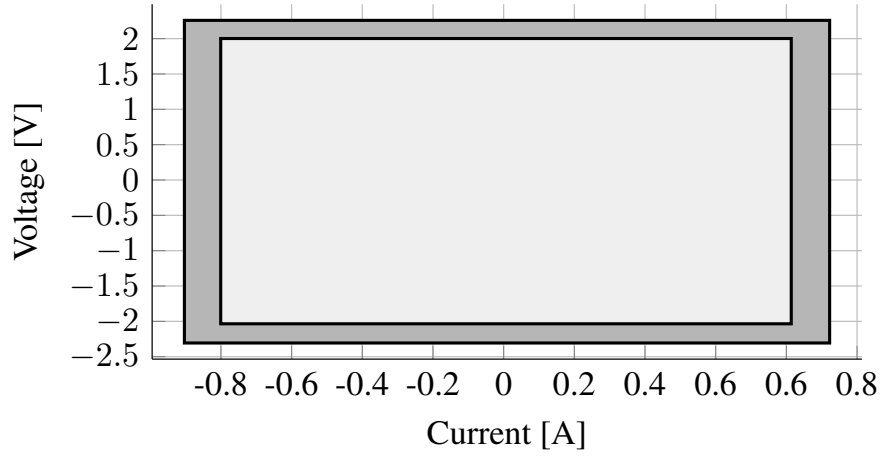


Figure 5.3: Cross-sections of the tube at time $t = 0s$ depicted with \blacksquare and at time $t = 15s$ depicted as \square . It can be seen that the closer the nominal voltage is to the lower bound of the constraint set the larger is the tube size.

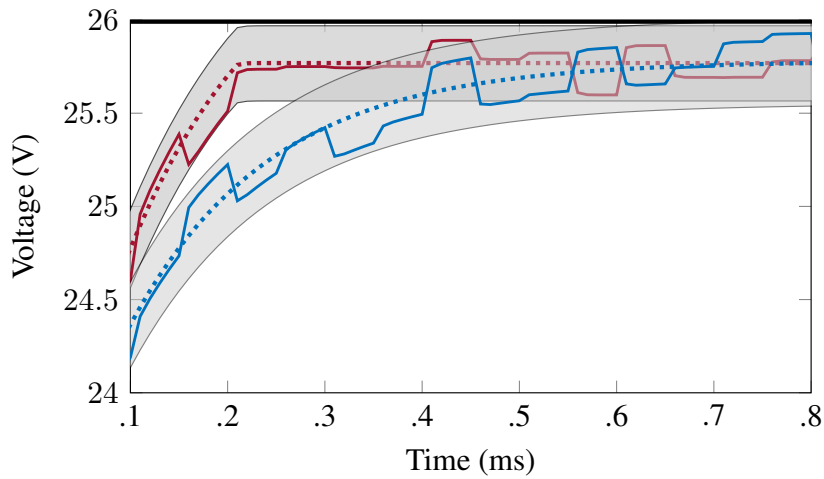


Figure 5.4: Comparison between the rigid-tube (—) approach presented in Chapter 4 and the dynamic tube (—) of this chapter. The rigid tube activates the constraint set and results in larger convergence time.

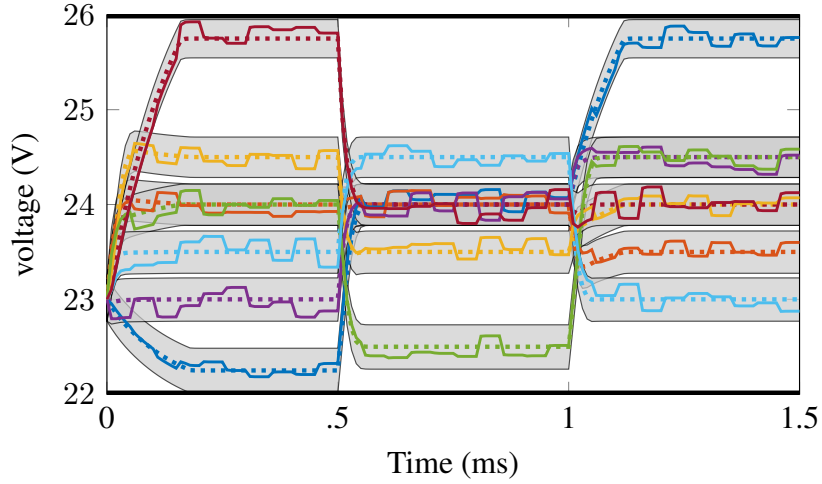


Figure 5.5: Node uncertain and nominal voltages of Node 1 (—,····), Node 2 (—,····), Node 3 (—,····), Node 4 (—,····), Node 5 (—,····), Node 6 (—,····), and Node 7 (—,····). The black solid lines represent the upper and lower bound respectively of the nodal constraint set.

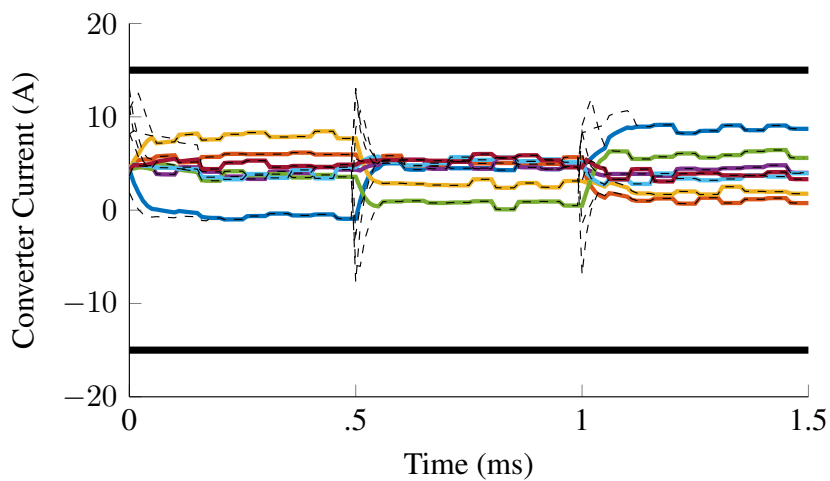


Figure 5.6: Current trajectories and references provided by the voltage layer.

5.6. CONCLUSIONS

constraint sets in order to reduce conservativeness arising from always assuming a worst-case scenario for the value of the nominal voltage.

Following the results on the invariance of the error dynamics, a MPC control scheme was proposed to achieve constrained regulation of the nominal trajectories to desired operating points. To this aim, the nominal control law was augmented by an additional feedback to counteract the negative impedance effect of the non-linearity at steady state. This allowed the construction of a positive invariance set for the MPC prediction model, which was then used to prove the recursive feasibility of the overall optimal control problem. Finally, an analytic stability proof for the closed loop dynamics was provided in two stages; first, the stability of the nominal dynamics was proven by exploiting the recursive feasibility property of the optimization problem to show monotonic decrease of the MPC value function. This was used to show that the value function is a Control Lyapunov function for the nominal dynamics and thus proving asymptotic stability of the respective feasible equilibrium points. Having established boundedness of the error dynamics, results from the theory of interconnected systems were applied to prove the asymptotic stability of the overall cascaded dynamics. The theoretic results of this study were illustrated in a simulated scenario of a meshed MG, where each node is locally connected to a CPL.

Chapter 6

Tube-based Control for Islanded AC Microgrids

The destabilising behaviour of constant power loads is also a predominant problem in the case of AC Microgrid networks. More importantly, the complexity of this problem is magnified due to the structure of the network dynamics. Instead of the single-phase converter, the integration of the DER units is performed through the three-phase inverters, where each dynamic component is represented by three states. This increase in complexity, entangles the adoption of the set-invariance techniques presented in the previous chapters, making the transition to the AC problem non-trivial. As it will be shown in this chapter, the complexity of the problem can be partially reduced by adopting the well-established dq transformation of the dynamical model, where the three-phase model can be simplified to a two-state counterpart. Nevertheless, the problem remains significantly more complicated compared with the DC scenario and necessitates an individual analysis to establish the desired bounded-input bounded-output results. This problem will be addressed in this chapter, where a particular attention will be given in the analytical behaviour induced by the CPL. Its effect of the two-dimensional state space will be discussed, and a characterisation of the respective subspace with a positive tangent vectorfield will be provided. Following similar principles with the previous chapters, the original uncertain dynamics are “split” into a nominal and an error model, and the proposed control law aims to bound the deviations between the nominal and the uncertain state trajectories into a positive invariant set. Then, following the necessary theoretical analysis, tuning guidelines are provided in the form of conditions on the controller parameters, such that the system displays robustness with respect to the destabilising effect of the CPL.

The problem statement is provided in Section 6.1, where the respective models of the load and the network system are defined. Then, Section 6.2 formally defines

the proposed control law and provides a preliminary discussion on the analytical approach. The properties of the CPL and its effect on the local node dynamics are investigated in Section 6.3, where the main results of this chapter are presented. Section 6.4 illustrates the properties of the closed-loop system in a simulated scenario and Section 6.5 provided some remarks on the network operation and discusses potential improvements in future approaches.

6.1 Problem Statement

The problem of designing a robust controller for isolated AC microgrids with local CPLs is investigated. Each interfacing inverter unit is considered as a controllable voltage source interfaced with the rest of the system with purely resistive lines. Similarly to previous chapters, in order to simplify the analysis, it is assumed that the inverter inner current is operating at a faster time scale than the voltage, *i.e.* the inner current has converged and is assumed as a control input in the voltage dynamics. Furthermore, the dq transformation of each local inverter model is adopted, rotating at a constant common frequency ω_c . Thus, the local dynamics are formulated as

$$C_i \frac{v_{d,i}}{dt} = i_{in,id} + \omega_c C_i v_{q,i} - \mathcal{L}_{ii} v_{d,i} - \sum_{j \in \mathcal{N}_i} \mathcal{L}_{ij} v_{d,j} - g_{d,i}(v_{d,i}, v_{q,i}, P_i, Q_i) \quad (6.1a)$$

$$C_i \frac{v_{q,i}}{dt} = i_{in,iq} - \omega_c C_i v_{d,i} - \mathcal{L}_{ii} v_{q,i} - \sum_{j \in \mathcal{N}_i} \mathcal{L}_{ij} v_{q,j} - g_{q,i}(v_{d,i}, v_{q,i}, P_i, Q_i) \quad (6.1b)$$

where C_i is the local output inverter capacitance, $\mathcal{L} \in \mathbb{R}^{n \times n}$ is the Laplacian matrix that describes the topology of the network, and $i_{in,i}$ is the inverter input current. The set $\mathcal{N}_i := \{j \in \mathcal{M} : \mathcal{L}_{ij} \neq 0, i \neq j\}$ denotes the neighbours of the i^{th} node. Finally, $[g_{d,i} \ g_{q,i}]^T$ represents the current drawn by the load in the respective dq components. Since this study considers purely constant power loads, which introduce a nonlinear behaviour to the dq inverter dynamics, the load model is explicitly expressed as

$$\begin{bmatrix} g_{d,i}(v_{d,i}, v_{q,i}, P_i, Q_i) \\ g_{q,i}(v_{d,i}, v_{q,i}, P_i, Q_i) \end{bmatrix} = \frac{2}{3} \begin{bmatrix} \frac{v_{d,i}}{v_{d,i}^2 + v_{q,i}^2} & \frac{v_{q,i}}{v_{d,i}^2 + v_{q,i}^2} \\ \frac{v_{q,i}}{v_{d,i}^2 + v_{q,i}^2} & -\frac{v_{d,i}}{v_{d,i}^2 + v_{q,i}^2} \end{bmatrix} \begin{bmatrix} P_i \\ Q_i \end{bmatrix} \quad (6.2)$$

The control problem considered in this paper is that of designing a feedback control law for the input currents such that system voltages remain bounded, despite the presence of CPLs.

6.2 Control Scheme Formulation

In this section, the first steps of the control design process are presented and the control objective is formally defined. It is assumed that both components of the load demand at the i^{th} node lie in polytopic sets with the origin within their interior, *i.e.* $P_i \in \mathbb{P}_i$ and $Q_i \in \mathbb{Q}_i$. This allows the expression of the load power demand as a deviation to constant values $\hat{P}_i \in \mathbb{R}_{>0}$ and $\hat{Q}_i \in \mathbb{R}_{>0}$ respectively, such that

$$\delta P_i = P_i - \hat{P}_i \in \mathbb{W}_{P,i} \subseteq \mathbb{P}_i, \quad (6.3)$$

$$\delta Q_i = Q_i - \hat{Q}_i \in \mathbb{W}_{Q,i} \subseteq \mathbb{Q}_i, \quad (6.4)$$

and

$$\mathbb{W}_{P,i} := \left\{ \delta P_i \in \mathbb{R} : \underline{\delta P}_i \leq \delta P_i \leq \overline{\delta P}_i \right\}, \quad (6.5)$$

$$\mathbb{W}_{Q,i} := \left\{ \delta Q_i \in \mathbb{R} : \underline{\delta Q}_i \leq \delta Q_i \leq \overline{\delta Q}_i \right\}. \quad (6.6)$$

where $\mathbb{W}_{P,i}$ and $\mathbb{W}_{Q,i}$ are also polytopic sets with $\{0\} \in \text{int}(\mathbb{W}_{P,i})$, $\text{int}(\mathbb{W}_{Q,i})$. In order to facilitate the control scheme formulation, an error state $e_i = [e_{d,i} \ e_{q,i}]^\top$ is introduced, with

$$\begin{bmatrix} e_{d,i} \\ e_{q,i} \end{bmatrix} = \begin{bmatrix} v_{d,i} - z_{d,i} \\ v_{q,i} - z_{q,i} \end{bmatrix} \quad (6.7)$$

where $[z_{d,i} \ z_{q,i}]^\top$ denotes the local nominal voltage, *i.e.* when $\delta P_i = \delta Q_i = 0$. The local nominal dynamics are, then, formulated as

$$\begin{aligned} C_i \dot{z}_{d,i} = & u_{d,i} + \omega_c C_i z_{q,i} - \mathcal{L}_{ii} z_{d,i} - \sum_{j \in \mathcal{N}_i} \mathcal{L}_{ij} z_{d,j} \\ & - \frac{2}{3} \bar{P}_i \frac{z_{d,i}}{z_{d,i}^2 + z_{q,i}^2} - \frac{2}{3} \bar{Q}_i \frac{z_{q,i}}{z_{d,i}^2 + z_{q,i}^2}, \end{aligned} \quad (6.8a)$$

$$\begin{aligned} C_i \dot{z}_{q,i} = & u_{q,i} - \omega_c C_i z_{d,i} - \mathcal{L}_{ii} z_{q,i} - \sum_{j \in \mathcal{N}_i} \mathcal{L}_{ij} z_{q,j} \\ & - \frac{2}{3} \bar{P}_i \frac{z_{q,i}}{z_{d,i}^2 + z_{q,i}^2} + \frac{2}{3} \bar{Q}_i \frac{z_{d,i}}{z_{d,i}^2 + z_{q,i}^2}, \end{aligned} \quad (6.8b)$$

where $u_i = [u_{d,i} \ u_{q,i}]^\top$ is the nominal control input. In order to simplify the dynamics, it is common to regulate the q-component of the voltage to zero. Similarly, it is assumed here that one can design a nominal control scheme for the uncertainty-free system in (6.8), such that $z_{q,i} = 0$ holds at all times. This allows the distinction of two separate cases. First, if the q-component of the error can be enforced to be zero at all times, then the remaining d-component of the dynamics is equivalent to

6.2. CONTROL SCHEME FORMULATION

the case of a DC Microgrid and one can achieve robust regulation similar to the DC scenario presented in the previous chapter. However, enforcing $e_{q,i} = 0$ at all times is not universally realistic, therefore the general case is considered, where $e_{q,i}$ cannot be trivially neglected. To this aim, the control law of the original dynamics is defined as

$$\dot{i}_{in,i} = -(K_{1,i} + K_{2,i})\mathbb{I}_2 e_i + u_i, \quad (6.9)$$

where $K_{1,i}, K_{2,i}$ are positive feedback gains. Although the feedback structure involving a summation of two scalar gains seems redundant, as will be shown in the following, the term $K_{2,i}$ will be used to decouple the overall network stability problem as of an isolated nodal stability problem. Then, the set-invariance analysis will be based on the second feedback term $K_{1,i}$. Following (6.7), the local error dynamics take the form

$$\begin{aligned} C_i \dot{e}_{d,i} = & \omega_c C_i e_{q,i} - (\mathcal{L}_{ii} + K_{1,i} + K_{2,i})e_{d,i} - \sum_{j \in \mathcal{N}_i} \mathcal{L}_{ij} e_{d,j} \\ & + \frac{2}{3} \left(\frac{\bar{P}_i(e_{d,i}(e_{d,i} + z_{d,i}) + e_{q,i}^2)}{z_{d,i}(e_{d,i} + z_{d,i})^2 + z_{d,i}e_{q,i}^2} - \frac{\hat{Q}_i e_{q,i}}{(e_{d,i} + z_{d,i})^2 + e_{q,i}^2} \right) \\ & - \frac{2}{3} \frac{\delta P_i(e_{d,i} + z_{d,i}) + \delta Q_i e_{q,i}}{(e_{d,i} + z_{d,i})^2 + e_{q,i}^2}, \end{aligned} \quad (6.10a)$$

$$\begin{aligned} C_i \dot{e}_{q,i} = & -\omega_c C_i e_{d,i} - (\mathcal{L}_{ii} + K_{1,i} + K_{2,i})e_{q,i} - \sum_{j \in \mathcal{N}_i} \mathcal{L}_{ij} e_{q,j} \\ & - \frac{2}{3} \left(\frac{\hat{P}_i e_{q,i}}{(e_{d,i} + z_{d,i})^2 + e_{q,i}^2} - \frac{\hat{Q}(e_{d,i}(e_{d,i} - z_{d,i}) - e_{q,i}^2)}{z_{d,i}(e_{d,i} + z_{d,i})^2 + z_{d,i}e_{q,i}^2} \right) \\ & + \frac{2}{3} \frac{\delta Q_i(e_{d,i} + z_{d,i}) - \delta P_i e_{q,i}}{(e_{d,i} + z_{d,i})^2 + e_{q,i}^2}. \end{aligned} \quad (6.10b)$$

The goal is to investigate under which conditions on the magnitude of $K_{1,i}$, the solution of the error dynamics obtains a uniform bound around the origin. To this aim the energy-like function, for the overall network dynamics, is defined as

$$V(e) = \frac{1}{2} e_d^\top C e_d + \frac{1}{2} e_q^\top C e_q, \quad (6.11)$$

with time derivative

$$\dot{V}(e) = e_d^\top C \dot{e}_d + e_q^\top C \dot{e}_q, \quad (6.12)$$

where $C = \text{diag}\{C_1, \dots, C_n\}$. The function $\dot{V}(\cdot)$ essentially describes the geometric behaviour of the error states. Therefore, particular interest will be given in characterising the subspaces of the state space, where the derivative obtains positive and negative values respectively. The core objective of the following set-invariance

analysis is showing that the former is enclosed in a closed and bounded set containing the origin, where outside of this set the derivative obtains strictly negative values. Therefore, analytic tools can be used to guarantee that any state trajectory emanating from an initial state within this closed set will remain in the set for all future times. Bounding the error state drastically simplifies the control design process, since the remaining, arguably simpler, task is regulating the uncertainty-free nominal state to a desired setpoint, while satisfying some parametrised version of the original operating constraints. If this is achieved, then the adopted control law “forces” the original uncertain state trajectory to “follow” the generated nominal.

Following the definition of the energy-like function of the system, it is noted that by the properties of the Laplacian matrix, it holds that the matrix $\mathcal{L} + K_{2,i}\mathbb{I}_n$ is positive definite for any arbitrarily small positive value of $K_{2,i}$. Therefore, substituting the error dynamics in \dot{V} and applying the scalar relations $e_d^\top(\mathcal{L} + K_{2,i}\mathbb{I}_n)e_d < 0$ and $e_q^\top(\mathcal{L} + K_{2,i}\mathbb{I}_n)e_q < 0$, results in the upper bound

$$\dot{V}(e) \leq \sum_{i \in \mathcal{M}} \frac{\tilde{V}_i(e_i)}{z_{d,i}((e_{d,i} + z_{d,i})^2 + e_{d,i})}, \quad (6.13)$$

where

$$\begin{aligned} \tilde{V}_i(e_i) = & \quad (6.14) \\ & e_{d,i}^4(-3K_{1,i}z_{d,i}) + e_{d,i}^3(-6K_{1,i}z_{d,i}^2 + 2\hat{P}_i) + \\ & e_{d,i}^2e_{q,i}^2(-3K_{1,i}z_{d,i}) + e_{d,i}^2e_{q,i}(-3K_{1,i}z_{d,i} + 2\hat{Q}_i) + \\ & e_{d,i}^2(-3K_{1,i}z_{d,i}^3 + 2\hat{P}_iz_{d,i} - 2\delta P_iz_{d,i}) + \\ & e_{d,i}e_{q,i}^2(-6K_{1,i}z_{d,i}^2 + 2\hat{P}_i) + e_{d,i}e_{q,i}(-4\hat{Q}_iz_{d,i}) + \\ & e_{q,i}^2(-3K_{1,i}z_{d,i}^3 - 2\hat{P}_iz_{d,i} - 2\delta P_iz_{d,i}) + \\ & e_{q,i}^3(-3K_{1,i}z_{d,i} - 2\hat{Q}_i) + e_{d,i}(-2\delta P_iz_{d,i}^2) + \\ & e_{q,i}(2\delta Q_iz_{d,i}^2). \end{aligned}$$

As a result, the right-hand side of the inequality is decoupled and it suffices to investigate the region where any of the i^{th} summands in the bound of (6.13) attains positive values.

6.3 Positive invariance of the dynamics

Following the problem formulation of the previous section, the task becomes finding a closed subset of the state space around the origin where (6.13) admits positive values and show that outside of the boundary of this set the time derivative becomes negative. This would imply that this subset is positive invariant under the trajectory

6.3. POSITIVE INVARIANCE OF THE DYNAMICS

of the error dynamics, hence the distance between the uncertain and nominal voltage trajectories is bounded. In the following, it will be initially assumed that the relation $z_{d,i} \geq 0$ holds at all times. However, in later parts of the section, a sufficient positive lower bound on the nominal state will be established such that the denominator of (6.13) is strictly positive.

First, the behaviour of the numerator of (6.13) is investigated. This term can be expressed as a summation of two functions

$$\tilde{V}_i(e_i) = f_i(e_{d,i}, e_{q,i}) + h_i(e_{d,i}, e_{q,i}, \delta P_i, \delta Q_i) \quad (6.15)$$

where,

$$\begin{aligned} f_i(e_{d,i}, e_{q,i}) := & \\ & e_{d,i}^4(-3K_{1,i}z_{d,i}) + e_{d,i}^3(-6K_{1,i}z_{d,i}^2 + 2\hat{P}_i) + \\ & e_{q,i}^3(-3K_{1,i}z_{d,i} - 2\hat{Q}_i) + e_{d,i}^2e_{q,i}^2(-3K_{1,i}z_{d,i}) + \\ & e_{d,i}^2e_{q,i}(-3K_{1,i}z_{d,i} + 2\hat{Q}_i) + e_{d,i}e_{q,i}^2(-6K_{1,i}z_{d,i}^2 + 2\hat{P}_i) + \\ & e_{d,i}e_{q,i}(-4\hat{Q}_iz_{d,i}) + e_{d,i}^2(-2K_{1,i}z_{d,i}^3 + 2\hat{P}_iz_{d,i}) + \\ & e_{q,i}^2(-2K_{1,i}z_{d,i}^3 - 2\hat{P}_iz_{d,i}), \end{aligned} \quad (6.16)$$

and a function gathering the uncertainty terms

$$\begin{aligned} h_i(e_{d,i}, e_{q,i}, \delta P_i, \delta Q_i) := & e_{d,i}^2(-K_{1,i}z_{d,i}^3 - 2\delta P_iz_{d,i}) + \\ & e_{q,i}^2(-K_{1,i}z_{d,i}^3 - 2\delta P_iz_{d,i}) + \\ & e_{d,i}(-2\delta P_iz_{d,i}^2) + e_{q,i}(2\delta Q_iz_{d,i}^2). \end{aligned} \quad (6.17)$$

The second summand of (6.15) describes the region of $\dot{V}(\cdot)$ where the CPL demand perturbations $(\delta P_i, \delta Q_i)$ impose a positive velocity on the closed loop vector field. Note that (6.17) is the general equation of a circular paraboloid surface. Since the analysis is focused on the subdomain of $\dot{V}(\cdot)$ that is mapped to non-negative values on the surface, the cross-section of the surface with the hyperplane of the origin can be perceived as the desired boundary set. This results in a two dimensional set, described by a circle with radius

$$r(z_{d,i}, \delta P_i, \delta Q_i) = \frac{z_{d,i}\sqrt{\delta P_i^2 + \delta Q_i^2}}{K_{1,i}z_{d,i}^2 + 2\delta P_i}, \quad (6.18)$$

and centre given by the function

$$c(z_{d,i}, \delta P_i, \delta Q_i) = \left(\frac{-\delta P_iz_d^2}{Kz_d^3 + 2\delta P_iz_d}, \frac{\delta Q_iz_d^2}{Kz_d^3 + 2\delta P_iz_d} \right). \quad (6.19)$$

The subdomain that is mapped to non-negative values is closed and bounded if the paraboloid opens downwards, *i.e.* the ‘‘peak’’ of the surface occurs in positive

values. This yields the condition

$$K_{1,i} > \frac{2|\delta P_i|}{z_{d,i}^2}. \quad (6.20)$$

Provided that (6.20) is satisfied, the above imply the existence of a closed set where its size “grows” proportionally to the magnitude of the load demand perturbations $(\delta P_i, \delta Q_i)$, as evident from (6.18). A sequence of maximum load demand perturbations is defined as

$$\mathcal{W}_i := \left\{ \begin{bmatrix} \overline{\delta P}_i & \overline{\delta Q}_i \end{bmatrix}^\top, \begin{bmatrix} \overline{\delta P}_i & \overline{\delta Q}_i \end{bmatrix}^\top \begin{bmatrix} \underline{\delta P}_i & \underline{\delta Q}_i \end{bmatrix}^\top, \begin{bmatrix} \underline{\delta P}_i & \underline{\delta Q}_i \end{bmatrix}^\top \right\} \quad (6.21)$$

with each k^{th} element denoted as $w(k) = [w_1(k) \ w_2(k)]^\top$, where $w_1(k)$ and $w_2(k)$ represent the active and reactive components respectively. Then, a worst-case scenario can be compactly defined for each element of \mathcal{W}_i with the set

$$\mathbb{B}_{i,k}(z_{d,i}) := \left\{ e_i \in \mathbb{R}^2 : d(e_i, c(z_{d,i}, w_1(k), w_2(k))) \leq r(z_{d,i}, w_1(k), w_2(k)) \right\}. \quad (6.22)$$

where $d(\cdot, \cdot)$ is the euclidean distance. Then, due to the linearity of (6.17) w.r.t. the load, boundedness of the function (6.17) can be deduced in the set resulting from the union

$$\mathcal{N}_i(z_{d,i}) := \bigcup_{k \in \{1, \dots, 4\}} \mathbb{B}_{i,k}(z_{d,i}). \quad (6.23)$$

Therefore, the above describes the closed subset of the state space, where the load demand perturbations impose a positive velocity on the dynamics. Note that the origin is a common point for all $\mathbb{B}_{i,k}(z_{d,i})$, hence the intersection of all $\mathbb{B}_{i,k}(z_{d,i})$ is also non-empty. This implies that $\mathcal{N}_i(z_{d,i})$ results from the union of overlapping sets, as opposed to four distinct sets in the state space. An example network is used to illustrate the above in Fig. 6.1. In order to conclude positive invariance of $\mathcal{N}_i(z_{d,i})$, it suffices to show that (6.16) is negative definite in a neighbourhood of every point in $\partial \mathcal{N}_i(z_{d,i})$ and the denominator of (6.13) is strictly positive for all $e_i \notin \mathcal{N}_i(z_{d,i})$. The following result provides sufficient conditions on the tuning parameters such that the first requirement is satisfied. In the proof, it is shown that if both conditions of the proposition are met, condition (6.20) is also implicitly satisfied.

Proposition 6.1. *If the feedback gain and the nominal voltage trajectory satisfy*

$$K_{1,i} \geq \frac{\hat{Q}_i}{z_{d,i}}, \quad (6.24)$$

and

$$z_{d,i} > \max_{\substack{\delta P_i \in \mathbb{W}_{P,i}, \\ \delta Q_i \in \mathbb{W}_{Q,i}}} \left\{ \frac{\hat{P}_i + 12\sqrt{\delta P_i^2 + \delta Q_i^2} + 2\overline{\delta P}_i}{\hat{Q}_i} \right\}, \quad (6.25)$$

respectively, then for all $i \in \mathcal{M}$:

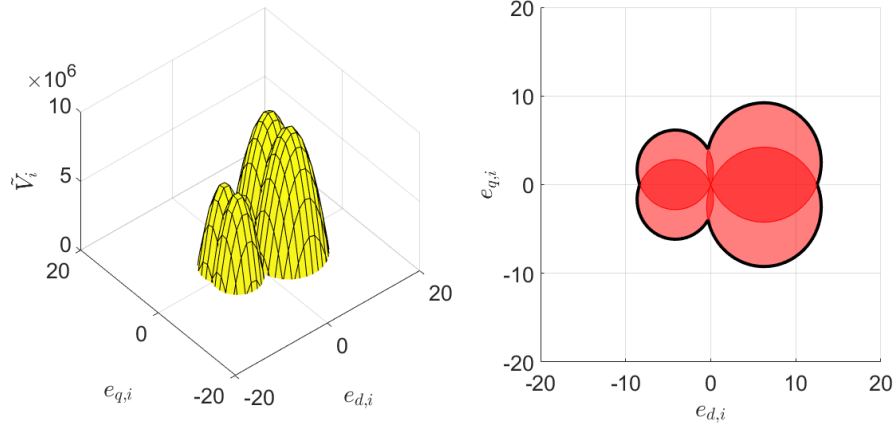


Figure 6.1: Example of the geometric effect of the CPL on the velocity of the energy-like function. **(Left)** The surface where $h_i(e_{d,i}, e_{q,i}, \delta P_i, \delta Q_i)$ is mapped to non-negative values. **(Right)** The projection of the surface on the state space (*red*) and the boundary of $\mathcal{N}_i(z_{d,i})$ (*black*). It can be seen from this figure that the control design and analysis in this case is indeed not as straightforward as in the DC scenario. The coupling between the d and q components leads to an invariant set that is not just a Cartesian product of the invariant sets depicted in the previous chapters.

- the function $f_i: \mathbb{R}^2 \rightarrow \mathbb{R}$ satisfies

$$f_i(e_i) \leq -\theta(\|e_i\|),$$

for all $e_i \in \mathcal{S}(z_{d,i})$ with

$$\mathcal{S}(z_{d,i}) := \{e_i \in \mathbb{R}^2: e_{q,i} \geq \underline{e}_{q,i}(z_{d,i}), e_{d,i} \geq \underline{e}_{d,i}(z_{d,i})\}, \quad (6.26)$$

where $\theta: \mathbb{R} \rightarrow \mathbb{R}^+$ is a class- \mathcal{K}_∞ function and

$$\underline{e}_{d,i}(z_{d,i}) = -\frac{K_{1,i}z_{d,i}^3 - \hat{P}_i z_{d,i}}{6K_{1,i}z_{d,i}^2 - 2\hat{P}_i}, \quad (6.27a)$$

$$\underline{e}_{q,i}(z_{d,i}) = -\frac{K_{1,i}z_{d,i}^3 + \hat{P}_i z_{d,i}}{3K_{1,i}z_{d,i} + 2\hat{Q}_i}. \quad (6.27b)$$

- The set inclusion $\mathcal{N}(z_{d,i}) \subset \text{int}(\mathcal{S}(z_{d,i}))$ is satisfied at all times.

Proof. The proof will be split in two parts. The first is dedicated to proving negative definiteness of $f_i: \mathbb{R}^2 \rightarrow \mathbb{R}$. To this aim, $f_i(e_{d,i}, e_{q,i})$ is expressed as a summation of the functions

$$f_{1,i}(e_{d,i}, e_{q,i}) :=$$

$$\begin{aligned}
 & e_{d,i}^4(-3K_{1,i}z_{d,i}) + e_{d,i}^3(-6K_{1,i}z_{d,i}^2 + 2\hat{P}_i) + \\
 & e_{q,i}^3(-3K_{1,i}z_{d,i} - 2\hat{Q}_i) + e_{q,i}^2(-K_{1,i}z_{d,i}^3 - \hat{P}_iz_{d,i}) + \\
 & e_{d,i}^2(-K_{1,i}z_{d,i}^3 + \hat{P}_iz_{d,i})
 \end{aligned}$$

and

$$\begin{aligned}
 f_{2,i}(e_{d,i}, e_{q,i}) := & \\
 & e_{d,i}^2 e_{q,i}^2 (-3K_{1,i}z_{d,i}) + e_{d,i}^2 e_{q,i} (-3K_{1,i}z_{d,i} + 2\hat{Q}_i) + \\
 & e_{d,i} e_{q,i}^2 (-6K_{1,i}z_{d,i}^2 + 2\hat{P}_i) + e_{d,i} e_{q,i} (-4\hat{Q}_iz_{d,i}) + \\
 & e_{d,i}^2 (-K_{1,i}z_{d,i}^3 + \hat{P}_iz_{d,i}) + e_{q,i}^2 (-K_{1,i}z_{d,i}^3 - \hat{P}_iz_{d,i})
 \end{aligned}$$

where the aim is to investigate under which conditions of $K_{1,i}$, both summands are negative. The first requirement is for every coefficient of the above to be negative. Then, a preliminary condition on the magnitude of the feedback gain can be derived as

$$K_{1,i} \geq \max \left\{ \frac{\hat{Q}_i}{z_{d,i}}, \frac{\hat{P}_i}{z_{d,i}^2} \right\}. \quad (6.28)$$

Applying this condition yields

$$\begin{aligned}
 f_{1,i}(e_{d,i}, e_{q,i}) \leq & e_{d,i}^3(-6K_{1,i}z_{d,i}^2 + 2\hat{P}_i) + e_{q,i}^3(-3K_{1,i}z_{d,i} - 2\hat{Q}_i) + \\
 & e_{q,i}^2(-K_{1,i}z_{d,i}^3 - \hat{P}_iz_{d,i}) + e_{d,i}^2(-K_{1,i}z_{d,i}^3 + \hat{P}_iz_{d,i}).
 \end{aligned}$$

The above implies that $f_{1,i}(e_{d,i}, e_{q,i})$ is negative definite for all states $(e_{q,i}, e_{d,i})$ in the set

$$\mathcal{S}(z_{d,i}) := \{e_i \in \mathbb{R}^2 : e_{q,i} \geq \underline{e}_{q,i}(z_{d,i}), e_{d,i} \geq \underline{e}_{d,i}(z_{d,i})\},$$

where

$$\begin{aligned}
 \underline{e}_{d,i}(z_{d,i}) &= -\frac{K_{1,i}z_{d,i}^3 - \hat{P}_iz_{d,i}}{6K_{1,i}z_{d,i}^2 - 2\hat{P}_i}, \\
 \underline{e}_{q,i}(z_{d,i}) &= -\frac{K_{1,i}z_{d,i}^3 + \hat{P}_iz_{d,i}}{3K_{1,i}z_{d,i} + 2\hat{Q}_i}.
 \end{aligned}$$

Also, substituting $e_{d,i} = \underline{e}_{d,i}(z_{d,i})$ in $f_{2,i}(e_{d,i}, e_{q,i})$ results in the simplified quadratic polynomial

$$f_{2,i}(\underline{e}_{d,i}, e_{q,i}) = \alpha_1 e_{q,i}^2 + \alpha_2 e_{q,i} + \alpha_3, \quad (6.29)$$

where

$$\begin{aligned}
 \alpha_1 = & -3\underline{e}_{d,i}^2 K_{1,i}z_{d,i} - 2\underline{e}_{d,i}(3K_{1,i}z_{d,i}^2 - \hat{P}_i) - K_{1,i}z_{d,i}^3 \\
 & - \hat{P}_iz_{d,i},
 \end{aligned}$$

6.3. POSITIVE INVARIANCE OF THE DYNAMICS

$$\begin{aligned}\alpha_2 &= -3e_{d,i}^2 K_{1,i} z_{d,i} + 2\hat{Q}_i - 4e_{d,i} \hat{Q}_i z_{d,i}, \\ \alpha_3 &= -e_{d,i}^2 K_{1,i} z_{d,i}^3 + e_{d,i}^2 \hat{P}_i z_{d,i}.\end{aligned}$$

In order to conclude negative definiteness of the above, its quadratic structure can be exploited to: (a) show that (6.29) obtains a global maximum, (b) the value of the function at the stationary point is negative. Regarding (a), the second derivative of (6.29) yields $\frac{\partial^2 f_{2,i}}{\partial e_{q,i}^2} = 2\alpha_1$, which by substituting with (6.27a) leads to the following necessary condition for (6.29) attaining a global maximum

$$-\frac{z_{d,i}(3K_{1,i}^3 z_{d,i}^6 + 66K_i^2 \hat{P}_i z_{d,i}^4 - 45K_{1,i} \hat{P}_i^2 z_{d,i}^2 + 8\hat{P}_i^3)}{4(\hat{P}_i - 3K_{1,i} z_{d,i}^2)^2} < 0.$$

Applying (6.28), the numerator of the above is strictly positive, therefore the condition holds and it can be concluded that (6.29) attains a global maximum at the point $e_{q,i}^* = -\frac{\alpha_2}{2\alpha_1}$. In order to prove (b), the sign of the function at the stationary point needs to be investigated, *i.e.*

$$\begin{aligned}f_{2,i}(e_{d,i}, e_{q,i}^*) &= \alpha_3 - \frac{\alpha_2^2}{2\alpha_1} + \frac{\alpha_2^2}{4\alpha_1} \leq \alpha_3 - \frac{\alpha_2^2}{2\alpha_1} \\ &\leq c_1 - \frac{c_2 c_3}{c_4} - c_5\end{aligned}$$

where

$$\begin{aligned}c_1 &= \frac{\hat{P}_i z_{d,i}^3 (-K_{1,i} z_{d,i}^2 + \hat{P}_i)^2}{4(\hat{P}_i - 3K_{1,i} z_{d,i}^2)^2}, \\ c_2 &= 2(-3K_{1,i} z_{d,i}^2 + \hat{P}_i)^2, \\ c_3 &= \left(2\hat{Q}_i - \frac{3K_{1,i} z_{d,i}^3 (-K_{1,i} z_{d,i}^2 + \hat{P}_i)^2}{4(\hat{P}_i - 3K_{1,i} z_{d,i}^2)^2} + \frac{4\hat{Q}_i z_{d,i}^2 (-K_{1,i} z_{d,i}^2 + \hat{P}_i)}{-6K_{1,i} z_{d,i}^2 + 2\hat{P}_i} \right)^2, \\ c_4 &= z_{d,i}(3K_{1,i}^3 z_{d,i}^6 + 66K_{1,i}^2 \hat{P}_i z_{d,i}^4 - 45K_{1,i} \hat{P}_i^2 z_{d,i}^2 + 8\hat{P}_i^3), \\ c_5 &= -\frac{K_{1,i} z_{d,i}^5 (-K_{1,i} z_{d,i}^2 + \hat{P}_i)^2}{4(\hat{P}_i - 3K_{1,i} z_{d,i}^2)^2}.\end{aligned}$$

Condition (6.28) is sufficient to guarantee $c_1 - c_5 \leq 0$ and, similarly to (a), it can be concluded that $c_4 \geq 0$. Therefore, since $c_2, c_3 \geq 0$, the right-hand side of (6.29) is a summation of non-positive terms and thus (6.29) is a negative semi-definite function. Similar conclusions can be drawn for the sign of $f_{2,i}(e_{d,i}, e_{q,i})$, therefore the above imply that conditions (6.24), (6.27a) and (6.27b) are sufficient to ensure the existence of a class- \mathcal{K} function $\theta: \mathbb{R} \rightarrow \mathbb{R}^+$ such that

$$f(e_i) \leq -\theta(\|e_i\|) \leq 0$$

6.3. POSITIVE INVARIANCE OF THE DYNAMICS

for all $e_i \in \mathcal{S}(z_{d,i})$. To prove the second part of the proposition, it is noted that $\{0\} \in \partial\mathbb{B}_{i,k}$ holds, for all $k \in |\mathcal{W}_i|$. This allows the formulation of a sufficient condition for the desired set inclusion as

$$\left| \underline{e}_{d,i}(z_{d,i}) \right| - 2r(z_{d,i}, w_{P,i}, w_{Q,i}) > 0,$$

where $w_{P,i} = \max_{\delta P_i \in \mathbb{W}_{P,i}} \{\delta P_i^2\}$ and $w_{Q,i} = \max_{\delta Q_i \in \mathbb{W}_{Q,i}} \{\delta Q_i^2\}$. Substituting the explicit form of each function yields the condition on the nominal state

$$z_{d,i}^2 > \frac{\hat{P}_i + 12\sqrt{w_{P,i} + w_{Q,i}} + 2\bar{\delta}P_i}{K_{1,i}}.$$

Considering the condition on the feedback gain (6.28), if $K_{1,i}$ obtains a lower bound value $K_{1,i} = \frac{\hat{P}_i}{z_{d,i}^2}$, then

$$\frac{12\sqrt{w_{P,i} + w_{Q,i}} + 2\bar{\delta}P_i}{\hat{P}_i} < 0.$$

needs to be satisfied. However, this does not hold, since by definition the above is a summation of strictly positive terms. The same result occurs if $K_{1,i}$ obtains the lower bound $K_{1,i} = \frac{2\bar{\delta}P_i}{z_{d,i}^2}$. In contrast, for $K_{1,i} = \frac{\hat{Q}_i}{z_{d,i}}$ results in the desired condition

$$z_{d,i} > \frac{\hat{P}_i + 12\sqrt{w_{P,i} + w_{Q,i}} + 2\bar{\delta}P_i}{\hat{Q}_i}$$

which, furthermore, implicitly implies

$$\frac{\hat{Q}_i}{z_{d,i}} > \max \left\{ \frac{2|\delta P_i|}{z_{d,i}^2}, \frac{\hat{P}_i}{z_{d,i}^2} \right\},$$

and results in $\underline{e}_{d,i}(z_{d,i}) > \underline{e}_{q,i}(z_{d,i})$. Therefore, the above imply that a necessary condition of the feedback gain is formulated as

$$K_{1,i} \geq \frac{\hat{Q}_i}{z_{d,i}}$$

This concludes the proof. \square

So far in the analysis, the set where (6.14) obtains positive values has been investigated and it has been shown that this set $\mathcal{N}_i(z_{d,i})$ is closed and bounded. Furthermore, Prop. 6.1 establishes that there exists a set $\mathcal{S}(z_{d,i})$ such that the set inclusion $\mathcal{N}(z_{d,i}) \subset \text{int}(\mathcal{S}(z_{d,i}))$ holds and for all states in the set complement $\mathcal{S}(z_{d,i}) \setminus \mathcal{N}_i(z_{d,i})$ the function obtains negative values. The next Theorem establishes sufficiency of the conditions of Prop. 6.1 to derive the desired result on the boundedness of the error trajectory.

Theorem 6.1 (Positive invariance of the error dynamics). *For each $i \in \mathcal{M}$, if*

$$z_{d,i} > \max_{\substack{\delta P_i \in \mathbb{W}_{P,i}, \\ \delta Q_i \in \mathbb{W}_{Q,i}}} \left\{ \frac{\hat{P}_i + 12\sqrt{\delta P_i^2 + \delta Q_i^2} + 2\delta \bar{P}_i}{\hat{Q}_i}, \frac{6\hat{P}_i - 8}{25\hat{P}_i - 12} \right\}, \quad (6.30)$$

then, the set $\mathcal{N}_i(z_{d,i})$ is positive invariant under the solution of the error dynamics given in (6.10).

Proof. Considering the energy function in (6.13), Prop. 6.1 provides sufficient conditions such that the nominator of the energy function obtains positive values in $\mathcal{N}_i(z_{d,i})$ and negative in a neighbourhood outside of the boundary $\partial\mathcal{N}_i(z_{d,i})$. The remaining condition is to show when the lower bound on the nominal voltage trajectory is sufficient to conclude that the denominator of (6.13) is strictly positive. Substituting for $e_{d,i} = \underline{e}_{d,i}(z_{d,i})$ and using the fact that $K_{1,i} > \frac{\hat{P}_i}{z_{d,i}^2}$, yields the condition

$$\begin{aligned} (z_{d,i} + e_{d,i})^2 + e_{d,i} &> z_{d,i}(25\hat{P}_i^2 - 12\hat{P}_i) + \frac{\hat{P}_i^2}{z_{d,i}^4} + 8\hat{P}_i - 6\hat{P}_i^2 \\ &> z_{d,i}(25\hat{P}_i^2 - 12\hat{P}_i) + 8\hat{P}_i - 6\hat{P}_i^2, \end{aligned}$$

where the first strict inequality is deduced by substituting $K_{1,i} = \frac{\hat{P}_i}{z_{d,i}^2}$. Then, the condition

$$z_{d,i} \geq \frac{6\hat{P}_i - 8}{25\hat{P}_i - 12}$$

is sufficient for right-hand side of the latter inequality to be positive semi-definite. Augmenting the condition of Prop. 6.1 with the above results in the desired lower bound on the nominal state. Therefore, conditions (6.24), (6.30) are sufficient to conclude that the vector assigned to any point $e_i \in \partial\mathcal{N}_i(z_{d,i})$ is sub-tangential to the set $\mathcal{N}_i(z_{d,i})$ and that the solution of the error dynamics is Lipschitz continuous. Then, by a direct application on Nagumo's theorem on set invariance, the set $\mathcal{N}_i(z_{d,i})$ is positive invariant under the solution of the error dynamics. This completes the proof. \square

Remark 6.1. *The above results on the existence of a positive invariant set indicate that by achieving a parameter-dependent lower bound on the nominal voltage and the feedback gain, the network demonstrates robustness to load demand perturbations. Thus, a constraint-based approach similar to the previous chapters can be used to satisfy the bound of Theorem 6.1 and regulate the uncertainty-free nominal system, while it is guaranteed that the distance between the nominal and the true voltage trajectories is bounded in $\mathcal{N}_i(z_{d,i})$. The proposed control scheme has two*

major practical advantages; first, having an explicit characterization of the bounded effect of the disturbance facilitates the development of more sophisticated methods that achieve satisfaction of operational constraints and protect the electronic components from damages. Secondly, the proposed control law (6.9) provides the designing capability of distributing the voltage fluctuations, which are commonly experienced by changes in the CPL demand, between both the voltage and the current states. This can be done by increasing the feedback gain, where the choice can be analytically made following the result that the deviations between the reference current u_i and the injected $i_{in,i}$ are guaranteed to be contained in the set $-(K_{1,i} + K_{2,i})\mathbb{I}_2\mathcal{N}_i(z_{d,i})$.

The main focus of this chapter was the characterisation of a positive invariant set for the case of AC Microgrids with CPLs. Once the explicit form of this set is derived, one can design a tube-based control scheme similarly with the previous chapters. In order to avoid repetition, the design of a nominal control scheme is omitted here, however it is noted that the results of the previous chapters can be also applied in this case.

6.4 Simulations

In this section, the theoretic results of Section 6.3 are demonstrated in a simulated scenario. The proposed control scheme is applied on a network composed of four nodes $\mathcal{M} := \{\mathcal{V}_1, \mathcal{V}_2, \mathcal{V}_3, \mathcal{V}_4\}$ with set of edges

$$\mathcal{E} := \{(\mathcal{V}_1, \mathcal{V}_2), (\mathcal{V}_1, \mathcal{V}_3), (\mathcal{V}_1, \mathcal{V}_4), (\mathcal{V}_2, \mathcal{V}_3)\}$$

and corresponding weights $Y_L = \{(1.5)^{-1}, (1.1)^{-1}, (0.9)^{-1}, (0.8)^{-1}\}$. Every local CPL shares a similar load profile with $\hat{P}_i = 0.5$ kW, $\hat{Q}_i = 0.4$ kVAR and respective load perturbations in the sets $\|\delta P_i\| \leq 0.5$ kW and $\|\delta Q_i\| \leq 0.4$ kVAR. In order to approximate the PI set developed in Section 6.3 with a convex set, a superset of this set is considered, defined with centre the origin and radius $r_s = 2 \max\{r(z_{d,i}, \delta P_i, \delta Q_i)\}$. This results in the PI set $v_i \in \{z_i\} \oplus \mathcal{N}_i(z_{d,i})$, where at the steady state $\bar{z}_{d,i} = 110\sqrt{2}$ yields $\mathcal{N}_i(\bar{z}_{d,i}) := \{e_i \in \mathbb{R}^n : \|e_i\| \leq 1.6 \text{ V}\}$. Note that this is still a PI set as the proof of the second statement of Prop. 6.1 is structured considering a similar superset as a worst-case scenario. An unconstrained control scheme is used to regulate every nominal state to $V_{rms} = 110$ V. As depicted in Fig. 6.2, the nominal RMS voltage of each node is regulated to the desired reference and the true voltage trajectory is contained in the designed positive invariant set centred around the nominal. It can be argued that the proposed approach may result in a conservative size of the PI set, due to the theoretic conditions being sufficient but not necessary, *i.e.* the adopted set is over-approximating the ultimate

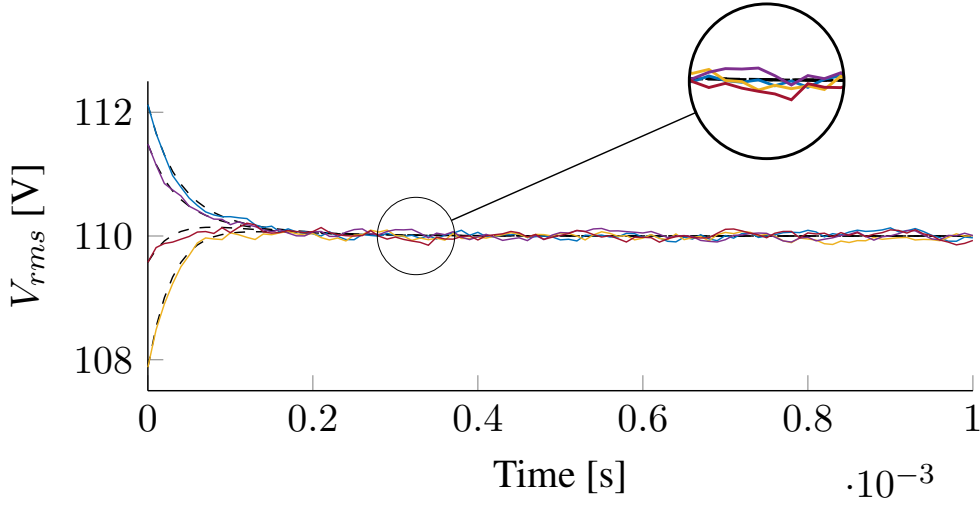


Figure 6.2: Voltage trajectories for nodes \mathcal{V}_1 (—), \mathcal{V}_2 (—), \mathcal{V}_3 (—), \mathcal{V}_4 (—) and respective nominal trajectories (---). It is seen that the RMS voltage of each node is kept close to the rated value despite the constant perturbations of the load demand.

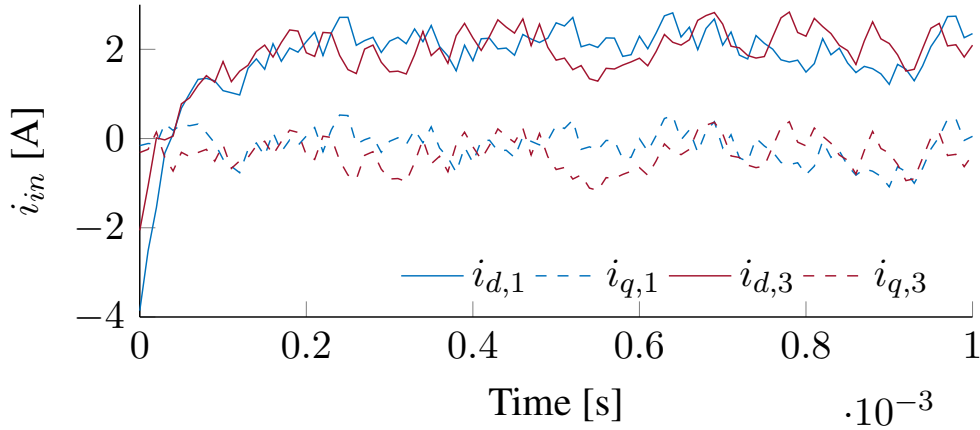


Figure 6.3: Input current trajectories for nodes \mathcal{V}_1 and \mathcal{V}_3 .

bounded region of the dynamics. Finally, Fig. 6.3 depicts the injected currents of the inverters \mathcal{V}_1 and \mathcal{V}_3 . Similarly to the previous chapters, the current trajectories experience fluctuations due to the effect of load demand changes. The magnitude of these fluctuations can be tuned according to the choice of the feedback gain K , where the inverse result will be seen in the voltage dynamics.

6.5 Conclusions

This chapter presented a control scheme for isolated AC Microgrids with local CPLs. By perceiving the load demand as a parametric time-varying disturbance, tools from the theory of set invariance control were utilised to design a control law that provides

6.5. CONCLUSIONS

robustness to the network dynamics with respect to load demand perturbations. Explicit parameter-based conditions of the control parameters were provided, such that the trajectory of the true voltage is always contained within a PI set centred on a constructed uncertainty-free nominal trajectory. Future iterations of this study are aimed in reducing possible conservativeness regarding the size of the PI set by deducing “stricter” sufficiency of the current theoretical conditions.

Chapter 7

Conclusions and future work

This chapter will provide a brief summary of the thesis and some concluding remarks on the results. In addition, the following part includes potential limitations and sources of conservativeness in the presented work. Finally, some ideas for future directions of this work are provided in the end of the chapter.

7.1 Summary

Chapter 3 presented a distributed, nonlinear, control design for isolated DC Microgrids with purely constant power loads and neighbour-to-neighbour communication. An extensive theoretical analysis was provided that guarantees both local and coupled constraint satisfaction. Sufficient conditions are provided such that the closed loop system is asymptotically stable and achieves the desired operation. The challenge of designing a distributed scheme for this particular type of systems, *i.e.* where a strong coupling term exists between the local dynamics, was addressed by introducing an upper bound on the error of the available information between sampling times. In this chapter, the error consisted of both the load demand and the neighbouring voltage values.

Chapter 4 investigated the geometric behaviour of the constant power load and its effect on the closed loop system. This analysis was used to establish sufficient conditions for the existence of a positive invariant set under the solution of the voltage dynamics. It was shown that the centre of this set was defined by a generated nominal trajectory, facilitating this way a tube-like behaviour, where the true voltage trajectory is guaranteed to remain within the positive invariant set around the nominal trajectory for all future times. Then, this set was used to parametrise the original constraint sets and reduce the error bound, formulated in Chapter 3, to only the transmitted information between the nodes, contrary to also including the local power demand. Finally, a Control Lyapunov function was introduced to

prove asymptotic stability of the inner current dynamics.

Chapter 5 utilised the locally available information on the generated reference trajectory to allow a time-varying behaviour of the bound on the voltage dynamics. This eliminates the conservativeness of the method presented in Chapter 4, where the entire analysis was based on a worst-case scenario of the nominal voltage trajectory. Furthermore, the investigation of the qualitative behaviour of the closed loop system under the proposed control law allowed the formulation of less restricting conditions on the values of the tuning parameters. The stability of the cascaded dynamics was analytically proven by the use of Control Lyapunov Functions and tools from the theory of interconnected systems.

Finally, Chapter 6 extended the proposed methods of the previous chapters to the case of isolated AC Microgrids. Even though the system model displayed a higher degree of complexity, compared with the DC case, an analytic characterisation of a positive invariant set was provided that is embedded in the two dimensional state space for each node. Guidelines were also outlined in order to approximate the PI set with a convex superset, by using the maximum distance between the centre and boundary of this set. Having characterized the PI set for the more challenging AC voltage dynamics, the tube-based MPC approach developed in previous chapters may then easily be applied to generate the desired nominal trajectories around which the perturbed dq voltage components remain. The closed loop system was assessed in a simulated scenario, where the rms voltage remained within the desired set at all times. Ultimately, a tube-like behaviour was proven to be achievable also in the case of AC Microgrids.

7.2 Discussion of assumptions and limitations

This section includes a discussion on the assumptions that are adopted in this research work and provides some remarks on the potential sources of conservatism in the proposed methods. The aim is to clarify their purpose and highlight their necessity, as well as demonstrate how one can overcome these during the implementation process.

- In order to simplify the analysis, every case study considered in this thesis considers purely resistive lines. While this may seem restrictive, it was shown in [116] that line inductances do not affect the system stability in the case of DC Microgrids. This assumption is justified in Chapter 6, by assuming low-voltage networks, where the effect of the inductance is less significant. Nevertheless, some effect will be present and future work could consider how to quantify and handle this.

- It is assumed that the input voltage of the converters is always constant. One could argue that this is not always the case, however it was shown in [178] that this assumption is not restrictive and it can be always satisfied by the use of batteries and supporting elements in the connection between the distributed renewable resource unit and the converter. Nevertheless, even in the presence of some variation in the input voltage, the proposed primary controller of Chapter 4 can be used to dynamically adjust the duty ratio, such that this variation does not affect the analytic and theoretic results.
- In Chapter 3, the bound on the error rate of change becomes more difficult to satisfy when the number of neighbours is increased. This problem is partially alleviated in the following chapters, however, during the practical implementation of this method, one may require short sampling times to satisfy Assumption 3.5, which increases the computational burden. One method to address this problem is to adopt multiple shooting methods, or other similar efficient algorithms, to solve the optimisation problems [179].
- The decoupling of the stability problem, in Chapter 4, as that of the stability problem of a single node may result in a more conservative bound on the nodal trajectories that experience a lower local load demand. This is necessary to obtain a scalar representation of the bound and derive a scalar condition on the feedback gain that achieves the desired positive invariance result in Proposition 4.2. If this decoupling method is not used, then one faces the problem of requiring the solutions of a matrix equation with nonlinear components, which significantly complicates the analysis and may result in use of approximation methods that could produce even more conservative trajectory bounds.
- Chapter 6 formulated the problem by considering a constant global frequency in the local node model. This is in order to simplify the approach, in an effort to highlight the main result without the need of including additional control layers. Nevertheless, as it will be discussed in the following section, the design of a control approach that considers the frequency and current dynamics is a possible future direction of this work.
- Each chapter provides a robustness analysis, where each case has a similar assumption; the load demand is assumed to be bounded in a predefined set. The use of tubes creates the implicit assumption that the maximal load perturbation results in nonempty nominal constraint sets and the controller can tolerate this without raising the issue of infeasibility of the optimisation problem. While it may be straightforward to overcome this problem during the

practical implementation by accordingly adjusting the constraint sets, investigating the interaction between the constraints and the robust positive invariant set is an interesting future direction.

7.3 Future directions

The research work presented in this thesis may take many different future directions. Some examples are:

- One may investigate the Plug-and-Play capability, *i.e.* the seamless introduction and removal of a node from the network, of the proposed distributed methods and the effect this has on the stability analysis of the Microgrid system. An important challenge in this direction is how to deal with the time-varying network topology. From an individual node point-of-view, this change is seen as an external input signal. This fact can be used to follow a uncertain-nominal system approach, where the nominal system perceives this external input as zero. Then, analytic conditions on stable and constrained operation can be formulated by perceiving the introduction, or loss, of a neighbour node as an external bounded signal in the uncertain dynamics.
- The proposed controller of Chapter 6 can be expanded to achieve frequency and current regulation, without assuming a constant common frequency. This would require the development of a separate control scheme for each case that can guarantee the respective boundedness specifications. In this direction, one may reformulate the sl-PI controller, introduced in Chapter 4, to bound the deviations from a rated value. The challenge here is the need for synchronization of the converter operation.
- It would be interesting to validate the results of the proposed methods in an experimental setup. This way, the practical implementability and possible technical restrictions can be assessed in a real world environment. A possible practical limitation is the need for solving optimisation problems in short time. During this thesis, some techniques were proposed that can make this process easier, e.g. the use of interior point and multiple shooting methods. In addition, the computation burden was reduced by removing the perturbations of the load demand from the optimisation problem. One possible area of improvement is using more than just the first element of the computed control sequence. This way, the need to constantly recalculate control actions can be overcome, however this could have implications on the recursive feasibility

7.3. FUTURE DIRECTIONS

property of the optimal control problem. Setting feasibility criteria to decide whether to compute a new control sequence could address this.

- This thesis developed necessary and sufficient boundedness conditions of the tuning parameters such that the desired closed-loop behaviour is achieved. In many cases, the desired control objective was set invariance and stability. An interesting topic would be to include the objective of performance improvement in the choice of the control parameters via an optimisation-based method. This way, the choice of the feedback gain, which affects the sizes of the parametrised input and state constraint sets as explained in Remarks 4.2 and 6.1, can be made in an optimal way. Another criterion can be that the size of the input and state constraint sets are such that no issue of recursive feasibility can occur, eliminating the need of implicitly assuming this.

Appendix A

Preliminaries: Theory and Notation

A.1 Common notations

The notation $|\mathcal{A}|$ denotes the cardinality of a set $\mathcal{A} \in \mathbb{R}^{n \times n}$. The closure, boundary and interior of a set \mathcal{A} are denoted as $\text{cl}(\mathcal{A})$, $\partial\mathcal{A}$ and $\text{int}(\mathcal{A})$ respectively. A polytope $\mathcal{A} \subset \mathbb{R}^n$ with complexity n_c is characterized by $\mathcal{A} = \{x \in \mathbb{R}^n : Px \leq q\}$ with $P \in \mathbb{R}^{n_c \times n}$ and $q \in \mathbb{R}^{n_c}$. The Pontryagin Difference of polytopes \mathcal{A} and \mathcal{B} is defined as $\mathcal{A} \ominus \mathcal{B} = \{a \in \mathbb{R}^n : a + b \in \mathcal{A}, \forall b \in \mathcal{B}\}$.

The notation $\mathbb{1}$ and $\mathbb{0}$ denotes an all-ones and all-zeros vector respectively of appropriate dimension, where the dimension will be clear from the context. For a vector $x \in \mathbb{R}^n$ the notation $[x]$ denotes a diagonal matrix on $\mathbb{R}^{n \times n}$, where $x_i = [x]_{ii}$, for $i = 1, 2, \dots, n$. For $x \in \mathbb{R}^n$, $[\cos x] = \text{diag}(\cos x_1, \dots, \cos x_n)$. The N element sequence is $\mathbf{a} = \{a(0), \dots, a(N-1)\}$. A sequence of length k is denoted as $\{x\}_k = \{x_1, x_2, \dots, x_k\}$. The Hausdorff distance between two sets $A, B \subset \mathbb{R}^n$ is $h(A, B) = \max \{ \sup_{a \in A} \inf_{b \in B} |a - b|^2, \sup_{b \in B} \inf_{a \in A} |a - b|^2 \}$.

According to [171], a set $m\mathcal{A}$ is called positive invariant for a system of the form,

$$\dot{x} = f(x(t))$$

if for all $x(0) \in \mathcal{A}$, it holds that the solution $x(t) \in \mathcal{A}$ for all $t > 0$.

A topological space M is called a smooth manifold if for any $p \in M$ there exist an open set in a neighbourhood of p , $\mathcal{O} \subset M$ and diffeomorphism $\psi: \mathcal{O} \rightarrow \mathbb{R}^n$. The combination (ψ, \mathcal{O}) is called a coordinate chart of M . The tangent space on a point $p \in M$ is denoted as $T_p M$, and a vector field X is a map assigning a vector $X(p) \in T_p M$ at each point $p \in M$. A Riemannian metric G represents the inner product of the tangent space of M at x , where $G: T_x M \times T_x M \rightarrow \mathbb{R}$. The

pair of a smooth manifold together with G is called a Riemannian manifold. Let $\gamma: [0, 1] \rightarrow M$ be a smooth function with $\gamma(0) = x_1$ and $\gamma(1) = x_2$ for $x_1, x_2 \in M$. The Riemannian distance between x_1 and x_2 is given by $d_R = \inf \ell_R(\gamma)$, where $\ell_R(\gamma)$ is the arc length of γ on M . The respective Riemannian norm is denoted as $\|\cdot\|_R$. The Lie derivative of a function $f \in C^\infty(M)$ along a vector field $X \in TM$ is given as $\mathcal{L}ie_X f = \sum_{i=1}^n X_i \frac{\partial f}{\partial x_i}$. The inner product between two vectors $a, b \in \mathbb{R}^n$ is denoted as $\langle a, b \rangle = \sum_{i=1}^n a_i b_i$.

A.1.1 Function properties

The following two definitions on the qualitative behaviour of a function can be found in [155].

Definition A.1 (class- \mathcal{K} function). *A continuous function $\alpha: [0, a] \times [0, \infty) \rightarrow [0, \infty)$ is said to belong to class- \mathcal{K} if it is strictly increasing and $\alpha(0)=0$. It is said to belong to class \mathcal{K}_∞ if $a = \infty$ and $\alpha(r) \rightarrow \infty$ as $r \rightarrow \infty$.*

Definition A.2 (class- \mathcal{KL} function). *A continuous function $\beta: [0, \alpha] \times [0, \infty) \rightarrow [0, \infty)$ is said to belong to class- \mathcal{KL} if, for each fixed s , the mapping $\beta(r, s)$ belongs to class- \mathcal{K} with respect to r and, for each fixed r , the mapping $\beta(r, s)$ is decreasing with respect to s and $\beta(r, s) \rightarrow 0$ as $s \rightarrow \infty$.*

A function $f: X \rightarrow Y$ is called Lipschitz continuous if there exists a real positive constant $K \in [0, \infty)$ such that for any $c_1 \in X$ and $c_2 \in X$ it holds

$$d(f(c_1), f(c_2)) \leq K d(c_1, c_2),$$

where $d(\cdot, \cdot)$ is an appropriate distant function defined for the respective metric spaces (d, X) and (d, Y) . In addition, a function is of class \mathcal{K} -continuous if the above equality holds for some class- \mathcal{K} function $\alpha(\cdot)$, *i.e.*

$$d(f(c_1), f(c_2)) \leq \alpha(d(c_1, c_2)),$$

The following definition utilises the notion of Lipschitz continuity to derive existence and uniqueness of the initial value problem $\dot{x} = f(x(t)), x(t_0) = x_0$.

Definition A.3 (Existence and Uniqueness of solution map). *Let $f(x)$ satisfy the Lipschitz continuity condition for any two values in its respective domain c_1, c_2 ,*

$$\|f(c_1) - f(c_2)\| \leq K \|c_1 - c_2\|.$$

Then, there exists a positive constant $\delta > 0$ such that the initial value problem $\dot{x} = f(x(t)), x(t_0) = x_0$ has a unique solution map over the time interval $[t_0, t_0 + \delta]$, see [155].

A.2 Linear Algebra

Definition A.4 (Matrix similarity). *Considering two matrices $A, B \in \mathbb{R}^{n \times n}$, then A and B are called similar, if there exist a matrix $P \in \mathbb{R}^{n \times n}$ such that $B = P^{-1}AP$.*

Definition A.5 (Hurwitz matrix). *A matrix $A \in \mathbb{R}^{n \times n}$ is called Hurwitz if $\text{Re}(\lambda_i) < 0$ holds for all eigenvalues $\{\lambda_i\}_{i=1}^n$ of A .*

Lemma A.1 (Quadratic Eigenvalue Problem). *Consider the quadratic polynomial*

$$Q(\lambda) = \lambda^2 M + \lambda C + K$$

with matrix coefficients $M, C, K \in \mathbb{C}^{n \times n}$ and $M \neq 0$. Then, for a Quadratic Eigenvalue Problem (QEP) with

$$|\lambda^2 M + \lambda C + K| = 0$$

it holds that $\text{Re}(\lambda_i) < 0$ for all $i \in 1, \dots, n$ if the matrix coefficients M, C, K are all positive definite.

Proof. see [180]. □

Lemma A.2 (Diagonalizable product of symmetric matrices). *If two matrices $A, B \in \mathbb{R}^{n \times n}$ are positive definite and symmetric, then their product AB is diagonalizable.*

Proof. Define $A^{\frac{1}{2}}$ as the unique, positive definite square root of A . Then, AB is similar to $A^{\frac{1}{2}}BA^{\frac{1}{2}}$ which is symmetric. Since $A^{\frac{1}{2}}BA^{\frac{1}{2}}$ is symmetric and thus, according to the spectral theorem, diagonalizable, AB is also diagonalizable. □

A.3 Nonlinear System Analysis

Definition A.6 (Solution Map). *Consider a system of n dimensions described by the differential equation $\dot{x} = f(x)$. Then, the solution map of the differential equation is given by the function $\phi : \mathbb{R}^n \times \mathbb{R} \rightarrow \mathbb{R}^n$ which described the state trajectory of the system in the respective state space.*

Definition A.7 (Lyapunov function). *A function $V : \mathbb{R}^n \rightarrow \mathbb{R}$ is said to be a Lyapunov function for the system $\dot{x} = f(x)$, if it is continuous, has continuous first derivative, $V(0) = 0$, is positive definite and the time derivative satisfies*

$$\dot{(V)}f \leq -\alpha(\|x\|)$$

where $\alpha : \mathbb{R}^n \rightarrow \mathbb{R}$ is a class- \mathcal{K} function.

Definition A.8 (Asymptotic stability). *Consider a system of n dimensions described by the differential equation $\dot{x} = f(x)$. Suppose that x^e is an equilibrium point for the system such that $f(x^e) = 0$. Then, for any initial state $x(0)$, the system is called asymptotically stable if there exists a Lyapunov function for the system and for a $\delta > 0$, if $\|x(0) - x^e\| \leq \delta$ then $\lim_{t \rightarrow \infty} \|x(t) - x^e\| = 0$.*

Definition A.9 (Reachable set). *Consider the system $\dot{x} = f(x, u)$, with $f: \mathbb{R}^n \times \mathbb{U} \rightarrow \mathbb{R}^n$ and \mathbb{U} the set of available control actions. Denote the solution of the system as $\phi: \mathbb{R} \times \mathbb{R}^n \times \mathbb{U} \rightarrow \mathbb{R}^n$, then the reachable set from initial state x_0 and time $t \geq 0$ is defined as*

$$\mathcal{R}(x_0) := \{y \in \mathbb{R}^n : y = \phi(t, x_0, u), t \geq 0, u \in \mathbb{U}\}.$$

Theorem A.1 (Stability around the origin via linearisation). *Consider the system $\dot{x} = f(x)$, with $f: D \rightarrow \mathbb{R}^n$ a continuous function with continuous first derivative. Let $x = 0$ be an equilibrium point of the system and $\{0\} \in D$. Define*

$$J = \frac{\partial f}{\partial x}(x)|_{x=0}$$

Then, if J is a Hurwitz matrix the origin is an asymptotically stable equilibrium point of the system.

Theorem A.2 (Ultimate Boundedness). *Let $D \subset \mathbb{R}^n$ be a domain that contains the origin and $V: [0, \infty) \times D \rightarrow \mathbb{R}$ be a continuously differentiable function such that*

$$\begin{aligned} \alpha_1(\|x\|) \leq V(t, x) \leq \alpha_2(\|x\|) \\ \frac{\partial V}{\partial t} + \frac{\partial V}{\partial x} f(t, x) \leq -W_3(x), \quad \forall \|x\| \geq \mu > 0 \end{aligned}$$

$\forall t \geq 0$ and $\forall x \in D$, where α_1, α_2 are class- \mathcal{K} functions and $W_3(x)$ is a continuous positive definite function. Take $r > 0$ such that $B_r \subset D$ and suppose that

$$\mu \leq \alpha_2^{-1}(\alpha_1(r))$$

Then, there exists a class \mathcal{KL} -function β and for any initial state $x(t_0)$, satisfying $\|x(t_0)\| \leq \alpha_2^{-1}(\alpha_1(r))$, there exist a $T \geq 0$ such that the solution of the system satisfies

$$\begin{aligned} \|x(t)\| \leq \beta(\|x(t_0)\|, t - t_0), \quad \forall t_0 \leq t \leq t_0 + T \\ \|x(t)\| \leq \alpha_2^{-1}(\alpha_1(\mu)), \quad \forall t \geq t_0 + T \end{aligned}$$

Morover, if $D = \mathbb{R}^n$ and α_1 belongs to class \mathcal{K}_∞ , then the above hold for any initial state $x(t_0)$, with no restriction on how large μ is.

Proof. see [155, Appendix C.9] □

Theorem A.3 (Nagumo’s Theorem). *Let $\dot{x} = f(x)$, where the map f is at least once continuously differentiable and the solutions exists inside an open set $\mathcal{O} \subseteq \mathbb{R}^n$. Then, the closed subset $S \subset \mathcal{O}$ is positive invariant under the flow of the system if and only if*

$$\liminf_{\lambda \rightarrow 0^+} \frac{d(S, x + \lambda f(x))}{\lambda} = 0$$

for all $x \in \partial S$, where $d(\cdot, \cdot)$ denotes the euclidean distance.

Proof. Original proof can be found in [181], and different formulations of the theorem, with respective proofs in [182, 183]. \square

Definition A.10 (Strict dissipativity). *For a system of dimension n described by the differential equation $\dot{x} = f(x, u)$, where $u \in \mathbb{R}^n$ defines the control input, let a storage function be defined as the lower bounded function $\lambda : \mathbb{R}^n \rightarrow \mathbb{R}$. Then, a system is called strictly dissipative if there exists a supply rate function $s : \mathbb{R}^n \times \mathbb{R}^n \rightarrow \mathbb{R}$, such that the inequality holds*

$$\lambda(x(\tau)) \leq \lambda(x_0) + \int_0^\tau s(x(t), u(t)) - \alpha \left(\|x(t) - x^e\| \right) dt,$$

where x^e is an equilibrium point for the dynamics, such that $f(x^e, u^e) = x^e$ holds, and $\alpha \in \mathcal{K}_\infty$.

Definition A.11 (Region of Attraction). *Consider a system of n dimensions described by the differential equation $\dot{x} = f(x)$ with respective solution $\phi(t, x(0))$ for any initial state $x(0)$. Then, the region of attraction of the origin is defined as*

$$\Omega = \{x \in \mathbb{R}^n : \lim_{t \rightarrow \infty} \phi(t, x(0)) = 0\}$$

A.4 Graph Theory

A Microgrid can be seen as an undirected and connected graph $\mathcal{G} = (\mathcal{M}, \mathcal{E})$ where the set of nodes \mathcal{M} represent a collection of power converters and local loads; the set of edges $\mathcal{E} \subseteq \mathcal{M} \times \mathcal{M}$ defining the Microgrid topology is characterized by the node-edge matrix $\mathcal{B} \in \mathbb{R}^{|\mathcal{E}| \times |\mathcal{M}|}$ which for edge $\varepsilon = (i, j) \in \mathcal{E}$ involving nodes i and j can be defined as $[\mathcal{B}]_{ei} = 1$ if node i is the source of $\varepsilon \in \mathcal{E}$, and $[\mathcal{B}]_{ej} = -1$ if node j is its sink, and zero otherwise. The weights of the edge ε , representing the admittances of the lines, are collected in the line admittances matrix R^{-1} .

Given an undirected graph G , the matrix $A(R) \in \mathbb{R}^{|\mathcal{M}| \times |\mathcal{M}|}$ denotes the weighted adjacency matrix of G , where $a_{ij} = R_{ij}^{-1}$ for the edge $\varepsilon = (i, j)$ and $a_{ij} = 0$ if the node

A.4. GRAPH THEORY

is not incident. Then, the topology of the graph can be expressed by the Laplacian matrix $\mathcal{L} = [A(R)\mathbb{1}_{|\mathcal{M}|}] - A(R)$. The components of the Laplacian matrix satisfy

$$\mathcal{L}_{ij} = \begin{cases} -R_{ij}^{-1}, & \text{if } i \neq j, \\ \sum_{k=1, k \neq i}^{|\mathcal{M}|} R_{ik}^{-1}, & \text{if } i = j. \end{cases}$$

Lemma A.3 (Zero row sums). *Consider the weighted graph \mathcal{G} , with n number of nodes and topology characterised by the Laplacian matrix \mathcal{L} . Then,*

$$\mathcal{L}\mathbb{1}_n = \mathbf{0}_n$$

Proof. See proof in [184, Lemma 6.2]. □

The above lemma implies that there exist a zero eigenvalue of the matrix \mathcal{L} with eigenvector $\mathbb{1}_n$. The following lemma draw results on the sign of the non-zero eigenvalues.

Lemma A.4 (Spectrum of the Laplacian Matrix). *Consider the weighted graph \mathcal{G} , with n number of nodes and topology characterised by the Laplacian matrix \mathcal{L} . Then, the eigenvalues of the Laplacian matrix satisfy,*

$$\lambda_1 = 0 \leq \lambda_2 \leq \dots \leq \lambda_n$$

Proof. See proof in [184, Lemma 6.5]. □

Bibliography

- [1] E. Parliament, [Infographic: how climate change is affecting europe](https://www.europarl.europa.eu/news/en/headlines/society/20180905ST011945/infographic-how-climate-change-is-affecting-europe), [Online; posted 28-03-2023] (March 2023).
URL <https://www.europarl.europa.eu/news/en/headlines/society/20180905ST011945/infographic-how-climate-change-is-affecting-europe>
- [2] E. Parliament, [Climate change in europe: facts and figures](https://www.europarl.europa.eu/news/en/headlines/society/20180703ST007123/climate-change-in-europe-facts-and-figures), [Online; posted 24-03-2023] (March 2023).
URL <https://www.europarl.europa.eu/news/en/headlines/society/20180703ST007123/climate-change-in-europe-facts-and-figures>
- [3] N. Hatziargyriou, H. Asano, R. Iravani, C. Marnay, Microgrids, IEEE power and energy magazine 5 (4) (2007) 78–94.
- [4] R. Lasseter, [MicroGrids: A Conceptual Solution](http://ieeexplore.ieee.org/lpdocs/epic03/wrapper.htm?arnumber=985003), 2002 IEEE Power Engineering Society Winter Meeting. Conference Proceedings (Cat. No.02CH37309) 1 (2002) 305–308. doi:10.1109/PESW.2002.985003.
URL <http://ieeexplore.ieee.org/lpdocs/epic03/wrapper.htm?arnumber=985003>
- [5] C. Marnay, S. Chatzivasileiadis, C. Abbey, R. Iravani, G. Joos, P. Lombardi, P. Mancarella, J. Von Appen, Microgrid evolution roadmap, in: 2015 international symposium on smart electric distribution systems and technologies (EDST), IEEE, 2015, pp. 139–144.
- [6] R. H. Lasseter, P. Paigi, Microgrid: A conceptual solution, in: 2004 IEEE 35th annual power electronics specialists conference (IEEE Cat. No. 04CH37551), Vol. 6, IEEE, 2004, pp. 4285–4290.
- [7] S. Sen, V. Kumar, Microgrid control: A comprehensive survey, Annual Reviews in Control 45 (June) (2018) 118–151. doi:10.1016/j.arcontrol.2018.04.012.

- [8] F. Katiraei, M. R. Iravani, Power management strategies for a microgrid with multiple distributed generation units, *IEEE transactions on power systems* 21 (4) (2006) 1821–1831.
- [9] F. Katiraei, M. R. Iravani, P. W. Lehn, Micro-grid autonomous operation during and subsequent to islanding process, *IEEE Transactions on power delivery* 20 (1) (2005) 248–257.
- [10] F. R. Badal, P. Das, S. K. Sarker, S. K. Das, A survey on control issues in renewable energy integration and microgrid, *Protection and Control of Modern Power Systems* 4 (1) (2019) 1–27.
- [11] Y. Xia, W. Wei, Y. Peng, P. Yang, M. Yu, Decentralized coordination control for parallel bidirectional power converters in a grid-connected dc microgrid, *IEEE Transactions on Smart Grid* 9 (6) (2017) 6850–6861.
- [12] T. Dragičević, X. Lu, J. C. Vasquez, J. M. Guerrero, Dc microgrids—part i: A review of control strategies and stabilization techniques, *IEEE Transactions on power electronics* 31 (7) (2015) 4876–4891.
- [13] T. Dragičević, X. Lu, J. C. Vasquez, J. M. Guerrero, Dc microgrids—part ii: A review of power architectures, applications, and standardization issues, *IEEE transactions on power electronics* 31 (5) (2015) 3528–3549.
- [14] S. Sudhoff, S. Pekarek, R. Swanson, V. Duppalli, D. Horvath, A. Kasha, R. Lin, B. Marquet, P. O’Regan, H. Suryanarayana, et al., A reduced scale naval dc microgrid to support electric ship research and development, in: *2015 IEEE Electric Ship Technologies Symposium (ESTS)*, IEEE, 2015, pp. 464–471.
- [15] A. Shekhar, L. Ramírez-Elizondo, P. Bauer, Dc microgrid islands on ships, in: *2017 IEEE Second International Conference on DC Microgrids (ICDCM)*, IEEE, 2017, pp. 111–118.
- [16] A. Alassi, S. Bañales, O. Ellabban, G. Adam, C. MacIver, HvdC transmission: Technology review, market trends and future outlook, *Renewable and Sustainable Energy Reviews* 112 (2019) 530–554.
- [17] D. Roch-Dupré, Á. J. López-López, R. R. Pecharromán, A. P. Cucala, A. Fernández-Cardador, Analysis of the demand charge in dc railway systems and reduction of its economic impact with energy storage systems, *International Journal of Electrical Power & Energy Systems* 93 (2017) 459–467.

BIBLIOGRAPHY

- [18] M. Ceraolo, G. Lutzemberger, E. Meli, L. Pugi, A. Rindi, G. Pancari, Energy storage systems to exploit regenerative braking in dc railway systems: Different approaches to improve efficiency of modern high-speed trains, *Journal of Energy Storage* 16 (2018) 269–279.
- [19] G. Graber, V. Calderaro, V. Galdi, A. Piccolo, R. Lamedica, A. Ruvio, Techno-economic sizing of auxiliary-battery-based substations in dc railway systems, *IEEE transactions on transportation electrification* 4 (2) (2018) 616–625.
- [20] D. J. Becker, B. Sonnenberg, Dc microgrids in buildings and data centers, in: 2011 IEEE 33rd International Telecommunications Energy Conference (INTELEC), IEEE, 2011, pp. 1–7.
- [21] G. AlLee, W. Tschudi, Edison redux: 380 vdc brings reliability and efficiency to sustainable data centers, *IEEE Power and Energy Magazine* 10 (6) (2012) 50–59.
- [22] P. C. Loh, D. Li, Y. K. Chai, F. Blaabjerg, Autonomous operation of hybrid microgrid with ac and dc subgrids, *IEEE transactions on power electronics* 28 (5) (2012) 2214–2223.
- [23] K. Uhlen, A. G. Endegnanew, T. M. Haileselassie, Operation and control of hybrid ac/dc transmission grids, in: *IECON 2019-45th Annual Conference of the IEEE Industrial Electronics Society*, Vol. 1, IEEE, 2019, pp. 4842–4847.
- [24] J. D. Watson, I. Lestas, Control of interlinking converters in hybrid ac/dc grids: network stability and scalability, *IEEE Transactions on Power Systems* 36 (1) (2020) 769–780.
- [25] P. Skentzos, G. C. Konstantopoulos, Current-limiting control of interlinking converter to maintain power balance in hybrid microgrids, in: 2022 IEEE PES Innovative Smart Grid Technologies Conference Europe (ISGT-Europe), IEEE, 2022, pp. 1–5.
- [26] P. Rault, X. Guillaud, F. Colas, S. Nguéfeu, Investigation on interactions between ac and dc grids, in: 2013 IEEE Grenoble Conference, IEEE, 2013, pp. 1–6.
- [27] S. Martínez, F. Torres, C. Roa, E. López, Interaction between ac grids and mt-dc systems based on droop controllers, in: 2018 IEEE International Conference on Automation/XXIII Congress of the Chilean Association of Automatic Control (ICA-ACCA), IEEE, 2018, pp. 1–6.

BIBLIOGRAPHY

- [28] A. Yazdani, R. Iravani, Voltage-sourced converters in power systems: modeling, control, and applications, John Wiley & Sons, 2010.
- [29] T. Hornik, Q.-C. Zhong, Control of power inverters in renewable energy and smart grid integration, John Wiley & Sons, 2012.
- [30] R. D. Middlebrook, S. Cuk, A general unified approach to modelling switching-converter power stages, in: 1976 IEEE power electronics specialists conference, IEEE, 1976, pp. 18–34.
- [31] R. Ortega, J. A. L. Perez, P. J. Nicklasson, H. J. Sira-Ramirez, Passivity-based control of Euler-Lagrange systems: mechanical, electrical and electromechanical applications, Springer Science & Business Media, 2013.
- [32] B. K. Bose, et al., Modern power electronics and AC drives, Vol. 123, Prentice hall Upper Saddle River, NJ, 2002.
- [33] R. W. Erickson, D. Maksimovic, Fundamentals of power electronics, Springer Science & Business Media, 2007.
- [34] C. J. O’Rourke, M. M. Qasim, M. R. Overlin, J. L. Kirtley, A geometric interpretation of reference frames and transformations: dq0, clarke, and park, IEEE Transactions on Energy Conversion 34 (4) (2019) 2070–2083.
- [35] N. Pogaku, M. Prodanovic, T. C. Green, Modeling, analysis and testing of autonomous operation of an inverter-based microgrid, IEEE Transactions on power electronics 22 (2) (2007) 613–625.
- [36] P. S. Kundur, O. P. Malik, Power system stability and control, McGraw-Hill Education, 2022.
- [37] S. Singh, A. R. Gautam, D. Fulwani, Constant power loads and their effects in dc distributed power systems: A review, Renewable and Sustainable Energy Reviews 72 (2017) 407–421.
- [38] E. Hossain, R. Perez, A. Nasiri, S. Padmanaban, A comprehensive review on constant power loads compensation techniques, IEEE access 6 (2018) 33285–33305.
- [39] S. Dedeoglu, G. C. Konstantopoulos, A. G. Paspatis, Grid-supporting three-phase inverters with inherent root mean square current limitation under balanced grid voltage sags, IEEE Transactions on Industrial Electronics 68 (11) (2020) 11379–11389.

- [40] L. Ahmethodzic, M. Music, Comprehensive review of trends in microgrid control, *Renewable Energy Focus* 38 (2021) 84–96.
- [41] J. Kumar, A. Agarwal, V. Agarwal, A review on overall control of dc microgrids, *Journal of energy storage* 21 (2019) 113–138.
- [42] Q. Shafiee, T. Dragičević, J. C. Vasquez, J. M. Guerrero, Hierarchical control for multiple dc-microgrids clusters, *IEEE transactions on energy conversion* 29 (4) (2014) 922–933.
- [43] J. M. Guerrero, J. C. Vasquez, J. Matas, L. G. De Vicuña, M. Castilla, Hierarchical control of droop-controlled ac and dc microgrids—a general approach toward standardization, *IEEE Transactions on industrial electronics* 58 (1) (2010) 158–172.
- [44] D. E. Olivares, A. Mehrizi-Sani, A. H. Etemadi, C. A. Cañizares, R. Iravani, M. Kazerani, A. H. Hajimiragha, O. Gomis-Bellmunt, M. Saeedifard, R. Palma-Behnke, et al., Trends in microgrid control, *IEEE Transactions on smart grid* 5 (4) (2014) 1905–1919.
- [45] U. N. Ekanayake, U. S. Navaratne, A survey on microgrid control techniques in islanded mode, *Journal of Electrical and Computer Engineering* 2020 (2020) 1–8.
- [46] D. Y. Yamashita, I. Vechiu, J.-P. Gaubert, A review of hierarchical control for building microgrids, *Renewable and Sustainable Energy Reviews* 118 (2020) 109523.
- [47] F. Dörfler, J. W. Simpson-Porco, F. Bullo, Breaking the hierarchy: Distributed control and economic optimality in microgrids, *IEEE Transactions on Control of Network Systems* 3 (3) (2015) 241–253.
- [48] A. Jaafar, A. Alawieh, R. Ortega, E. Godoy, P. Lefranc, Pi stabilization of power converters with partial state measurements, *IEEE Transactions on control systems technology* 21 (2) (2012) 560–568.
- [49] R. A. Ferreira, H. A. Braga, A. A. Ferreira, P. G. Barbosa, Analysis of voltage droop control method for dc microgrids with simulink: Modelling and simulation, in: *2012 10th IEEE/IAS International Conference on Industry Applications*, IEEE, 2012, pp. 1–6.
- [50] T. Dragičević, X. Lu, J. C. Vasquez, J. M. Guerrero, Dc microgrids—part i: A review of control strategies and stabilization techniques, *IEEE Transactions on power electronics* 31 (7) (2015) 4876–4891.

- [51] Q. C. Zhong, Robust droop controller for accurate proportional load sharing among inverters operated in parallel, *IEEE Transactions on Industrial Electronics* 60 (4) (2013) 1281–1290. doi:10.1109/TIE.2011.2146221.
- [52] Z. Shuai, D. He, J. Fang, Z. J. Shen, C. Tu, J. Wang, Robust droop control of dc distribution networks, *IET Renewable Power Generation* 10 (6) (2016) 807–814.
- [53] G. Liu, T. Caldognetto, P. Mattavelli, P. Magnone, Power sharing analysis of power-based droop control for dc microgrids considering cable impedances, in: 2017 19th European Conference on Power Electronics and Applications (EPE'17 ECCE Europe), IEEE, 2017, pp. P–1.
- [54] Y. Chen, A. Luo, Z. Peng, Robust droop multiple loop control method for resistance output parallel inverters, 2nd IET Renewable Power Generation Conference (RPG 2013) (2013).
- [55] Q.-C. Zhong, Y. Wang, B. Ren, Ude-based robust droop control of inverters in parallel operation, *IEEE Transactions on Industrial Electronics* 64 (9) (2017) 7552–7562.
- [56] Q. Xu, Y. Xu, C. Zhang, P. Wang, A robust droop-based autonomous controller for decentralized power sharing in dc microgrid considering large-signal stability, *IEEE Transactions on Industrial Informatics* 16 (3) (2019) 1483–1494.
- [57] J. C. Vasquez, J. M. Guerrero, A. Luna, P. Rodríguez, R. Teodorescu, Adaptive droop control applied to voltage-source inverters operating in grid-connected and islanded modes, *IEEE transactions on industrial electronics* 56 (10) (2009) 4088–4096.
- [58] V. Nasirian, A. Davoudi, F. L. Lewis, J. M. Guerrero, Distributed adaptive droop control for dc distribution systems, *IEEE Transactions on Energy Conversion* 29 (4) (2014) 944–956.
- [59] N. R. Chaudhuri, B. Chaudhuri, Adaptive droop control for effective power sharing in multi-terminal dc (mtdc) grids, *IEEE Transactions on Power Systems* 28 (1) (2012) 21–29.
- [60] X. Lu, K. Sun, J. M. Guerrero, J. C. Vasquez, L. Huang, State-of-charge balance using adaptive droop control for distributed energy storage systems in dc microgrid applications, *IEEE Transactions on Industrial electronics* 61 (6) (2013) 2804–2815.

- [61] Z. Huang, Adaptive integrated coordinated control strategy for mmc-mtde systems, in: 2018 International Conference on Power System Technology (POWERCON), IEEE, 2018, pp. 2440–2447.
- [62] S. Augustine, M. K. Mishra, N. Lakshminarasamma, Adaptive droop control strategy for load sharing and circulating current minimization in low-voltage standalone dc microgrid, *IEEE Transactions on Sustainable Energy* 6 (1) (2014) 132–141.
- [63] J. W. Simpson-Porco, F. Dorfler, F. Bullo, Voltage stabilization in microgrids via quadratic droop control, in: 52nd IEEE Conference on Decision and Control, Dec 2013, pp. 7582–7589.
- [64] J. W. Simpson-Porco, F. Dörfler, F. Bullo, Voltage stabilization in microgrids via quadratic droop control, *IEEE Transactions on Automatic Control* 62 (3) (2016) 1239–1253.
- [65] P. Prabhakaran, Y. Goyal, V. Agarwal, Novel nonlinear droop control techniques to overcome the load sharing and voltage regulation issues in dc microgrid, *IEEE Transactions on power electronics* 33 (5) (2017) 4477–4487.
- [66] Y. Zhang, X. Qu, M. Tang, R. Yao, W. Chen, Design of nonlinear droop control in dc microgrid for desired voltage regulation and current sharing accuracy, *IEEE Journal on Emerging and Selected Topics in Circuits and Systems* 11 (1) (2021) 168–175.
- [67] A. Elrayyah, F. Cingoz, Y. Sozer, Construction of nonlinear droop relations to optimize islanded microgrid operation, *IEEE Transactions on Industry Applications* 51 (4) (2015) 3404–3413.
- [68] P. D. Ferreira, P. M. Carvalho, L. A. Ferreira, M. D. Ilic, Distributed energy resources integration challenges in low-voltage networks: Voltage control limitations and risk of cascading, *IEEE Transactions on Sustainable Energy* 4 (1) (2012) 82–88.
- [69] F. Zhang, X. Duan, M. Liao, J. Zou, Z. Liu, Statistical analysis of switching overvoltages in uhv transmission lines with a controlled switching, *IET Generation, Transmission & Distribution* 13 (21) (2019) 4998–5004.
- [70] N. Bottrell, T. C. Green, Comparison of current-limiting strategies during fault ride-through of inverters to prevent latch-up and wind-up, *IEEE Transactions on Power Electronics* 29 (7) (2013) 3786–3797.

- [71] G. C. Konstantopoulos, Q.-C. Zhong, Current-limiting dc/dc power converters, *IEEE Transactions on Control Systems Technology* 27 (2) (2018) 855–863.
- [72] A.-C. Braitor, G. C. Konstantopoulos, V. Kadiramanathan, Enhanced primary droop controller for meshed dc micro-grids with overvoltage protection, in: 2021 29th Mediterranean Conference on Control and Automation (MED), IEEE, 2021, pp. 368–373.
- [73] A. Paspatis, G. Konstantopoulos, S. Dedeoglu, Control design and small-signal stability analysis of inverter-based microgrids with inherent current limitation under extreme load conditions, *Electric Power Systems Research* 193 (2021) 106929.
- [74] J. Neely, S. Pekarek, R. DeCarlo, N. Vaks, Real-time hybrid model predictive control of a boost converter with constant power load, in: 2010 Twenty-Fifth Annual IEEE Applied Power Electronics Conference and Exposition (APEC), IEEE, 2010, pp. 480–490.
- [75] Q. Xu, Y. Yan, C. Zhang, T. Dragicevic, F. Blaabjerg, An offset-free composite model predictive control strategy for dc/dc buck converter feeding constant power loads, *IEEE Transactions on Power Electronics* 35 (5) (2019) 5331–5342.
- [76] Q. Xu, N. Vafamand, L. Chen, T. Dragičević, L. Xie, F. Blaabjerg, Review on advanced control technologies for bidirectional dc/dc converters in dc microgrids, *IEEE Journal of Emerging and Selected Topics in Power Electronics* 9 (2) (2020) 1205–1221.
- [77] S. Yousefizadeh, J. D. Bendtsen, N. Vafamand, M. H. Khooban, T. Dragičević, F. Blaabjerg, EKF-based predictive stabilization of shipboard dc microgrids with uncertain time-varying load, *IEEE Journal of Emerging and Selected Topics in Power Electronics* 7 (2) (2018) 901–909.
- [78] F. Garcia-Torres, A. Zafra-Cabeza, C. Silva, S. Grieu, T. Darure, A. Estanqueiro, Model predictive control for microgrid functionalities: Review and future challenges, *Energies* 14 (5) (2021) 1296.
- [79] C. Chen, S. Duan, T. Cai, B. Liu, G. Hu, Smart energy management system for optimal microgrid economic operation, *IET renewable power generation* 5 (3) (2011) 258–267.

BIBLIOGRAPHY

- [80] E. Espina, J. Llanos, C. Burgos-Mellado, R. Cardenas-Dobson, M. Martinez-Gomez, D. Saez, Distributed control strategies for microgrids: An overview, *IEEE Access* 8 (2020) 193412–193448.
- [81] M. H. Cintuglu, T. Youssef, O. A. Mohammed, Development and application of a real-time testbed for multiagent system interoperability: A case study on hierarchical microgrid control, *IEEE Transactions on Smart Grid* 9 (3) (2016) 1759–1768.
- [82] Y. Han, K. Zhang, H. Li, E. A. A. Coelho, J. M. Guerrero, Mas-based distributed coordinated control and optimization in microgrid and microgrid clusters: A comprehensive overview, *IEEE Transactions on Power Electronics* 33 (8) (2017) 6488–6508.
- [83] M. Tucci, S. Rivero, J. C. Vasquez, J. M. Guerrero, G. Ferrari-Trecate, A decentralized scalable approach to voltage control of dc islanded microgrids, *IEEE Transactions on Control Systems Technology* 24 (6) (2016) 1965–1979.
- [84] Y. Sun, X. Hou, J. Yang, H. Han, M. Su, J. M. Guerrero, New perspectives on droop control in ac microgrid, *IEEE Transactions on Industrial Electronics* 64 (7) (2017) 5741–5745.
- [85] Y. Han, H. Li, L. Xu, X. Zhao, J. M. Guerrero, Analysis of washout filter-based power sharing strategy—an equivalent secondary controller for islanded microgrid without lbc lines, *IEEE Transactions on Smart Grid* 9 (5) (2017) 4061–4076.
- [86] L. Meng, T. Dragicevic, J. C. Vasquez, J. M. Guerrero, Tertiary and secondary control levels for efficiency optimization and system damping in droop controlled dc–dc converters, *IEEE Transactions on Smart Grid* 6 (6) (2015) 2615–2626.
- [87] C. Jin, P. Wang, J. Xiao, Y. Tang, F. H. Choo, Implementation of hierarchical control in dc microgrids, *IEEE transactions on industrial electronics* 61 (8) (2013) 4032–4042.
- [88] L. Che, M. Shahidehpour, Dc microgrids: Economic operation and enhancement of resilience by hierarchical control, *IEEE Transactions on Smart Grid* 5 (5) (2014) 2517–2526.
- [89] D. I. Hidalgo-Rodríguez, J. Myrzik, Optimal operation of interconnected home-microgrids with flexible thermal loads: a comparison of decentralized,

- centralized, and hierarchical-distributed model predictive control, in: 2018 Power Systems Computation Conference (PSCC), IEEE, 2018, pp. 1–7.
- [90] K. Hajar, A. Hably, S. Bacha, A. Elrafhi, Z. Obeid, An application of a centralized model predictive control on microgrids, in: 2016 IEEE Electrical Power and Energy Conference (EPEC), IEEE, 2016, pp. 1–6.
- [91] F. Garcia-Torres, C. Bordons, J. Tobajas, J. J. Márquez, J. Garrido-Zafra, A. Moreno-Muñoz, Optimal schedule for networked microgrids under deregulated power market environment using model predictive control, *IEEE Transactions on Smart Grid* 12 (1) (2020) 182–191.
- [92] L. K. Gan, P. Zhang, J. Lee, M. A. Osborne, D. A. Howey, Data-driven energy management system with gaussian process forecasting and mpc for interconnected microgrids, *IEEE Transactions on Sustainable Energy* 12 (1) (2020) 695–704.
- [93] P. R. Baldivieso-Monasterios, G. C. Konstantopoulos, A. T. Alexandridis, Model-based two-layer control design for optimal power management in wind-battery microgrids, *Journal of Energy Storage* 48 (2022) 104005.
- [94] J. L. Jerez, P. J. Goulart, S. Richter, G. A. Constantinides, E. C. Kerrigan, M. Morari, Embedded online optimization for model predictive control at megahertz rates, *IEEE Transactions on Automatic Control* 59 (12) (2014) 3238–3251.
- [95] K. E. Antoniadou-Plytaria, I. N. Kouveliotis-Lysikatos, P. S. Georgilakis, N. D. Hatziargyriou, Distributed and decentralized voltage control of smart distribution networks: Models, methods, and future research, *IEEE Transactions on smart grid* 8 (6) (2017) 2999–3008.
- [96] Y. Khayat, Q. Shafiee, R. Heydari, M. Naderi, T. Dragičević, J. W. Simpson-Porco, F. Dörfler, M. Fathi, F. Blaabjerg, J. M. Guerrero, et al., On the secondary control architectures of ac microgrids: An overview, *IEEE Transactions on Power Electronics* 35 (6) (2019) 6482–6500.
- [97] J. Zhao, F. Dörfler, Distributed control and optimization in dc microgrids, *Automatica* 61 (2015) 18–26.
- [98] S. Moayedi, A. Davoudi, Distributed tertiary control of dc microgrid clusters, *IEEE Transactions on Power Electronics* 31 (2) (2015) 1717–1733.

BIBLIOGRAPHY

- [99] C. De Persis, E. R. Weitenberg, F. Dörfler, A power consensus algorithm for dc microgrids, *Automatica* 89 (2018) 364–375.
- [100] S. Sahoo, S. Mishra, A distributed finite-time secondary average voltage regulation and current sharing controller for dc microgrids, *IEEE Transactions on Smart Grid* 10 (1) (2017) 282–292.
- [101] L. Ding, Q.-L. Han, X. Ge, X.-M. Zhang, An overview of recent advances in event-triggered consensus of multiagent systems, *IEEE transactions on cybernetics* 48 (4) (2017) 1110–1123.
- [102] J. Peng, B. Fan, Q. Yang, W. Liu, Distributed event-triggered control of dc microgrids, *IEEE Systems Journal* 15 (2) (2020) 2504–2514.
- [103] P. Shafiee, Y. Khayat, Y. Batmani, Q. Shafiee, J. M. Guerrero, On the design of event-triggered consensus-based secondary control of dc microgrids, *IEEE Transactions on Power Systems* 37 (5) (2021) 3834–3846.
- [104] L. Xing, Q. Xu, F. Guo, Z.-G. Wu, M. Liu, Distributed secondary control for dc microgrid with event-triggered signal transmissions, *IEEE Transactions on Sustainable Energy* 12 (3) (2021) 1801–1810.
- [105] D. Pullaguram, S. Mishra, N. Senroy, Event-triggered communication based distributed control scheme for dc microgrid, *IEEE Transactions on Power Systems* 33 (5) (2018) 5583–5593.
- [106] S. Peyghami, H. Mokhtari, P. C. Loh, P. Davari, F. Blaabjerg, Distributed primary and secondary power sharing in a droop-controlled lvdc microgrid with merged ac and dc characteristics, *IEEE Transactions on Smart Grid* 9 (3) (2016) 2284–2294.
- [107] F. Gao, S. Bozhko, G. Asher, P. Wheeler, C. Patel, An improved voltage compensation approach in a droop-controlled dc power system for the more electric aircraft, *IEEE Transactions on Power Electronics* 31 (10) (2015) 7369–7383.
- [108] A. Khorsandi, M. Ashourloo, H. Mokhtari, A decentralized control method for a low-voltage dc microgrid, *IEEE Transactions on Energy Conversion* 29 (4) (2014) 793–801.
- [109] Q. Xu, X. Hu, P. Wang, J. Xiao, P. Tu, C. Wen, M. Y. Lee, A decentralized dynamic power sharing strategy for hybrid energy storage system in autonomous dc microgrid, *IEEE transactions on industrial electronics* 64 (7) (2016) 5930–5941.

- [110] P. Lin, P. Wang, J. Xiao, J. Wang, C. Jin, Y. Tang, An integral droop for transient power allocation and output impedance shaping of hybrid energy storage system in dc microgrid, *IEEE Transactions on Power Electronics* 33 (7) (2017) 6262–6277.
- [111] Q. Xu, J. Xiao, X. Hu, P. Wang, M. Y. Lee, A decentralized power management strategy for hybrid energy storage system with autonomous bus voltage restoration and state-of-charge recovery, *IEEE Transactions on Industrial Electronics* 64 (9) (2017) 7098–7108.
- [112] Q. Xu, J. Xiao, P. Wang, X. Pan, C. Wen, A decentralized control strategy for autonomous transient power sharing and state-of-charge recovery in hybrid energy storage systems, *IEEE Transactions on Sustainable Energy* 8 (4) (2017) 1443–1452.
- [113] J. Schiffer, R. Ortega, A. Astolfi, J. Raisch, T. Sezi, Conditions for stability of droop-controlled inverter-based microgrids, *Automatica* 50 (10) (2014) 2457–2469.
- [114] A. H. Etemadi, E. J. Davison, R. Iravani, A decentralized robust control strategy for multi-der microgrids—part i: Fundamental concepts, *IEEE Transactions on Power Delivery* 27 (4) (2012) 1843–1853.
- [115] S. Rivero, F. Sarzo, G. Ferrari-Trecate, Plug-and-play voltage and frequency control of islanded microgrids with meshed topology, *IEEE Transactions on Smart Grid* 6 (3) (2014) 1176–1184.
- [116] A. P. N. Tahim, D. J. Pagano, E. Lenz, V. Stramosk, Modeling and stability analysis of islanded dc microgrids under droop control, *IEEE Transactions on power electronics* 30 (8) (2014) 4597–4607.
- [117] L. Guo, S. Zhang, X. Li, Y. W. Li, C. Wang, Y. Feng, Stability analysis and damping enhancement based on frequency-dependent virtual impedance for dc microgrids, *IEEE Journal of emerging and selected topics in power electronics* 5 (1) (2016) 338–350.
- [118] Z. Liu, M. Su, Y. Sun, W. Yuan, H. Han, J. Feng, Existence and stability of equilibrium of dc microgrid with constant power loads, *IEEE Transactions on Power Systems* 33 (6) (2018) 6999–7010.
- [119] J. Liu, W. Zhang, G. Rizzoni, Robust stability analysis of dc microgrids with constant power loads, *IEEE Transactions on Power Systems* 33 (1) (2017) 851–860.

BIBLIOGRAPHY

- [120] X. Liu, Y. Bian, Large signal stability analysis of the dc microgrid with the storage system, in: 2017 20th International Conference on Electrical Machines and Systems (ICEMS), IEEE, 2017, pp. 1–5.
- [121] M. Srinivasan, A. Kwasinski, Control analysis of parallel dc-dc converters in a dc microgrid with constant power loads, *International Journal of Electrical Power & Energy Systems* 122 (2020) 106207.
- [122] X. Li, X. Zhang, W. Jiang, J. Wang, P. Wang, X. Wu, A novel assorted nonlinear stabilizer for dc–dc multilevel boost converter with constant power load in dc microgrid, *IEEE Transactions on Power Electronics* 35 (10) (2020) 11181–11192.
- [123] D. Karimipour, F. R. Salmasi, Stability analysis of ac microgrids with constant power loads based on popov’s absolute stability criterion, *IEEE Transactions on Circuits and Systems II: Express Briefs* 62 (7) (2015) 696–700.
- [124] K. E. Lucas-Marcillo, D. A. P. Guingla, W. Barra, R. L. P. De Medeiros, E. M. Rocha, D. A. Vaca-Benavides, S. J. R. Orellana, E. V. H. Muentes, Novel robust methodology for controller design aiming to ensure dc microgrid stability under cpl power variation, *IEEE Access* 7 (2019) 64206–64222.
- [125] I. Rai, R. Anand, A. Lashab, J. M. Guerrero, Hardy space nonlinear controller design for dc microgrid with constant power loads, *International Journal of Electrical Power & Energy Systems* 133 (2021) 107300.
- [126] M. Su, Z. Liu, Y. Sun, H. Han, X. Hou, Stability analysis and stabilization methods of dc microgrid with multiple parallel-connected dc–dc converters loaded by cpls, *IEEE Transactions on Smart Grid* 9 (1) (2016) 132–142.
- [127] Y. Xue, J. M. Guerrero, Smart inverters for utility and industry applications, in: *Proceedings of PCIM Europe 2015; International Exhibition and Conference for Power Electronics, Intelligent Motion, Renewable Energy and Energy Management*, VDE, 2015, pp. 1–8.
- [128] H. Wang, X. Yue, X. Pei, Y. Kang, Improved software current-limiting protection strategy for starting the high-power motor, in: 2009 International Conference on Electrical Machines and Systems, IEEE, 2009, pp. 1–4.
- [129] F. Salha, F. Colas, X. Guillaud, Virtual resistance principle for the overcurrent protection of pwm voltage source inverter, in: 2010 IEEE PES Innovative Smart Grid Technologies Conference Europe (ISGT Europe), IEEE, 2010, pp. 1–6.

- [130] X. Pei, Y. Kang, Short-circuit fault protection strategy for high-power three-phase three-wire inverter, *IEEE Transactions on Industrial Informatics* 8 (3) (2012) 545–553.
- [131] J. M. Bloemink, M. R. Iravani, Control of a multiple source microgrid with built-in islanding detection and current limiting, *IEEE Transactions on Power Delivery* 27 (4) (2012) 2122–2132.
- [132] H. Chen, P. D. S. Assala, Y. Cai, P. Yang, Intelligent transient overvoltages location in distribution systems using wavelet packet decomposition and general regression neural networks, *IEEE Transactions on Industrial Informatics* 12 (5) (2016) 1726–1735.
- [133] J. B. Rawlings, D. Q. Mayne, M. Diehl, *Model predictive control: theory, computation, and design*, Vol. 2, Nob Hill Publishing Madison, WI, 2017.
- [134] B. Kouvaritakis, M. Cannon, *Model predictive control*, Switzerland: Springer International Publishing 38 (2016).
- [135] D. Q. Mayne, M. M. Seron, S. V. Raković, Robust model predictive control of constrained linear systems with bounded disturbances, *Automatica* 41 (2) (2005) 219–224. [doi:10.1016/j.automatica.2004.08.019](https://doi.org/10.1016/j.automatica.2004.08.019).
- [136] S. V. Raković, E. C. Kerrigan, K. I. Kouramas, D. Q. Mayne, Invariant approximations of the minimal robust positively invariant set, *IEEE Transactions on Automatic Control* 50 (3) (2005) 406–410. [doi:10.1109/TAC.2005.843854](https://doi.org/10.1109/TAC.2005.843854).
- [137] M. Cannon, J. Buerger, B. Kouvaritakis, S. Rakovic, Robust tubes in nonlinear model predictive control, *IEEE Transactions on Automatic Control* 56 (8) (2011) 1942–1947.
- [138] S. V. Rakovic, A. R. Teel, D. Q. Mayne, A. Astolfi, Simple robust control invariant tubes for some classes of nonlinear discrete time systems, *Proceedings of the 45th IEEE Conference on Decision and Control* (2006) 6397–6402.
- [139] D. Q. Mayne, E. C. Kerrigan, E. Van Wyk, P. Falugi, Tube-based robust nonlinear model predictive control, *International journal of robust and nonlinear control* 21 (11) (2011) 1341–1353.
- [140] X. Liu, Y. Shi, D. Constantinescu, Robust distributed model predictive control of constrained dynamically decoupled nonlinear systems: A contraction theory perspective, *Systems & Control Letters* 105 (2017) 84–91.

- [141] B. T. Lopez, J.-J. E. Slotine, J. P. How, Dynamic tube mpc for nonlinear systems, in: 2019 American Control Conference (ACC), IEEE, 2019, pp. 1655–1662.
- [142] S. Yu, C. Maier, H. Chen, F. Allgöwer, Tube mpc scheme based on robust control invariant set with application to lipschitz nonlinear systems, *Systems & Control Letters* 62 (2) (2013) 194–200.
- [143] M. Farina, R. Scattolini, Distributed predictive control: A non-cooperative algorithm with neighbor-to-neighbor communication for linear systems, *Automatica* 48 (6) (2012) 1088–1096.
- [144] S. Riverso, G. Ferrari-Trecate, Tube-based distributed control of linear constrained systems, *Automatica* 48 (11) (2012) 2860–2865.
- [145] C. Hans, P. Braun, J. Raisch, L. Grüne, C. Reincke-Collon, Hierarchical Distributed Model Predictive Control of Interconnected Microgrids, *IEEE Transactions on Sustainable Energy* 3029 (c) (2018) 1–10. [doi:10.1109/TSTE.2018.2802922](https://doi.org/10.1109/TSTE.2018.2802922).
- [146] B. Jin, H. Li, W. Yan, M. Cao, Distributed Model Predictive Control and Optimization for Linear Systems with Global Constraints and Time-Varying Communication, *IEEE Transactions on Automatic Control* 66 (7) (2021) 3393–3400. [doi:10.1109/TAC.2020.3021528](https://doi.org/10.1109/TAC.2020.3021528).
- [147] J. Kohler, M. A. Muller, F. Allgower, Nonlinear reference tracking: An economic model predictive control perspective, *IEEE Transactions on Automatic Control* 64 (1) (2019) 254–269. [doi:10.1109/TAC.2018.2800789](https://doi.org/10.1109/TAC.2018.2800789).
- [148] S. Riverso, K. Kouramas, G. Ferrari-Trecate, Decentralized and distributed robust control invariance for constrained linear systems, 2017 IEEE 56th Annual Conference on Decision and Control, CDC 2017 2018-Janua (Cdc) (2018) 5978–5984. [doi:10.1109/CDC.2017.8264564](https://doi.org/10.1109/CDC.2017.8264564).
- [149] M. Lazar, M. Tetteroo, Computation of terminal costs and sets for discrete-time nonlinear mpc, *IFAC-PapersOnLine* 51 (20) (2018) 141–146.
- [150] D. Ferreira, S. Silva, W. Silva, D. Brandao, G. Bergna, E. Tedeschi, Overview of consensus protocol and its application to microgrid control, *Energies* 15 (22) (2022) 8536.
- [151] F. Dorfler, F. Bullo, Synchronization and transient stability in power networks and nonuniform kuramoto oscillators, *SIAM Journal on Control and Optimization* 50 (3) (2012) 1616–1642.

- [152] P. Vorobev, P.-H. Huang, M. Al Hosani, J. L. Kirtley, K. Turitsyn, A framework for development of universal rules for microgrids stability and control, 2017 IEEE 56th Annual Conference on Decision and Control (CDC) (2017) 5125–5130.
- [153] A.-C. Braitor, G. C. Konstantopoulos, V. Kadiramanathan, Current-limiting droop control design and stability analysis for paralleled boost converters in dc microgrids, *IEEE Transactions on Control Systems Technology* 29 (1) (2020) 385–394.
- [154] G. C. Konstantopoulos, P. R. Baldivieso-Monasterios, State-limiting pid controller for a class of nonlinear systems with constant uncertainties, *International Journal of Robust and Nonlinear Control* 30 (5) (2020) 1770–1787.
- [155] H. K. Khalil, *Nonlinear systems third edition*, Patience Hall 115 (2002).
- [156] D. Limón, A. Ferramosca, T. Alamo, A. H. González, D. Odloak, Model predictive control for changing economic targets, *IFAC Proceedings Volumes* 45 (17) (2012) 384–391.
- [157] L. Grüne, Dissipativity and optimal control, arXiv preprint arXiv:2101.12606 (2021).
- [158] T. Faulwasser, L. Grüne, Turnpike properties in optimal control: An overview of discrete-time and continuous-time results, *Handbook of numerical analysis* 23 (2022) 367–400.
- [159] C. I. Byrnes, W. Lin, Losslessness, feedback equivalence, and the global stabilization of discrete-time nonlinear systems, *IEEE Transactions on automatic control* 39 (1) (1994) 83–98.
- [160] T. Faulwasser, D. Bonvin, On the design of economic nmpc based on an exact turnpike property, *IFAC-PapersOnLine* 48 (8) (2015) 525–530.
- [161] L. Grüne, M. Stieler, *Asymptotic stability and transient optimality of economic MPC without terminal conditions*, *Journal of Process Control* 24 (8) (2014) 1187–1196. doi:10.1016/j.jprocont.2014.05.003.
URL <http://dx.doi.org/10.1016/j.jprocont.2014.05.003>
- [162] G. Grimm, M. J. Messina, S. E. Tuna, A. R. Teel, Model predictive control: For want of a local control Lyapunov function, all is not lost, *IEEE Transactions on Automatic Control* 50 (5) (2005) 546–558. doi:10.1109/TAC.2005.847055.

BIBLIOGRAPHY

- [163] G. Grimm, M. J. Messina, S. E. Tuna, A. R. Teel, Examples when nonlinear model predictive control is nonrobust, *Automatica* 40 (10) (2004) 1729–1738.
- [164] S. V. Rakovic, A. R. Teel, D. Q. Mayne, A. Astolfi, Simple robust control invariant tubes for some classes of nonlinear discrete time systems, in: *Proceedings of the 45th IEEE Conference on Decision and Control*, IEEE, 2006, pp. 6397–6402.
- [165] M. Doff-Sotta, M. Cannon, Difference of convex functions in robust tube nonlinear mpc, in: *2022 IEEE 61st Conference on Decision and Control (CDC)*, IEEE, 2022, pp. 3044–3050.
- [166] S. V. Raković, L. Dai, Y. Xia, Homothetic tube model predictive control for nonlinear systems, *IEEE Transactions on Automatic Control* (2022).
- [167] V. Jurdjevic, *Geometric control theory*, Cambridge university press, 1997.
- [168] F. Colonius, W. Kliemann, *The dynamics of control*, Springer Science & Business Media, 2012.
- [169] A.-C. Braitor, G. Konstantopoulos, On the existence and uniqueness of equilibria in meshed dc microgrids with cpls, in: *30th Mediterranean Conference on Control and Automation, Proceedings, Institute of Electrical and Electronics Engineers (IEEE)*, 2022, pp. 1030–1035.
- [170] T. M. Apostol, *Calculus, Volume 1*, John Wiley & Sons, 1991.
- [171] F. Blanchini, Set invariance in control, *Automatica* 35 (11) (1999) 1747–1767. [doi:10.1016/S0005-1098\(99\)00113-2](https://doi.org/10.1016/S0005-1098(99)00113-2).
- [172] L. Grüne, J. Pannek, *Nonlinear model predictive control*, in: *Nonlinear model predictive control*, Springer, 2017, pp. 45–69.
- [173] M. Diehl, H. G. Bock, H. Diedam, P.-B. Wieber, Fast direct multiple shooting algorithms for optimal robot control, *Fast motions in biomechanics and robotics: optimization and feedback control* (2006) 65–93.
- [174] D. Mayne, An apologia for stabilising terminal conditions in model predictive control, *International Journal of Control* 86 (11) (2013) 2090–2095.
- [175] I. Kolmanovsky, E. G. Gilbert, Theory and computation of disturbance invariant sets for discrete-time linear systems (1998). [doi:10.1155/S1024123X98000866](https://doi.org/10.1155/S1024123X98000866).

BIBLIOGRAPHY

- [176] A. Isidori, E. Sontag, M. Thoma, *Nonlinear control systems*, Vol. 3, Springer, 1995.
- [177] Y. Nie, O. Faqir, E. C. Kerrigan, Iclocs2: Try this optimal control problem solver before you try the rest, in: 2018 UKACC 12th international conference on control (CONTROL), IEEE, 2018, pp. 336–336.
- [178] J. Schiffer, D. Zonetti, R. Ortega, A. M. Stanković, T. Sezi, J. Raisch, A survey on modeling of microgrids—from fundamental physics to phasors and voltage sources, *Automatica* 74 (2016) 135–150.
- [179] M. Diehl, H. J. Ferreau, N. Haverbeke, Efficient numerical methods for nonlinear mpc and moving horizon estimation, *Nonlinear model predictive control: towards new challenging applications* (2009) 391–417.
- [180] F. Tisseur, K. Meerbergen, The quadratic eigenvalue problem, *SIAM review* 43 (2) (2001) 235–286.
- [181] M. Nagumo, Über die lage der integralkurven gewöhnlicher differentialgleichungen, *Proceedings of the Physico-Mathematical Society of Japan*. 3rd Series 24 (1942) 551–559.
- [182] H. Brezis, On a characterization of flow-invariant sets, *Communications on Pure and Applied Mathematics* 23 (2) (1970) 261–263.
- [183] T. C. Gard, V. Lakshmikantham, Strongly flow-invariant sets, *Applicable Analysis* 10 (4) (1980) 285–293.
- [184] F. Bullo, *Lectures on network systems*, Vol. 1, Kindle Direct Publishing, 2020.